

STUDY OF CHLOROPHYLL BASED COMPOSITES FOR RADIATION DOSIMETRY IN RADIOTHERAPY

Thesis Submitted for the Award of the Degree of

DOCTOR OF PHILOSOPHY
in
Physics

By
Bhagat Chand

Registration No. 41800595

Supervised By
Dr. Mukesh Kumar
Professor



LOVELY PROFESSIONAL UNIVERSITY
PUNJAB

2022

DECLARATION

I hereby declare that the thesis entitled “**Study of Chlorophyll Based Composites for Radiation Dosimetry in Radiotherapy**” submitted by me for the degree of **Doctor of Philosophy** in Physics to the Lovely Professional University Phagwara is the result of my original and independent work under the guidance of **Dr. Mukesh Kumar**. This work has not previously formed the basis for the award of any degree, fellowship, diploma or other similar titles in this or any other University.

Dated:

Bhagat Chand
Registration No. – 41800595

CERTIFICATE

This is to certify that Mr. Bhagat Chand has completed Ph.D. Thesis titled “**Study of Chlorophyll Based Composites for Radiation Dosimetry in Radiotherapy**” under my Guidance and supervision. To the best of my knowledge, the present work is the result of his original investigation and study. No part of the project has ever been submitted for any other Degree or Diploma at any University.

The Project is fit for the submission and the partial fulfilment of the conditions for the award of Doctor of Philosophy in Physics.

Dated:

Signature of supervisor

Dr. Mukesh Kumar
Professor
Department of Physics
Lovely Professional
University
Phagwara, Punjab

Abstract

Cancer is the term used to describe the abnormal and uncontrolled growth of tissues in the body. It is caused by several factors and may manifest at any stage of life. It is one of the major causes of death worldwide with more than 10 M deaths globally per year. Radiotherapy is one of the major techniques for treating cancers. It utilizes high-energy electromagnetic and particulate radiations in the form of x-rays, gamma rays, and charged particles such as electrons and protons, etc. respectively for the treatment of cancers. Since the radiations are associated with the induction of somatic and genetic changes in the living organisms, it is required that the radiation dose be measured very precisely before delivering it to the patient. For this purpose, several national and international agencies have prescribed several standard protocols. The quantity of interest in radiation dosimetry is the absorbed dose to water (D_w).

A wide variety of dosimeters are also available for measuring D_w directly or indirectly. However, in economically weaker countries, the dosimetry systems pose an additional burden on treatment due to their cost, availability, and periodic calibrations. Hence a dosimetry system that overcomes these limitations and possesses some properties of an ideal dosimeter is required. The presented research has introduced a chemical dosimeter and a film dosimeter based on chlorophyll molecule as an active substance.

The chlorophylls have been extracted from plants commonly available in the region using some common organic solvents. Chlorophylls have been extracted from mango, hibiscus, pine, and spinach using acetone (80%), Dimethyl sulfoxide (DMSO), N, N Dimethyl formamide (DMF), and ethanol. An optimum pair of plants and solvent has been chosen based on chlorophyll yield and the seasonal availability of the plant. The samples have been analyzed by Ultraviolet-Visible (UV-Vis) spectrophotometry. The absorption spectra have shown two major peaks in the red region corresponding to 664 nm and in the blue region corresponding to 434 nm. The chlorophyll concentrations have been simultaneously determined by using the established algorithms. Two-way analysis of variance (ANOVA) has been tested to determine the variations among the plant group and solvent group for yielding and extracting the chlorophylls respectively. Based on the results

of ANOVA and practical considerations on the seasonal availability, mango, and acetone (80%) have been considered as the optimal pair for further study.

This optimal pair has been tested for the radiation dosimetric properties under high-energy x-ray and electron beam radiations from a medical linear accelerator (linac). The radiation response, linearity, energy, and dose rate dependence have been tested. The radiation-induced changes in the dosimeter have been quantified by UV-Vis absorption spectroscopy by analyzing changes at 664 nm in the region corresponding to the absorption maxima of chlorophyll-a (*chl-a*) in the red region of UV-Vis spectra. The dosimeter has been found sensitive to a small therapeutic dose of 0.012 Gy. This dosimeter has shown a good response in the therapeutic range of doses from 0.012 Gy to 2 Gy of 6 MV x-ray beam. The dosimeter possesses linearity in the response up to the conventional therapeutic dose of 2 Gy with a Pearson's correlation coefficient value of 0.91. Beyond that, it shows saturation in response.

The dosimeter exhibit energy and dose rate dependence. A maximum change of 5.8% in the response has been observed for 15 MV x-rays as compared to that for 6 MV x-rays. Similarly, the energy dependence has been observed for the electron beams. The flattening filter-free (FFF) x-rays have also shown response variations as compared to 6 MV x-rays. A variation of 1.2 % in the response of the dosimeter has been observed for 10 MV x-rays as compared to 6 MV x-rays. The results suggest that the dosimeter exhibits small dependence on beam qualities. Similarly, the small energy dependence within 5% of the response has been recorded for the electron beams. The dosimeter has been found to exhibit a weak dose rate dependence also. The dosimeter is dependent on dose rates up to 3 Gy/min, beyond that its response has been found to be independent of the dose rate.

A two-dimensional (2D) film dosimeter has been synthesized for dose determination in a plane. The casting method has been used to form the composite films. Polyvinyl alcohol (PVA) has been selected for the formation of the composite films. 10 ml of the PVA solution and 10 ml of the chlorophyll solution have been mixed thoroughly using a magnetic stirrer to make a homogenous mixture. This mixture has been cast in Petri

plates to form the films. This thickness of the films has been regulated by the volume of the solution. The casted solution has been subjected to freezing and thawing cycles of 12 h and 30 min respectively for the preparation of the copolymer films. Six such cycles have yielded films of optimal quality.

The films have been characterized by UV-Vis, photoluminescent (PL), Fourier transforms Infrared (FTIR), flatbed scanning, x-ray diffraction (XRD), and field emission scanning electron microscopy (FESEM) spectroscopy techniques. These techniques confirmed the preparation and presence of the pigment in the PVA matrix. Along with chlorophylls, small amounts of other pigments and chlorophyll degradation products have also been detected in the films. The UV-Vis spectra show discrete peaks in the blue and red regions of the spectra around 400 nm and 670 nm respectively. The shifts in peak locations in the composites as compared to that in solvents have been due to high polarity of the system and the formation of some inter-molecular transition levels in the composite. The FTIR spectra show transmission peaks corresponding to different functional groups present in chlorophyll, confirming the successful fusion of the chlorophyll to the PVA matrix. The flatbed scanning, 3D surface analysis, and RGB analysis have further confirmed the presence of green-coloured pigments in the composite films. The XRD spectra have shown peaks at locations slightly shifted from that corresponding to pure PVA with reduced sharpness. This indicates the reduction in crystalline nature with the infusion of chlorophyll. Further, the surface morphology of the films has shown a discrete fusion of chlorophyll on the PVA surface.

The film dosimeter has been irradiated under similar conditions as applied to the liquid dosimeter. The dosimeter has shown a response toward the therapeutic dose of x-rays from 0.25 Gy to 32 Gy. The quantification of the decrease in absorption at 670 nm (A_{670}) in the UV-Vis spectrum has been quantified as the measure of radiation-induced changes. The dosimeter shows the linearity of response up to 1 Gy with a Pearson correlation coefficient value of 0.96. It has been found to have energy dependence in the electron and photon beams.

The radiation response of the composite films has been analysed by different characterization techniques viz., PL, FTIR, XRD, and FESEM. The PL spectra indicate a change in the physical properties of the films with increasing dose. The spectrum indicates a change in the concentration of photoelectrons with increasing radiation dose. The FTIR spectra have also shown a decrease in transmission intensity at 32 Gy due to possible radiation-induced geometrical changes in the composite leading to a change in the dipole moment of the composite structure.

The XRD spectra have also indicated the radiation-induced change in the composite films leading to change in the orientations of the composite molecules and hence a decrease in the intensity of the diffraction peaks. The peak intensities around the location of maximum intensity have been found to decrease with increasing doses. The FESEM images have also confirmed the radiation-induced structural changes with localized cracks and pitting observed with increasing radiation dose. The highest level of pitting effect has been observed at a 32 Gy dose.

The optimal storage conditions for chlorophyll solution have been tested at temperatures of 5 °C and 20 °C in ambient light and darkness. The degradation rate constant (k), half-life ($t_{1/2}$) and activation energy (E) have been calculated for *chl-a* and *chl-b* in the solution. The E of *chl-a* has been 60.242 kJ/mol at 5 °C in dark and 36.174 kJ/mol at 20 °C in light and that of *chl-b* was 110.9 kJ/mol at 5 °C in dark and 53.9 kJ/mol 20 °C in light. The half-life and temperature quotient for *chl-b* have been higher than that for *chl-a* indicating overall higher stability of the former. These parameters have suggested that the chlorophyll solution and the films must be stored at 5 °C in darkness for a long and stable life.

In the present study, the chlorophyll dosimeter has been contained in a polypropylene (PPE) vial of 1 cc volume of a wall of 0.05 cm thickness. The dosimeter has a finite volume, and the dose is perturbed by the density differences from water. Hence, the non-water equivalence of the dosimeter correction factor ($f_{w,chl}$), a wall correction factor (P_{wall}), and volume averaging correction factors (P_v) have been calculated. The values of

correction factors: $f_{w,chl} = 0.969$, $P_{wall} = 0.995$ and $P_v = 0.999$ have been obtained. The largest correction comes from the non-water equivalence of the dosimeter followed by polypropylene wall and volume averaging respectively. These correction factors can be utilized for the determination of D_w from dose to chlorophyll (D_{chl}).

The present study concludes that the proposed dosimeters can be tested and used for clinical dosimetry of therapeutic x-rays and electron beam radiations.

Acknowledgments

I did not include a list of names in this section, however, if you recognize yourself elsewhere in this manuscript, then you are all acknowledged herein...

I am heartily thankful to my supervisor Dr. Mukesh Kumar; Professor, Department of Physics, LPU Phagwara, who meticulously undertook to act as my supervisor despite his hectic teaching schedule and other academic duties. I thank him for guiding me in the right direction. His wisdom, knowledge, and commitment to the highest standard inspired and motivated me. I am also highly thankful to Dr. Kailash Juglan, Head of the School of Chemical Engineering and Physical Sciences, LPU Phagwara; whose advice, wisdom and vision inspired me always and helped in each step of this work. I am highly obliged to all the faculty members of the Department of Physics, LPU Phagwara for their time-to-time motivation and support in completing this work. I am also thankful to all the technical staff in the Department of Physics, Chemistry and Central Instrument Facility, LPU, for allowing me to use all the necessary equipment and facilities which enabled me to complete my work.

I am extremely thankful to all the members of the Research Degree Committee for their academic support, valuable input from time to time, and motivational remarks.

I spent my time in between DRPGMC Tanda and LPU Phagwara, within two very different worlds. I will keep a very good memory of the morning coffee breaks, the brainstorming in the labs, and the coursework class bunks. My sincere gratitude to Dr. Sangeeta Prasher, Assistant Professor, Kanya Maha Vidyalaya, Jalandhar for her continuous guidance and support throughout the project. My sincere thanks to Dr. Muninder Kumar Negi, Head of the Department of Radiotherapy, AIIMS, Bilaspur for his most valuable support, encouragement, and positive attitude toward this research. Special thanks to the entire faculty and staff of the department of Radiotherapy, DRPGMC, Tanda for their support and suggestions from time to time.

Special thanks to my parents Sh. Khem Chand Bhardwaj and Smt. Chander Prabha Bhardwaj and my brother Mr. Prajapati Bhardwaj for their moral support and blessings. A

very special thanks to the one with whom I realized the true meaning of my life, my better half Ms. Priyamvda Bhardwaj for her immense and unconditional love, cooperation, and support in accomplishing my work. Thank you all for filling me with enthusiasm from time to time to complete this manuscript.

Last but not least I thank the Almighty “MAA MANGLAKALI” to give me an opportunity to be among wise people and giving me the strength and courage to continue my work for the betterment of the cancer patients.

Bhagat Chand

Table of Contents

DECLARATION	i
CERTIFICATE	ii
Abstract	iii
Acknowledgments	vii
List of Figures	xiv
List of Tables	xix
List of Abbreviations and Symbols	xx
1. Introduction	
1.1 Introduction	1
1.2 Cancer	2
1.3 Radiation therapy	3
1.4 Radiation Dosimetry	6
1.4.1 Requirements of a dosimetry system	9
1.5 Review of Literature	13
1.6 Research objectives:	20
Bibliography	22
2. Methodology	
2.1 Introduction	29
2.2 Extraction of chlorophylls	29
2.2.1 Selection and preparation of leaves	30
2.2.2 Selection of chemicals	30
2.2.3 Extraction in acetone (80%) and DMF	31
2.2.4 Extraction in DMSO	31
2.2.5 Extraction in ethanol	31
2.2.6 Sample analysis	32
2.2.6.1 UV-Vis spectrophotometry	32
2.2.6.2 FTIR spectroscopy	34
2.3 Preparation of polymer films	36
2.3.1 Selection of polymer	36
2.3.2 Preparation of chlorophyll polymer composite	36

2.3.3 Characterization of the copolymer films	37
2.3.3.1 Flatbed scanning	37
2.3.3.2. Photoluminescence (PL) spectroscopy	38
2.3.3.3. X-ray diffraction (XRD) spectroscopy for crystallographic study	39
2.3.3.4. Scanning electron microscopy (SEM) for morphological study	40
2.4 Radiometric analysis	41
2.4.1 Dose calculation system	41
2.4.2 Radiation delivery system	41
2.4.3 Irradiation setup	43
2.4.3.1 x-ray beams	43
2.4.3.2 Electron beams	43
2.4.4 Characterization of chlorophyll dosimeter	43
2.4.4.1 Accuracy and precision	43
2.4.4.2 Dose linearity	44
2.4.4.3 Dose rate dependence	44
2.4.4.4 Energy dependence	45
2.5 Monte Carlo simulations	45
2.5.1 MC simulation of the linac	45
2.5.2 MC simulation of the chlorophyll dosimeter	45
Bibliography	46
3. Analysis of Chlorophyll extraction and storage conditions	
3.1 Introduction	47
3.2 Analysis of chlorophyll extraction	47
3.2.1 Spectrum Parameters	49
3.2.3 Choice of Solvent and Plant Species	51
3.2.4 Analysis of the FTIR spectra of chlorophyll solution	54
3.3 Analysis of storage conditions	55
3.3.1 Temporal analysis of chlorophyll contents	57
3.3.2 Spectral analysis	59
3.3.3 Kinetic Analysis	62
3.4 Conclusion	66
Bibliography	66

4. Synthesis and characterization of the chlorophyll-PVA composite films	
4.1 Introduction	69
4.2 Preparation of composite films	69
4.3 Analysis of UV-Vis absorbance	71
4.4 Analysis of FTIR spectra	73
4.5 Analysis of PL spectra	75
4.6 Flatbed scanning	77
4.7 Morphological study of the composite films using SEM	79
4.8 Crystallographic study from XRD spectra	81
4.9 Conclusion	83
Bibliography	84
5. Radiometric analysis of chlorophyll solution and polymer composites	
5.1 Introduction	89
5.2 Radiation dosimetric properties of chlorophyll solution	89
5.2.1 Physical properties of the dosimeter	89
5.2.2 UV-Vis absorption spectra	90
5.2.3. Accuracy and Precision	91
5.2.4 Dose linearity	93
5.2.5 Energy Dependence	95
5.2.6 Dose rate dependence	96
5.2.7 Determination of absorbed dose to water using chlorophyll dosimeter	98
5.3 Radiation Dosimetric properties of Chl-PVA composite films	99
5.3.1 UV-Vis spectrophotometry	99
5.3.2 Flatbed scanning	100
5.3.3 Dose linearity	102
5.3.4 Energy dependence	102
5.4 Characterization of the radiation effects on chlorophyll solution	104
5.4.1 PL spectroscopy	105
5.4.2 FTIR spectroscopy	106
5.4.3 X-Ray Diffraction analysis	107
5.4.4 SEM analysis	108
5.5 Convenience of use and cost effectiveness	110
5.6 Conclusion	111

Bibliography	112
6. Monte Carlo simulation of chlorophyll dosimeter	
6.1 Introduction	116
6.2 MC Simulation of the linac	116
6.2.1 Radiation beam profiles	120
6.2.2. MLC modeling	124
6.2.3 Output factors	125
6.3 MC Simulation of the chlorophyll dosimeter	127
6.4 Conclusion	130
Bibliography	131
7. Summary and Conclusion	
Appendix - 1	
List of Patents and Publications	135
Patent	136
Publications	138

List of Figures

Figure 1.1 The illustration of the propagation of EM radiation is described by its wavelength (λ), amplitude (A), and direction of propagation. The electric and magnetic fields are propagating perpendicular to each other and to the direction of propagation.	02
Figure 1. 2 The mechanism of radiation-induced DNA strand break and cytoplasmic changes leading to cell death	04
Figure 1.3 The TCP (A) and NTCP (B) curves, the ratio of TCP to NTCP is called therapeutic ratio and determines the probability of tumor control at any normal tissue reactions	06
Figure 1.4 The IAEA TRS 398 based absolute dosimetry system applied in dosimetry of radiotherapy beams	08
Figure 1.5 The properties of an ideal radiation dosimeter	12
Figure 1.6 Chemical structure of chl-a and chl-b molecules	17
Figure 1.7 Energy level diagram of chlorophyll showing the ground state and first and second singlet excited states. The absorption of light causes an excitation to first and second singlet excited states respectively, and the conversion to ground state occurs through emission of heat or fluorescence radiation in red and blue regions. The third singlet excited state is a long-lived state	19
Figure 2.1 The process of chlorophyll extraction from the leaves	32
Figure 2.2 The UV 1800 UV-Vis spectrophotometer used in this study	33
Figure 2.3 The Shimadzu 8400 S FTIR spectrometer used in this study	35
Figure 2.4 The EPSON 12000XL flatbed scanner used in this study	38
Figure 2.5 The Bruker x-ray diffractometer utilized for XRD analysis of the sample	39
Figure 2.6 The JOEL SEM equipment utilized for sample analysis	40

Figure 2.7 Setup conditions for irradiation of chlorophyll and chlorophyll-based polymer composite films dosimeter under x-ray beams from a medical linear accelerator	42
Figure 2.8 The irradiation setup for x-rays (a) and electron beam radiations (b)	44
Figure 3.1 The comparative analysis of the chlorophyll extraction from different plants in different solvents	49
Figure 3.2 Variations of chl-a/b ratio with solvent polarity. The connecting lines are for representations only not as a trendline	50
Figure 3.3 The UV-Vis absorption spectra of the chlorophyll solution from different plants in different solvents	52
Figure 3.4 The FTIR spectra of leaf extracts obtained from different plants species in acetone (80%)	54
Figure 3.5 The degradation pathways of chlorophyll in vitro under the effect of different biochemical and physical conditions	57
Figure 3.6 The temporal variations of total chlorophyll concentration stored at different conditions of light and temperature	58
Figure 3.7 Trend of the change in color of chlorophyll solution over one month time	60
Figure 3.8 Variations observed in the UV-Vis absorbance spectra of chlorophyll samples over a period of one month at 20°C in dark (a), 20°C in light (b), 5°C in dark (c) and 5°C in light (d) storage conditions	61
Figure 3.9 Thermal and photo degradation kinetics of chl-a and (a), chl-b (b) under different storage conditions	63
Figure 4.1 The chl-PVA composite film during the freeze and thaw cycles (a) and the dried films(b)	70
Figure 4.2 The UV-Vis absorption spectra of PVA film and chl-PVA composite film	71

Figure 4.3 The FTIR spectra of pure PVA and chl-PVA composite thin film	74
Figure 4.4 The photoluminescence spectrum of chl-PVA thin film composites	76
Figure 4.5 The flatbed scanning image of the chl-PVA composite film (a), and the region of interest chosen for RGB analysis in imagej (b)	77
Figure 4.6 The 3D surface mapping of the RGB analysis of the ROI selected in the <i>chl-PVA</i> composite film	79
Figure 4.7 The SEM images of <i>chl-PVA</i> films ($\times 70000$) showing the chlorophyll distributed over the PVA matrix	80
Figure 4.8 The EDS spectra and EDS mapping of the elements in the chl-PVA composite film	81
Figure 4.9 The XRD spectra of pure PVA and chl-PVA composite films. The values of 2θ corresponding to the peaks are indicated in the figure	83
Figure 5.1 The UV-Vis absorption spectra of the chlorophyll dosimeter irradiated to therapeutic range of doses. The dose response has been observed by absorbance at 664 nm	90
Figure 5.2 The precision of the chlorophyll dosimeter for a dose of 2 Gy of 6 MV x-rays delivered under same setup conditions	92
Figure 5.3 The dose linearity region of the chlorophyll dosimeter. The dose, A664 linearity has been observed up to 2 Gy	93
Figure 5.4 The radiation response of the chlorophyll dosimeter in the tested range of therapeutic doses	94
Figure 5.5 The energy dependence of the chlorophyll dosimeter in the therapeutic range of x-rays (a) and electron beams (b)	96

Figure 5.6 Effect of different dose rates utilized to deliver 1 Gy dose of 6 MV x-ray beam to the chlorophyll dosimeter. The figure presents the mean \pm standard deviation (indicated by bars) for all energies compared against 600 cGy/min	97
Figure 5.7 The UV-Vis absorption spectra of the composite films showing the change in absorbance with radiation dose at around 670 nm	100
Figure 5.8 The 3D surface analysis of the chl-PVA films at 2 Gy and 32 Gy dose showing a decrease in the green colour content in the film	101
Figure 5.9 The dose response up to 32 Gy of therapeutic dose shown by the chl-PVA films	102
Figure 5.10 The energy dependence of the chl-PVA film dosimeter for x-ray beam energies (a) and electron beam energies (b)	104
Figure 5.11 The excitation and emission spectra of the chl-PVA dosimeter	105
Figure 5.12 The FTIR spectra of chl-PVA composite films irradiated to different doses of 6 MV x-rays	106
Figure 5.13 The XRD spectra of the chl-PVA composite films irradiated to different doses of 6MV x-ray	107
Figure 5.14 The FESEM images of the chl-PVA composite films irradiated at 2 Gy(a) and 32 Gy (b) dose of 6 MV x-rays. The radiation induced damage can be visualised in the film irradiated at 32 Gy	109
Figure 6.1 The relative locations of the components in Agility treatment head installed in Elekta VersaHD linac [Source: Monaco TPS reference manual	117
Figure 6.2 The comparative analysis of MC calculated and measured PDD profiles in SSD setup shows the dose difference at respective depths (a) and SAD setup for a range of field sizes (b)	121

Figure 6.3 Dose difference in measured and calculated off axis beam profiles in crossline (a) and inline (b) directions	123
Figure 6.4 The inline and cross line beam profiles for range of square field sizes of sides of length ranging from 5 cm to 30 cm	124
Figure 6.5 The radiation beam penumbra for Agility 160 leaves MLCs for a 10×10 cm ² field size. The congruence of measured and MC simulated parameters show the accuracy of the model parameters used to define the MLCs	125
Figure 6.5 Calculated and measured beam output factors as a function of field sizes	126
Figure 6.7 2D gamma analysis of the measured (a, d, and g) and MC calculated (b, e and, h) dose distributions at 90 cm SSD, 10 cm depth for 5 × 5 cm ² (a-c), 10 × 10 cm ² (d-f), and 20 × 20 cm ² (g-i)	127
Figure 6.6 Illustration of the irradiation setup for a chlorophyll dosimeter and Agility head simulated in EGSnrc MC simulation toolkit for determination of the correction factors	129

List of Tables

Table 2.1 The equations used to determine simultaneously the chlorophyll concentrations.	34
Table 3.1 Chlorophyll concentrations $\mu\text{g}/\text{mg}$ (of fresh leaves' weight) obtained in different solvents from selected plants	48
Table 3.2 The solvent and plant wise values of chlorophyll spectrum characterization by sorbet ratio and FWHM of the red peak absorption	51
Table 3.3 (a) ANOVA results comparing selected plant species and solvents for extraction of chlorophylls	53
Table 3.3 (b) ANOVA results comparing se selected solvents for chlorophyll extraction.	53
Table 3.4 The rate constants k ($\times 10^{-3}$; h^{-1}) and coefficients of determination (R^2) for photo and thermal degradation of chlorophyll in mango leaves, obtained from chemical analysis and plot of $\ln(C/C_0)$ vs observation time are given along with E_a and $t_{1/2}$	65
Table 4.1 The RGB analysis of the composite film.	78
Table 5.1 The values of A_{664} obtained from continuous irradiation of the chlorophyll dosimeter. The precision has been calculated from the standard deviation	92
Table 5.2 the RGB analysis of the chl-PVA films irradiated up to 32 Gy.	101
Table 6.1 The value of estimated errors (ϵ) and gamma index (3%/3mm) for PDD, inline and crossline profiles at 100 cm SSD and 10×10 cm ² field size	120
Table 6.2 Comparison of the parameters describing radiation beam quality of a 6 MV photon beam for 10×10 cm ² field size.	120
Table 6.3 The MC calculated values of the correction factors for chlorophyll dosimeter.	128

List of Abbreviations and Symbols

- 1.** DMSO: Dimethyl sulfoxide.
- 2.** DMF: N, N Dimethyl formamide.
- 3.** ANOVA: Analysis of variance.
- 4.** UV-Vis: Ultraviolet and visible spectroscopy.
- 5.** MV: Megavoltage or Million volt.
- 6.** Chl-a: Chlorophyll-a.
- 7.** FFF: Flattening filter free.
- 8.** PVA: Polyvinyl alcohol.
- 9.** PL: Photoluminescent spectroscopy.
- 10.** FTIR: Fourier transform infrared spectroscopy.
- 11.** FESEM: Field emission scanning electron microscopy.
- 12.** Gy: Gray; the unit of radiation absorbed dose.
- 13.** PPE: Polypropylene.
- 14.** EM: Electromagnetic radiations.
- 15.** PET: Positron emission tomography.
- 16.** CT: Computed tomography scan.
- 17.** MRI: Magnetic resonance imaging.
- 18.** DNA: Deoxyribose nucleic acid.
- 19.** kV: kilo volt.
- 20.** TCP: Tumour control probability.
- 21.** NTCP: Normal tissues complication probability.
- 22.** OSLD: Optically stimulated luminescent dosimeter.
- 23.** TLD: thermoluminescent dosimeter.
- 24.** QA: Quality assurance.
- 25.** PSQA: Patient specific quality assurance.
- 26.** 2DRT: Two-dimensional radiotherapy.
- 27.** 3DCRT: Three-dimensional conformal radiotherapy.
- 28.** IMRT: Intensity modulated radiotherapy.

29. IMAT: Intensity modulated arc therapy.
30. AAPM: American association of physicists in medicine.
31. IAEA: International atomic energy agency.
32. ICRU: International commission on radiation units and measurements.
33. CCD: Charge couple device.
34. RGB: Red green blue.
35. MU: Monitor units.
36. SSD: Source to surface distance.
37. SAD: Source to axis distance.
38. MLC: Multileaf collimators.
39. EGSnrc: Electron gamma shower; national research centre.
40. FWHM: Full width half maxima.
41. OD: Optical density.
42. LET: Linear energy transfer.
43. DD: Dose difference.
44. DTA: Distance to agreement.
45. D_{det} : Absorbed dose to detector volume.
46. D_{med} : Absorbed dose to medium.
47. D_w : Absorbed dose to water.
48. D_F : Absorbed dose to Fricke dosimeter.
49. D_{chl} : Absorbed dose to chlorophyll dosimeter.
50. N_{DWQ_0} : The absorbed dose to water calibration factor in reference beam quality Q_0 .
51. k : The combination of correction factors used in dosimetry.
52. P_{wall} : The wall correction factor.
53. P_v : The volume averaging correction factor.
54. $f_{w,chl}$: The absorbed dose from chlorophyll to water conversion factor.

Chapter 1

Introduction

1.1 Introduction

The propagation of energy in the space and material medium is called radiation. One form of radiation namely Electromagnetic (EM) radiation is one of the most common sources of energy from natural and artificial sources. It ranges from very high-frequency cosmic rays to low-energy radio waves. For a long, EM radiations have been used in various human ventures. It has numerous applications in telecommunication, industrial radiography, food safety, agriculture, medicine, etc. [1]. The radiations in the form of rays and particles have several applications in academic research and development as well. The ionizing radiations like the x-rays, gamma rays, and some particle radiations are specifically used in diagnostic and therapeutic radiology.

The radiations are broadly classified as non-ionizing and ionizing. Non-ionizing radiations don't possess enough energy to produce ionization events in the atoms or molecules and hence are not considered harmful to body tissue. The ionizing radiations, on the other hand, deposit dose in the matter by the process of ionization and/or excitation. The ionizing radiations are further classified in a wide variety. However, the region of interest in the present study is the x-rays and the electron radiations produced from a medical linear accelerator (linac), which are used for cancer treatment in radiotherapy [2].

The medicinal use of radiations is mainly of two types: radio-diagnostic and radio-therapeutic. Diagnostic radiology is one of the most useful and interdependent branches of medicine. It provides solutions to several other medical applications by providing qualitative and quantitative information on a specific type of physiological condition [3]. The diagnostic use includes diagnostic x-rays radiography, computed tomography scanning, x-ray angiography, gamma scanning, positron emission tomography (PET) scanning, etc. [4]. These techniques mostly use kilovoltage x-rays and gamma rays in small quantities. The radiation dose in such procedures is usually low in the ranges of a few mGy

to cGy. The therapeutic use of radiation is mainly in the treatment of benign and malignant cancers.

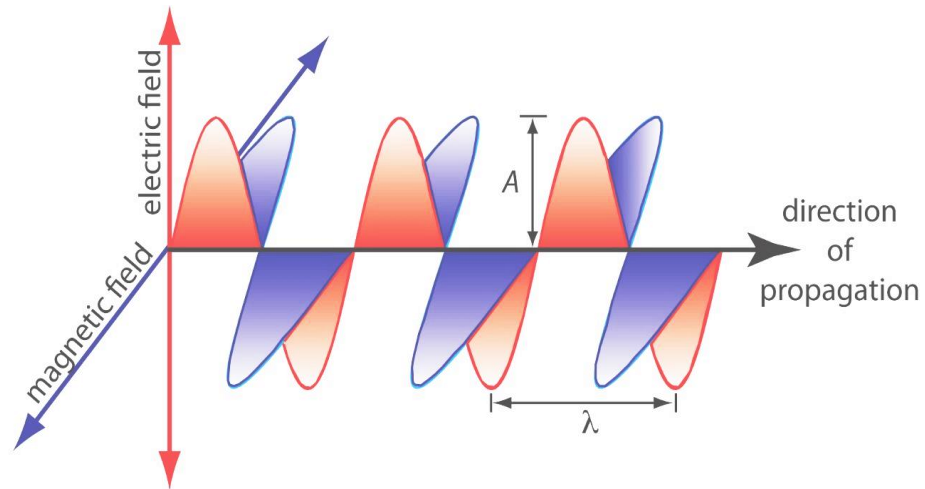


Figure 1.1 The illustration of the propagation of EM radiation is described by its wavelength (λ), amplitude (A), and direction of propagation. The electric and magnetic fields are propagating perpendicular to each other and to the direction of propagation.

1.2 Cancer

Cancer is the term used to describe the abnormal and uncontrolled growth of cells in the body. It has been a major cause of social and financial toxicity along with its physiological and mental traumatic effects on the patients [5,6]. Cancer incidence is a major concern worldwide. It is a major cause of death in developing nations. In the year 2020; 19.3 M new cancer cases have been detected worldwide with over 10 M cancer-caused deaths. Breast cancer has been the leading cause of cancer followed by lung, colorectal, prostate, and stomach. Cancer is the first to the second leading cause of death in the western world while in India it is the third to the fourth-largest cause of death [7]. In India as per Indian Council of Medical Research (ICMR) data, 11,57294 new cases of cancer have been registered in the year 2018 and 7,24,821 cancer deaths have been reported

[8,9]. There has been an estimate that one out of nine Indians will develop cancer once in their lifetime [9]. It has been reported as the second largest disease in India [10,11].

Cancers are caused mainly by gene alterations due to several different factors [12]. The genetic abnormalities leading to the development of cancers are of two types: growth-promoting genes and growth-suppressing genes. If the growth-promoting genes are excessive, they lead to cell proliferation and if growth-suppressing genes are defective in activity or amount, they fail to halt the proliferative cells and lead to uncontrolled cell replication. The growth-promoting genes are called oncogenes while the growth suppressing genes are called tumour suppressor genes. The oncogenes cause the cancer cells to grow rapidly in an undefined fashion with a rapid doubling time in several cases. At a certain stage, these cells can metastasize, causing the spread of the disease to other parts of the body. The treatment is given to these cancer cells [13]. The most common means of treating cancer are surgery, chemotherapy, radiation therapy, and immunotherapy [14]. For about 70% of cases, surgery, chemotherapy, and radiotherapy are combined to achieve the intent of treatment. The specific kind of treatment choice depends upon the tumour type, stage, volume, location, and general condition (GC) of the patient [15].

1.3 Radiation therapy

Radiotherapy is the technique of treatment of benign or malignant tumours by use of ionizing radiations. The ionizing radiations can either be obtained from a radioactive source or produced artificially in numerous types of generators [16]. Radiotherapy works on the principle of radiation-induced DNA damage and eventual cell death [17]. Figure 1.2 illustrates the mechanism of radiation-induced cell killing. The use of radiation in therapy is as old as the discovery of x-rays by Roentgen and the discovery of radioactivity by Becquerel [18]. The first use of x-rays in medical therapy is generally attributed to Emil Grubbé, a manufacturer living in Chicago who manufactured incandescent lamps and Crookes tubes and treated a patient with breast cancer using the x-rays [19, 20].

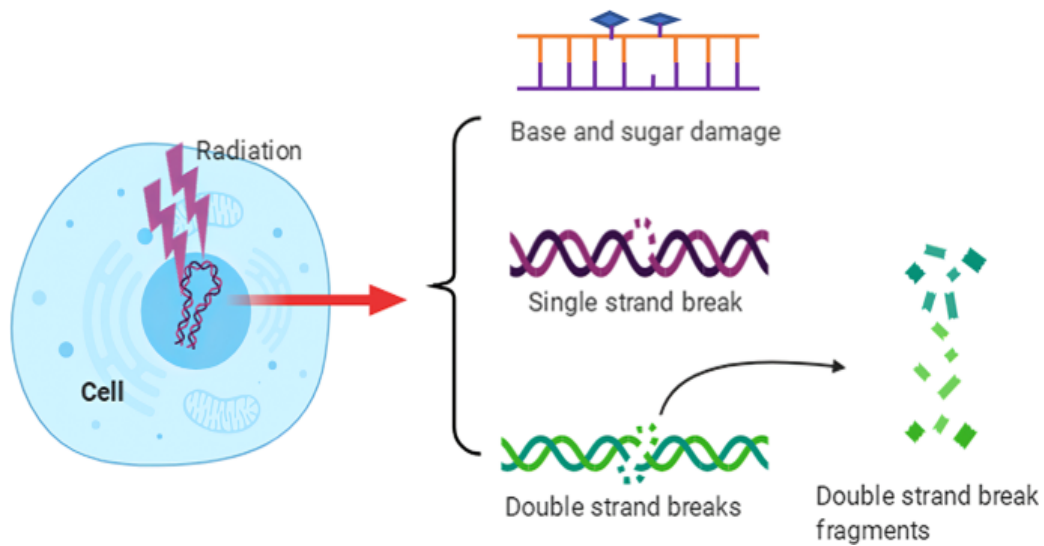


Figure 1.2 The mechanism of radiation-induced DNA strand break and cytoplasmic changes leading to cell death [21].

Radiotherapy aims to deliver a maximum radiation dose to the tumours i.e., to increase the tumour control probability (TCP) while simultaneously sparing surrounding normal structure i.e., to keep the normal tissue complication probability (NTCP) as low as reasonably achievable [23,24]. The NTCP and TCP curves (Figure 1.3) have a steep gradient in the centre and hence necessitate the accurate determination of the dose to avoid any radiation-induced damage to normal tissues [25]. This aim is achieved by a multistep process involving the clinical and radiological diagnosis, identification of the target volume and normal structure on the 2D or 3D radiological images, dose prescription to target, treatment planning, treatment plan verification and finally the treatment delivery [26].

Earlier the radiations have been delivered using low energy kilo volt (kV) x-rays. In the successive years, from 1930 to 1950, continuous scientific progress has been made to treat deep-seated tumours. The use of Radium based internal radiation therapy (brachytherapy) has also been largely performed during this era. The development of orthovoltage and super voltage x-ray tubes has also been a remarkable achievement. The introduction of electron beam therapy has been another milestone in this era [16]. The

evolution in radioactivity and induction of Co⁶⁰ radioactive source and the development of modern linear accelerator (linac) technology has led to the evolution of high-energy x-ray radiation therapy.

The megavoltage (MV) beams have been able to treat deep-seated tumours with very less side effects. The linacs have the advantage of producing variable dose rates and a range of electron and x-ray energies. Simultaneously the development of CT and MRI changed the scenario of radiation therapy by providing three-dimensional (3D) localization of the target. The 3D localization of the tumour and surrounding normal tissues proved to be an efficient tool to achieve the goal of radiotherapy. The radiation beams could now be placed more precisely to deliver the dose to the tumour with minimal damage to the normal tissues. Radiation delivery can be of many types ranging from conventional 2D therapy to three-dimensional conformal radiation therapy (3D CRT), intensity-modulated radiation therapy (IMRT) and now the most modern intensity-modulated arc therapy (IMAT) and particle therapy [22].

The output of the radiation source is one of the major factors determining the treatment accuracy. To maintain the accuracy and consistency of radiation dose delivery, the radiation sources need to be monitored and calibrated on regular basis in a well-defined and standardized setup following well-established protocols. Currently, this task in radiotherapy is performed following the guidelines of the American Association of Physicists in Medicine (AAPM) Task Group (TG) 51 and International Atomic energy Agency (IAEA) Technical report series (TRS) 398 respectively [27,28]. The air-filled ionization chambers are the recommended radiation dosimeters for absolute and reference dosimetry of therapeutic x-rays and electron beams. The thermo-luminescent dosimeter (TLD), radiographic and radio-chromic films, solid-state diode detectors, and diamond detectors are among the most used radiation dosimeters in relative dosimetry of the therapeutic radiations [29,30]. The radiation effectiveness, accuracy, spatial dose accuracy and precision, various dosimetric checks of the equipment and consistent accurate delivery etc. are performed with the radiation dosimeters [31].

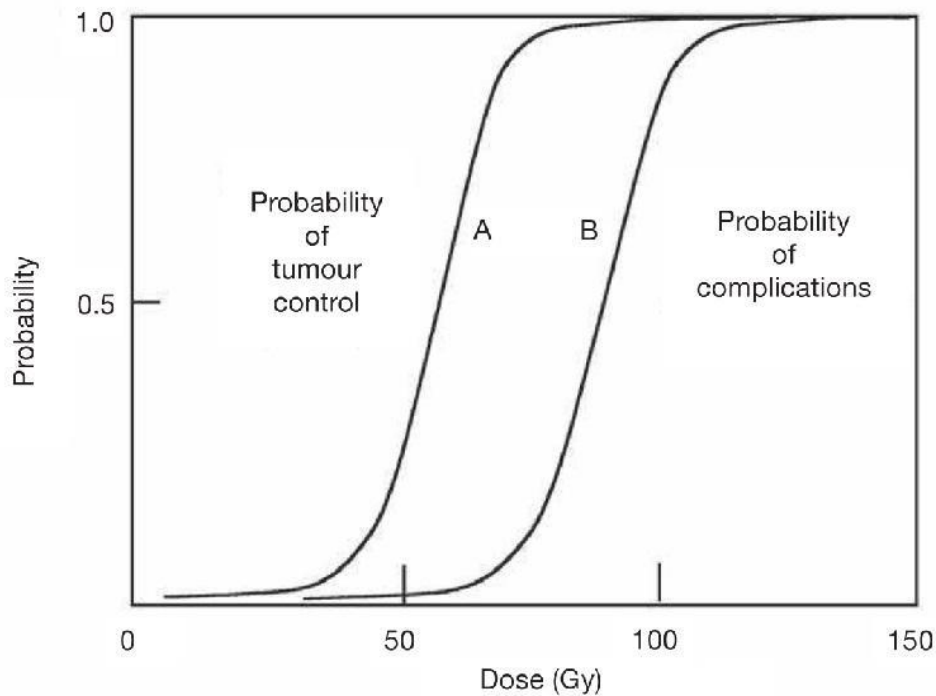


Figure 1.3 The TCP (A) and NTCP (B) curves, the ratio of TCP to NTCP is called the therapeutic ratio and determines the probability of tumour control at any level of normal tissue reactions. [32]

In radiotherapy, the biologically significant amount of radiation dose is directly delivered to the patient. Therapeutic radiations are known to cause radiation-induced damage in tissues other than the tumour. Overdosing or underdosing of the tumour can also have serious consequences in achieving the goal of therapy [23]. Hence it is vital to determine the accuracy of the absolute dose and spatial distribution of the dose on the patient. Further, the estimation of radiation dose is necessary for the safety of the radiation workers operating the radiation source and the public in the vicinity of the radiation source.

1.4 Radiation Dosimetry

Radiation dosimetry in radiation therapy involves the estimation of the radiation dose delivered to cancer patients. Dosimetry is as vital as the treatment itself and plays an

important role in the determination of the accuracy of radiation dose delivery. A radiation dosimeter is a device used to measure either the absolute dose or able to derive the dose in relative terms based on the effects produced in it because of the radiation interactions [32]. Several physical, biological, and chemical processes and phenomena can be utilized to observe and quantify the radiation effects [33]. Also, it is now evident that gamma radiations are capable of somatic changes in living organisms [34]. These changes if quantified precisely can also be used to estimate the radiation effect and hence the amount of radiation absorbed dose received by the organism.

The fundamental quantity in radiation dosimetry is the radiation absorbed dose. The dose is defined as the mean energy ($\bar{\epsilon}$) deposited in the unit mass (dm) of the medium. The absorbed dose is a non-stochastic quantity [32]. The radiation dosimetry is generally carried out in a phantom made up of some tissue equivalent material. Water is considered one of the most common phantom materials due to its dosimetric properties nearly equivalent to that of human soft tissues and its global availability [35]. The detector is placed inside the phantom and connected to a measuring assembly. The ionization produced by the radiation interactions inside the detectors is measured by the measuring assembly (figure 1.4). The detectors along with the measuring assembly are collectively called radiation dosimeters. The measuring assembly gives the measure of radiation absorbed dose in terms of a meter reading or other type of signals depending upon the type of detector used. The signal that is collected from the detector is multiplied by certain correction factors to determine the dose to the sensitive volume of the detector (D_{det}).

The desired quantity is the dose at a reference point in the medium (D_{med}) in the absence of the detector. This conversion of D_{det} to D_{med} is a crucial step requiring the knowledge of several correction factors as per the conditions of cavity theory [36]. The D_{med} gives the actual dose deposited by the radiations in the medium and is the quantity of interest. Unit of radiation absorbed dose is J/kg and the special unit is Gray.

$$D = \frac{d\bar{\epsilon}}{dm} \quad (1.1)$$

The dose to water measured by a detector placed inside a water phantom is given by:

$$D_{med} = M_{w,Q}^{user} \times N_{D,w,Q_0} \times k_i \quad (1.2)$$

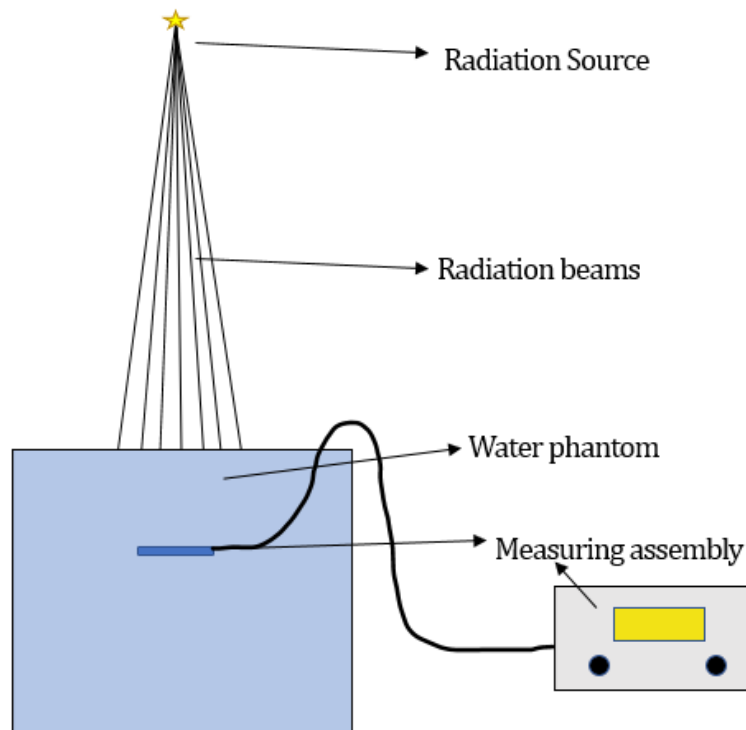


Figure 1.4 The IAEA TRS 398 based absolute dosimetry system applied in dosimetry of radiotherapy beams.

Where, $M_{w,Q}^{user}$ is the meter reading or the detector response in the user's radiation beam quality (Q). N_{DWQ_0} is the absorbed dose to water calibration factor determined in a reference beam quality (Q_0) of cobalt-60 (Co^{60}) gamma rays under reference conditions in the water phantom. " k_i " is the general correction factor used to correct for the effect of the difference in the value of an influence quantity between the calibration of a dosimeter under reference conditions in the standards laboratory and the use of the dosimeter in the user

facility under different conditions. [28]. The (IAEA) technical report series (TRS 398) [28] has recommended water as the phantom medium for absolute dosimetry of medical x-ray and electron radiation beams. The detector for absolute dosimetry is an ionisation chamber connected to an electrometer.

Radiation dosimetry has enormous applications in radiotherapy. The absolute dosimetry is used to standardize the radiation beams for delivering the known dose under certain specific setup conditions. The reference dosimetry is performed to verify the beam calibrations periodically. The relative dosimetry is performed in several ways to check the accurate dose delivery. This may be performed using a single detector, a detector array or a high resolution radiographic or radiochromic film dosimeter. The patient treatment plans are verified to check the accuracy of various parameters in the complex treatments like IMRT in a process called patient specific quality assurance (PSQA) [30].

The dosimetry system must possess at least one physical property characterizing the quantity under observation. Other desirable characteristics should also be satisfied by the dosimeter for better results and intended use. There are a variety of dosimetry systems currently being used in various applications in radiotherapy. The air-vented ion chambers are the most used instrument for reference and relative dosimetry. A class of dosimeters ranging from ion chambers, radiographic and radio chromic films, solid-state detectors, diamond dosimeters, chemical dosimeters like Fricke and its derivatives, optical fibres, TLDs, and optically stimulated luminescent dosimeters (OSLDs) are employed in certain specific applications in dosimetry of therapeutic radiations [29,37].

1.4.1 Requirements of a dosimetry system

The dosimetry systems in radiotherapy applications are expected to give radiation response accurately at a point as well as in planar and three-dimensional measurements. The ideal dosimeters are characterized by good accuracy, precision, and linearity. The response of such a dosimeter shouldn't be dose rate and energy dependence. In case of multiple dependencies, it becomes very difficult to standardize the response of the dosimeter and hence establish the calibrations. An ideal dosimeter is expected to have a

high spatial resolution especially in dosimetry applications involving small fields and high dose gradients. IAEA and other researchers [29,32] have defined certain properties of an ideal dosimeter as described below:

1. Sensitivity
2. Accuracy and precision
3. Linearity
4. Dose rate dependence
5. Energy dependence
6. Directional dependence
7. Spatial resolution and physical size
8. Readout convenience
9. The convenience of use
10. Cost-effectiveness

These parameters are explained in some detail in the context of the proposed chlorophyll dosimeter.

1. **Sensitivity:** Sensitivity is the measure of output per unit absorbed dose by the detector. It is the measure of the minimum amount of energy detected by the dosimeter. The sensitivity determines the lower limit on detection of radiation dose or energy. It is dependent on the detector area, several molecules of the active substance in the dosimeter, and any shielding material. The noise is a determining factor for sensitivity, as the inherent or readout noise can greatly affect the sensitivity of the dosimeter.

Another parameter that is of special interest concerning sensitivity is the detector **response**. The response is the relationship between the deposited amount of the physical quantity (I) in the medium and the output (M) generated in the detector in the form of voltage, current, or changes in absorbance, etc.

2. **Accuracy and precision:** These parameters are measures of uncertainty associated with the measurements made with the dosimeter. Precision is specified by the reproducibility of response under similar conditions of measurement. It is determined from the data obtained with frequently repeated measurements under the same setup conditions. High precision is associated with a small standard deviation. The analogy of precision is an archer hitting the target. The true value is the centre of the target with maximum points, while the arrow hitting the outer circles increases the error and hence reduced precision.

The accuracy of a dosimetry measurement is the proximity of its expected value to the true value of a measured quantity (I). The results of a measurement cannot be absolutely accurate, and the inaccuracy is characterized by its uncertainty.

3. **Linearity:** The dosimetry system must possess linearity in terms that M should be linearly proportional to I . However, beyond a certain limit, a non-linearity sets in. These properties are dependent on the type of dosimeter and its physical characteristics.
4. **Dose rate dependence:** While measuring the dose at different dose rates, the dosimetry system must give the same response. The quantity, M/I should remain constant at different dose rates. However, this condition is not met all the time and some dosimeters may possess a dose rate dependence. Such dependence may be useful in resolving different dose rates when such measurements are necessary to carry out. However, to correct the dependence of the response on the dose rate, appropriate correction factors can be incorporated.
5. **Energy dependence:** The response of a dosimetry system is generally a function of radiation beam quality (energy). Since, the calibrations are performed at a certain specific beam quality and used over a wide range, in such cases, the dosimetry system requires correction factors.
6. **Directional dependence:** In an ideal dosimeter, M should not vary with the angle of incidence of the radiation. The directional dependence is a property of the design of the dosimeter. Many dosimeters possess directional dependence due to their

construction, physical size, and energy of incident radiation. The dosimetry system in radiotherapy is generally used in the same geometry as calibration and hence the direction dependence if any is already corrected for. However, in some cases where measurements are made at different beam angles, either correction factors are used, or changes are made in the geometry of the dosimetry system.

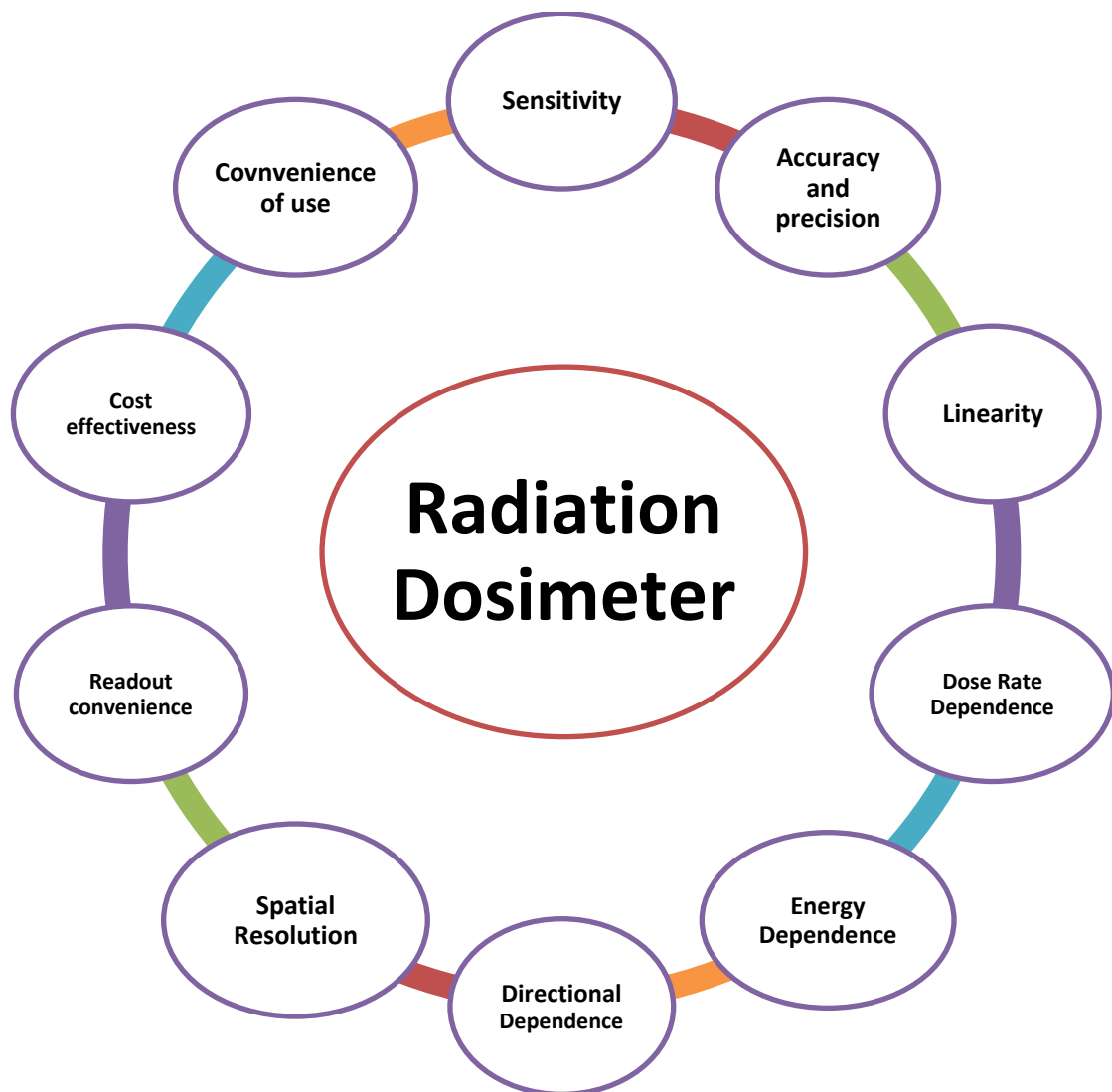


Figure 1.5 The properties of an ideal radiation dosimeter.

7. **Spatial resolution and physical size:** The radiation dose is a point quantity, and the dosimeter should allow the determination of the dose from a very small volume. The position of the point where the dose is determined should be well defined in a reference coordinate system.
8. **Readout convenience:** The readout system plays a significant role in determining the properties of a dosimetry system. The direct reading dosimetry systems are generally more convenient than the passive systems.
9. **Convenience of use:** The dosimeters must be used in several applications to attain similar results. The system should possess the property of reusabilities like ion chambers and solid-state detectors. However, some dosimeters like chemical detectors are single-use and need replacement. In such cases, the easy availability, stability, and rapid response of the readout system are desired.
10. **Cost-effectiveness:** The radiation dosimeters used in radiotherapy are of special importance as these are used to determine the radiation dose delivered to cancer patients. Along with the general requirements of an ideal dosimeter, these dosimeters should also be cost-effective as the overall cost pose a burden on the cost of treatment for the patient.

All these properties cannot be possessed by any single dosimeter. However, any system used for dosimetry, depending upon its application must possess some of these ideal properties. For example, the dosimeters used to discriminate different energies must respond differently to different energies, while those designed to measure in low doses must have sensitivity high enough that they can measure even the lowest doses under consideration.

1.5 Review of Literature

Several chemical compounds have been investigated in past for their application in radiation therapy dosimetry [38–40]. Fricke is one of the most used chemical dosimeters and is also adopted as a secondary standard dosimeter in secondary calibration laboratories [34]. Its derivatives have also been investigated by researchers to obtain better results and

enhance its response [41]. The dosimeter solution contains hydrated ferrous ammonium sulphate. The quantification of the radiation chemical yield (G) of Fe^{3+} against the radiation absorbed dose is taken as the measure of radiation effect. The concentration of Fe^{3+} is measured using UV-Vis spectrophotometry by application of the Beer-Lambert law [42]. The Fricke dosimeter has a stable response, and the process of its manufacturing is easy, robust, and cost-effective. However, this solution can only be used for point dosimetry. The ingredients of Fricke are toxic, biohazardous in nature and capable of producing issues of environmental pollution.

To overcome the limitations of measuring point dose only by the chemical dosimeters, 2D films have been developed for dosimetry. Radiographic films are one of the most basic film dosimeters. These are based on the ionization of silver halides as per the Gurney Mott theory. The dose characterization is proportional to the degree of blackening of the irradiated films [43]. Another type of film namely the radio-chromic film is now extensively being used in radiation therapy due to its wide and stable response and easy handling. These films contain leuco dyes, that polymerize on irradiation followed by a change in colour. The degree of change in colour is a measure of radiation dose in these films. These films can be handled in ambient light [43][44].

More recently, radio-chromic films have been developed based on a polystyrene base containing a fluran leuco dye, perovskite, scintillator and a photoacid generator for visualization of x-ray dose [45]. The device has been tested in a range of doses above 15 Gy and shown a good response. These films have been based on the change in colour of the film from yellow to black with increasing radiation dose. Investigators have studied the radio-chromic films for low-dose diagnostic x-ray dosimetry in the dose ranges of a few mGy [46] and up to 5 Gy [47]. The film dosimeters have shown the dose-response acceptable in clinical applications and shown stable response.

The development of new radiation detectors is a continuous process. The advances in radiation delivery techniques have increased the treatment effectiveness and increased the complexity of the delivery. This demands the adoption of a strict and sophisticated

dosimetry procedure to be adopted to check the accuracy of complex treatments. There is a growing demand for sophisticated detectors specific to delivery techniques. Radiation dosimetry, hence, has become very complicated and demands very accurate, reliable, and customised tools [48]. For example, a fibre optics detector can't be used for the dosimetry of large fields as it is designed for small fields and a 0.6cc farmer chamber is not suitable for small field dosimetry [49]. However, a great advantage in terms of the Monte Carlo (MC) simulation technique is that this technique can be used to calculate the desired quantities and study the radiation effects at any setup conditions that may not be experimentally possible. The MC simulations offer the highest level of accuracy and best possible congruence with the physical and radiological properties of the materials and radiation sources. MC simulations can be used for the characterization of any new dosimeters against an ideal measurement condition [50].

The dosimetry systems viz. air-filled ionization chambers, TLDs, OSLDs, diode detectors, optical fibre detectors, and chemical dosimeters like the 2D films and 3D gel dosimeters have their respective uses in different aspects of radiation dosimetry. The ionization chambers are versatile dosimeters having applications in most radiotherapy dosimetry. The solid-state detectors are mainly used in small field dosimetry, machine quality assurance (QA) and PSQA systems. Similarly, optical fibre detectors and scintillators have applications in small field dosimetry. The films are utilized for small field dosimetry, PSQA and machine QA owing to their high spatial resolution [30].

These dosimeters are mostly manufactured outside India, which hinders their easy availability. In addition to this, an additional cost in terms of various taxes has to be paid by the user which in the end has to be paid by the patient [6,51,52]. The maintenance of these systems is another issue as the lack of authorized service stations forces the customer to send this equipment to their original manufacturer overseas. This process adds the cost to the end-user. Many of the dosimeters demand periodic calibrations, the procedure adding cost to the user. Further, the dosimeters are mostly made up of inorganic materials, posing an issue of environmental hazard at the end of life.

The conventional dosimeters along with their technical shortcomings have cost-related factors and their availability in the country. Hence, such a system is required that can be prepared by medical physicists very easily and cost-effectively. Also, this system must have no additional cost and third-party dependence for its operation and calibrations. In this research, a novel dosimeter has been proposed for radiotherapy dosimetry. This dosimeter shall be based on the naturally abundant chlorophyll molecules. The feasibility of this molecule as a radiation dosimeter in therapeutic x-ray and electron beams shall be studied.

Chlorophyll is one of the most abundant natural compounds which is responsible for the green colour of plants. The name chlorophyll has been derived from Greek *khloros* (green) and *phyllon* (leaf). The name chlorophyll was proposed by Pierre Joseph Pelletier and Joseph Bienaimé Caventou in 1818 [53]. The central Magnesium (Mg^{2+}) atom was discovered in 1906. The chlorophylls are responsible for the green colour of leaves due to their absorbance properties. These are alcohol soluble molecules and can easily be extracted into alcohols. A detailed examination of chlorophylls was carried out by Willstatter and Fischer. Willstatter has been the first one to isolate the chlorophylls [54]. The absorbance and quantification on that basis have been proposed by Mackinney who successfully measured the absorbance coefficients of chlorophylls in a mixture and derived the simultaneous equations for its quantification [55].

Chlorophylls have a tetrapyrrole ring with a central Mg^{2+} and a long chain of hydrophobic phytol in its structure. The chlorophylls exist in six different forms namely chlorophyll a, b, c, d, e, and f. The chlorophyll a (*chl-a*) is a major photosynthetic pigment found in all plants capable of photosynthesis. Chlorophyll b (*chl-b*) is found as an accessory pigment in higher plants and in yellow-green algae. The chlorophylls c, d, e, and f are found in various algae. The chlorophylls in vivo are responsible for various properties of plants. Also, they are predictive of physiological behaviour. The chlorophylls are also used to study the effect of various factors on plant physiology in vivo. The chlorophylls are distinguished by their appearance with *chl-a* appearing bluish-green, *chl-b* bright green, chlorophyll c (*chl-c*) yellowish-green, chlorophyll d (*chl-d*) bright forest green, and

chlorophyll f (*chl-f*) emerald green [56,57]. The differences arise due to the structural differences among these molecules.

The chlorophylls are energy harvesting and transducing molecules in the photosynthesis process. The *chl-a* and *chl-b* molecules are present approximately in 3:1 respectively in the higher vascular plants in the sunny areas [58]. These molecules absorb the energy of light photons from the sun in the blue and red regions of the spectrum and transduce it further in the chain to initiate a light reaction. This process ends up giving glucose and oxygen; both of which are essential components of life on earth. The delocalized π electron clouds and the central magnesium atom of the chlorophylls are responsible for the pattern of radiation absorption. The transitions between the highest occupied π electron orbital and lowest unoccupied π electron orbitals cause the red band. The transitions between the orbital just lower than the highest occupied π electron orbital and the lowest unoccupied π electron orbital cause the absorbance in the blue region [59,60].

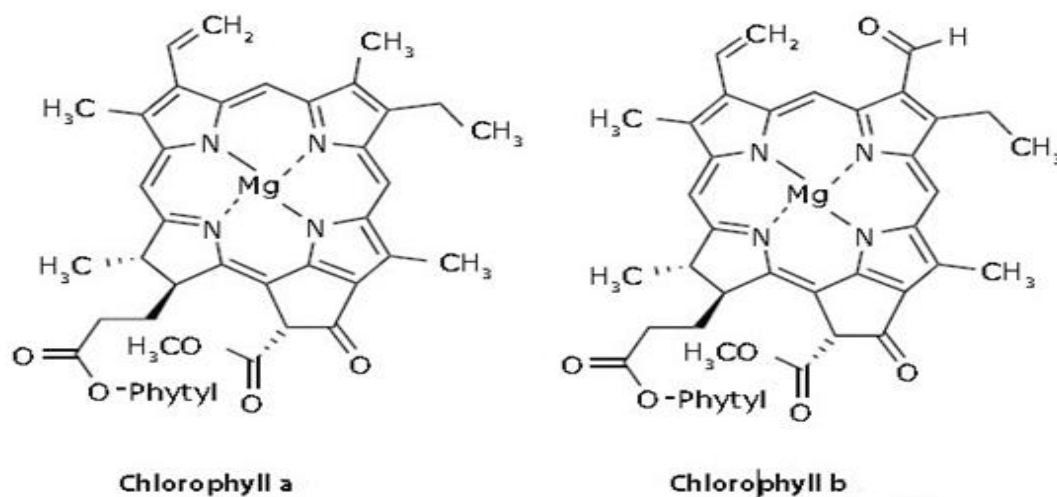


Figure 1.6 Chemical structure of *chl-a* and *chl-b* molecules. (From: <https://www.sigmaaldrich.com>)

Chlorophylls can be easily extracted in non-polar solvents [61,62]. Its response to ionizing radiations motivates the studies of this molecule as a radiation dosimeter. There have been a few attempts to develop a chlorophyll dosimeter in past also. J. Ramirez-Nino [63,64] has studied in detail the effects of UV and gamma radiations on the optical properties of chlorophyll and carotene. They found that the optical absorbance of chlorophyll solution decreased with increasing the dose of gamma radiation. The same author [65] studied the radiation effects on the chlorophyll solution embedded in a SiO₂ gel matrix prepared by sol-gel technique. The authors expected a free radical reaction involving cleavage of C=C and C-H bonds and then a polymerization reaction following the high-dose radiation exposures. They irradiated the matrix in a dose range of 1 cGy – 1000 Gy of gamma radiations followed by optical absorption measurements at 300 – 1000Å and observed a change in the opacity of the spectra. The opacity changes in the solution have been found higher than that in the matrix most probably due to reduced free radicle formation in the matrix. Saturation has been observed in opacity changes after a certain dose of gamma radiation.

Nouh and Abutalib, [66] have studied the effects of UV and gamma rays on chlorophyll and carotene by using an optical absorption readout for its quantification. A study by Abdelrazak et al., [67] has shown the effects of gamma irradiation on some physical properties of chlorophyll-Polymethylene methacrylate (PMMA) copolymer films. In this study, the chlorophyll extracted in ethanol from spinach leaves was cast in PMMA to make films of about 2 mm thickness. The whole setup has been done in a light-tight environment. The addition of chlorophyll to PMMA resulted in an enhancement of the thermal stability of PMMA. The films have been irradiated to a gamma-ray dose range of 20 kGy - 100 kGy followed by readout methods using FTIR, UV-Vis absorption spectroscopy, and galvanometric measurements. They found the sensitivity of these films towards photon radiation doses by observing a decrease in optical absorbance and FTIR transmission intensities with increasing radiation dose.

Hassan et al.,[68] have studied the dosimetric properties of chlorophyll polyvinyl alcohol (PVA) composite films. The authors have extracted chlorophyll from spinach with

90% acetone. Copolymer films have been prepared using a combination of compositions of PVA, chlorophyll and chitosan. The films were irradiated to a gamma dose of 50 - 500 kGy. They have found an optimum response in spectroscopic studies. A linear response has also been observed in a dose range of 1-100 kGy. The fading of this copolymer under the effect of light and oxygen is rapid and hence requires immediate readout.

In the liquid state, the chlorophyll can be utilised as a point dosimeter, however, its composite with polymer as a film will be for planar dose determination. This dosimeter will be beneficial in several applications ranging from industrial radiography, laboratory research and radiotherapy dosimetry. The major advantage of using chlorophyll polymer composites is that chlorophyll is available everywhere unambiguously and can be standardized in terms of dosimetric properties.

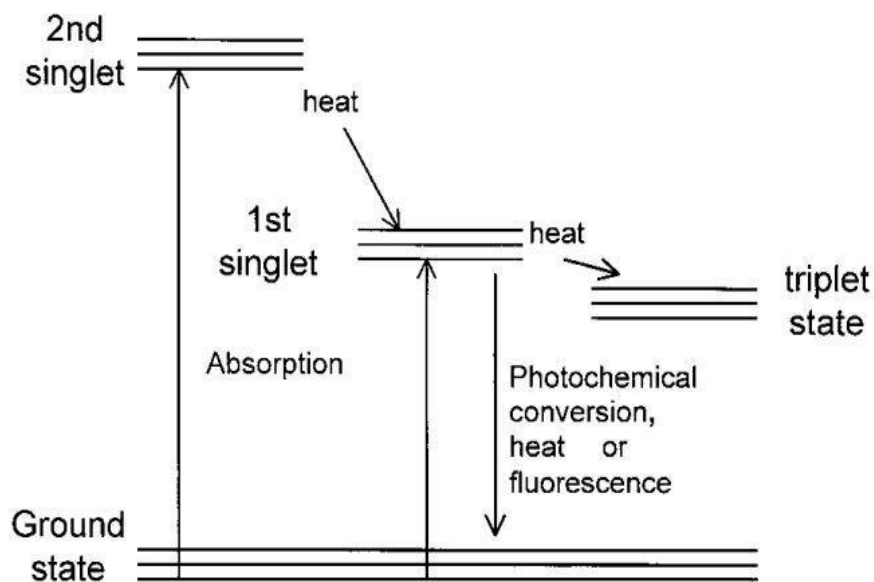


Figure 1.7 Energy level diagram of chlorophyll showing the ground state and first and second singlet excited states. The absorption of light causes an excitation to first and second singlet excited states respectively, and the conversion to the ground state occurs

through the emission of heat or fluorescence radiation in red and blue regions. The third singlet excited state is a long-lived state [69].

Chlorophyll dosimeter will be beneficial in radiotherapy applications due to its global availability and similar nature throughout the plant species. This dosimeter will be an alternative to commercially available, high-cost dosimeters, which are currently in use for radiotherapy dosimetry. This dosimeter will require only a few reagents for preparation and once prepared it can be used in a wide variety of applications ranging from relative dosimetry to in-vivo dosimetry, PSQA and machine quality checks etc. Since the dosimeter will require a single time calibration against the secondary standard detector, which can be performed in-house, so the calibration and maintenance cost will also be negligible. This dosimeter will benefit cancer patient care, providing a low-cost, efficient and viable system for the determination of radiation dose.

The aim of this research is to develop a radiation dosimeter based on chlorophyll as an active substance. A thorough investigation of chlorophyll solution will be done for dosimetric properties in radiation beam under different conditions of energy ranges, dose and dose rates of x-rays and electrons. The composite of chlorophyll with suitable polymers will be prepared to make a physically suitable 2D film dosimeter. This film will be investigated under similar conditions of irradiation as for the chlorophyll solution. The qualitative and quantitative analysis shall be done by UV-Vis spectroscopy, FTIR spectroscopy, flatbed scanning, XRD, SEM and PL spectroscopy.

1.6 Research objectives:

The aim of this research is to develop a chlorophyll-based chemical dosimeter for therapeutic radiations. For this purpose, leaves from *Spinacia oleracea* (Spinach), *Mangifera indica* (Mango), *Pinus* (Pine) and *Abroma augusta* (Hibiscus), will be used. For extraction, Acetone (80%), Ethanol, Dimethyl sulfoxide (DMSO) and N, N dimethyl formamide (DMF) will be tested. The extracted chlorophyll solution will then be tested

under x-rays and electron beams of a medical linear accelerator for its radiation dosimetric behaviour.

A 2D film for planar dose determination has also been synthesized. This film will also be characterized under similar conditions of dose, dose rate and energy ranges of x-rays and electron beams from the medical linear accelerator. Methods for the preparation, storage and handling of these films will be given. For quantification of chlorophyll content in solution and to check the radiation effects on chlorophyll in solution and in the film, different analytical methods viz. UV-Vis spectroscopy, PL spectroscopy, FTIR spectroscopy and XRD and SEM will be analysed. The focus is to develop a cheap and convenient point dosimeter and 2-D dosimeter for radiation beam dosimetry.

The following objectives will be studied in this research:

1. To extract chlorophyll from different plants using different solvents to achieve maximum yield.
2. Study the radiation dosimetric properties of chlorophyll solution in radiation therapy beams.
3. Synthesis and characterization of a chlorophyll-polymer composite.
4. Radiometric analysis of chlorophyll-based composites in a range of energies, dose rates and dose in different radiotherapy beams.
5. Standardize the preparation procedure and storage conditions of chlorophyll solution and chlorophyll based composites.
6. Application of Monte Carlo methods to study the effects of therapeutic x-rays and electron radiations on chlorophyll based dosimeter.

Bibliography

- [1] IAEA Radiation protection | IAEA
- [2] Faiz M. Khan and John P. Gibbons 2014 *Khan's the Physics of Radiation Therapy* (Lippincott Williams and Wilkins, a Wolters Kluwer Health business)
- [3] Bushberg J T, Seibert J A, Leidholdt E M Jr and Boone J M 2011 *The Essentials Physics of Medical Imaging* (LWW)
- [4] IAEA 2015 *Nuclear Medicine Physics: A handbook for teachers and students* (Vienna: IAEA)
- [5] Desai A, Sachdeva S, Parekh T and Desai R 2020 COVID-19 and Cancer: Lessons from a Pooled Meta-Analysis *JCO Global Oncology* 557–9
- [6] Azzani M, Roslani A C and Su T T 2015 The perceived cancer-related financial hardship among patients and their families: a systematic review *Support Care Cancer* **23** 889–98
- [7] Sung H, Ferlay J, Siegel R L, Laversanne M, Soerjomataram I, Jemal A and Bray F 2021 Global Cancer Statistics 2020: GLOBOCAN Estimates of Incidence and Mortality Worldwide for 36 Cancers in 185 Countries *CA: A Cancer Journal for Clinicians* **71** 209–49
- [8] Bray F, Ferlay J, Soerjomataram I, Siegel R L, Torre L A and Jemal A 2018 Global cancer statistics 2018: GLOBOCAN estimates of incidence and mortality worldwide for 36 cancers in 185 countries *CA: A Cancer Journal for Clinicians* **68** 394–424
- [9] Mathur P, Sathishkumar K, Chaturvedi M, Das P, Sudarshan K L, Santhappan S, Nallasamy V, John A, Narasimhan S and Roselind F S 2020 Cancer Statistics, 2020: Report from National Cancer Registry Programme, India *JCO Global Oncology* 1063–75
- [10] Ali I, Wani W A and Saleem K 2011 Cancer Scenario in India with Future Perspectives *Cancer Therapy* **8** 56–70

- [11] Rastogi T, Devesa S, Mangtani P, Mathew A and Cooper N 2008 Cancer incidence rates among South Asians in four geographic regions: India , Singapore , UK and US 147–60
- [12] Jimmy Caudell, Richard C. Miller And Barry Rosenstein 2019 *Radiation Biology Fundamentals of Radiation Oncology: Physical, Biological and Clinical Aspects* vol 1, ed MURSHED HASAN (London: Academic Press) pp 57–87
- [13] Edward C. Halperin, David E. Wazer and Carlos A. Perez 2013 *The Discipline of Radiation Oncology Principles and Practices of Radiation Oncology* vol 1, ed Halperin Edward C., Wazer David E., Perez Carlos A. and Brady Luther W. (Philadelphia: Lippincott Williams & Wilkins) pp 2–60
- [14] National Cancer Institute Treatment for Cancer - NCI
- [15] Loïc Grevillot 2012 *Monte Carlo simulation of active scanning proton therapy system with Gate/Geant4 : Towards a better patient dose quality assurance*
- [16] Gianfaldoni S, Gianfaldoni R, Wollina U, Lotti J, Tchernev G and Lotti T 2017 An Overview on Radiotherapy: From Its History to Its Current Applications in Dermatology *Open Access Macedonian Journal of Medical Sciences* **5** 521
- [17] Joiner Michael and Kogel Albert van der 2009 *Basic Clinical Radiobiology* vol 1 (London: Edward Arnold)
- [18] Halperin E C, Brady L W, Wazer D E and Perez C A 2019 *Perez & Brady's Principles and Practice of Radiation Oncology, Sixth Edition- Halperin, Edward C*, (Philadelphia: Wolters Kluwer)
- [19] Lederman M 1981 The early history of radiotherapy: 1895-1939. *Int J Radiat Oncol Biol Phys* **7** 639–48
- [20] Benedict S H and Goetsch S J 2015 *Stereotactic Radiosurgery and Stereotactic Body Radiation Therapy* (Taylor & Francis Group, LLC)
- [21] Huang R X and Zhou P K 2020 DNA damage response signaling pathways and targets for radiotherapy sensitization in cancer *Signal Transduction and Targeted Therapy* **5** 1–27

- [22] Van Dyk J (Jake) 1999 *The modern technology of radiation oncology : a compendium for medical physicists and radiation oncologists* (Medical Physics Pub)
- [23] Bentzen S M and Joiner M 2009 Fractionation: the linear-quadratic approach *Basic Clinical Radiobiology* 102–19
- [24] IAEA 2010 *Radiation Biology: a handbook for teachers and students* (Vienna: IAEA)
- [25] Mayers S 2011 *Characterisation of gafchromic EBT2 film for use in radiation therapy dosimetry*
- [26] Webb S 1997 *The Physics of Conformal Radiotherapy Advances in Technology IOP Publishing Ltd*
- [27] Almond P R, Biggs P J, Coursey B M, Hanson W F, Huq M S, Nath R and Rogers D W O 1999 AAPM's TG-51 protocol for clinical reference dosimetry of high-energy photon and electron beams *Medical Physics* **26** 1847–70
- [28] INTERNATIONAL ATOMIC ENERGY AGENCY 2000, *Absorbed Dose Determination in External Beam Radiotherapy*, Technical Reports Series No. 398, IAEA, Vienna
- [29] Shani Gad 1991 *Radiation dosimetry: instrumentation and methods* (CRC Press)
- [30] Andreo P, Burns D T, Nahum A E, Seuntjens J and Attix F H 2016 *Fundamentals of Ionizing Radiation Dosimetry (Introduction to Radiological Physics and Radiation Dosimetry, 2nd ed.)* vol 1, ed P Andreo, D T Burns, A E Nahum, J Seuntjens and F H Attix (Wiley-VCH)
- [31] Klein E E, Hanley J, Bayouth J, Simon W, Dresser S, Serago C, Aguirre F, Ma L, Arjomandy B, Liu C, Sandin C and Holmes T 2009 Task Group 142 report: Quality assurance of medical accelerators a... Fang-Fang Yin
- [32] Podgorsak E B 2005 *Radiation Oncology Physics: A Handbook for Teachers and Students* (Vienna)

- [33] Chu R D H, McLaughlin W L, Miller A and Sharpe P H G 2008 Report 80 *JICRU* **8** NP.1-NP
- [34] Slavik Tabakov, Franco Milano P S 2002 Effect of gamma and UV-B / C radiation on plant cells **33** 199–210
- [35] Gibbons J P and Khan F M 2020 *Khan's the physics of radiation therapy* ed J P Gibbons (Wolters Kluwer)
- [36] Attix F H 2007 *Cavity Theory Introduction to Radiological Physics and Radiation Dosimetry* (Weinheim, Germany: Wiley-VCH Verlag GmbH) pp 231–63
- [37] Abdelgawad M H, Soliman Y S, ElGohry M I, Eldib A A, Ma C M C and Desouky O S 2017 Measurements of radiotherapy dosimetric parameters using Fricke gel dosimeter *Biomedical Physics and Engineering Express* **3** 025021
- [38] Adamovics J A and Coakley R J 2019 Chemical dosimeters *Journal of Physics: Conference Series* **1305** 012028
- [39] Liosi G M, Dondi D, vander Griend D A, Lazzaroni S, D'Agostino G and Mariani M 2017 Fricke-gel dosimeter: overview of Xylenol Orange chemical behavior *Radiation Physics and Chemistry* **140** 74–7
- [40] Rabaeh K A, Hammoudeh I M E, Moftah B, Oglat A A, Eyadeh M M, Aldweri F M, Abdel-Qader A J and Devic S 2022 A normoxic acrylic acid polymer gel for dosimetry in radiation therapy *Journal of Radioanalytical and Nuclear Chemistry* **331** 665–72
- [41] Del Lama L S, Petchevist P C D and de Almeida A 2017 Fricke Xylenol Gel characterization at megavoltage radiation energy *Nuclear Instruments and Methods in Physics Research Section B: Beam Interactions with Materials and Atoms* **394** 89–96
- [42] Boag J W, Epp E, Fielden E M and Parker R P. 1982 3. Chemical Dosimetry *Journal of the International Commission on Radiation Units and Measurements* **os18** 14–21
- [43] Engeler C E 1991 *Christensen's Physics of Diagnostic Radiology*. (New Delhi: Wolter Kluwer Lippincot Williams and Wilkins)

- [44] Niroomand-Rad A, Blackwell C R, Coursey B M, Gall K P, Galvin J M, McLaughlin W L, Meigooni A S, Nath R, Rodgers J E and Soares C G 1998 Radiochromic film dosimetry: Recommendations of AAPM Radiation Therapy Committee Task Group 55 *Medical Physics* **25** 2093–115
- [45] Iwata T, Kinashi K, Doan H N, Vo P P, Sakai W and Tsutsumi N 2019 Leuco-Based Composite Resin Dosimeter Film *ACS Omega* **4** 9946–51
- [46] Alashrah S, El-Ghoul Y and Omer M A A 2021 Synthesis and characterization of a new nanocomposite film based on polyvinyl alcohol polymer and nitro blue tetrazolium dye as a low radiation dosimeter in medical diagnostics application *Polymers (Basel)* **13**
- [47] Tamura M, Monzen H, Matsumoto K, Otsuka M and Nishimura Y 2021 Feasibility study of a photochromic diarylethene film as a clinical dosimeter for kV x-rays *Radiation Measurements* **145**
- [48] ICRU 2014 Prescribing, Recording, And Reporting Small Beam SRT *Journal of the International Commission on Radiation Units and Measurements* **14** 31–53
- [49] Sherouse G and Dieterich S 2010 SU-GG-T-330: Experimental Comparison of Six Commercial Dosimetry Diodes for Measurement of Stereotactic Radiosurgery Cone Factors *Medical Physics*
- [50] Andreo P 2018 Monte Carlo simulations in radiotherapy dosimetry *Radiation Oncology* **13** 121
- [51] Mehlis K, Witte J, Surmann B, Kudlich M, Apostolidis L, Walther J, Jäger D, Greiner W and Winkler E C 2020 The patient-level effect of the cost of Cancer care-financial burden in German Cancer patients *BMC Cancer* **20** 1–8
- [52] Altice C K, Banegas M P, Tucker-Seeley R D and Yabroff K R 2017 Financial hardships experienced by cancer survivors: A systematic review *J Natl Cancer Inst* **109**
- [53] Jacobs E E, Vatter A E and Holt A S 1954 Crystalline chlorophyll and bacteriochlorophyll *Archives of Biochemistry and Biophysics* **53** 228–38

- [54] Govindjee 1967 Photosynthesis
- [55] Mackinney G 1941 Absorption of Light by Chlorophyll 315–23
- [56] Jacob-Lopes E, Zepka L Q and Queiroz M I 2017 Chlorophyll ed E Jacob-Lopes, L Q Zepka and M I Queiroz (InTech)
- [57] Queiroz Zepka L, Jacob-Lopes E and Roca M 2019 Catabolism and bioactive properties of chlorophylls *Current Opinion in Food Science* **26** 94–100
- [58] Kumari R, Ashraf S, Bagri G K, Khatik S K, Bagri D K and Bagdi D L 2018 Extraction and estimation of chlorophyll content of seed treated lentil crop using DMSO and acetone *Journal of Pharmacognosy and Phytochemistry* **7** 249–50
- [59] Marquez, U.M.L. & Sinnecker P 2007 Chlorophylls: Properties, Biosynthesis, Degradation and Functions *Food Colorants* ed C Socaciu (CRC Press) pp 39–64
- [60] Kang Y R, Park J, Jung S K and Chang Y H 2018 Synthesis, characterization, and functional properties of chlorophylls, pheophytins, and Zn-pheophytins *Food Chemistry* **245** 943–50
- [61] Porra R J, Thompson W A and Kriedemann P E 1989 Determination of accurate extinction coefficients and simultaneous equations for assaying chlorophylls a and b extracted with four different solvents: verification of the concentration of chlorophyll standards by atomic absorption spectroscopy *Biochimica et Biophysica Acta (BBA) - Bioenergetics* **975** 384–94
- [62] Barnes J D, Balaguer L, Manrique E, Elvira S and Davison A W 1992 *A reappraisal of the use of DMSO for the extraction and determination of chlorophylls a and b in lichens and higher plants. Environmental and Experimental Bota* **32** 85–100
- [63] Ramírez-Niño J, Mendoza D and Castaño V M 1998 A comparative study on the effect of gamma and UV irradiation on the optical properties of chlorophyll and carotene *Radiation Measurements* **29** 195–202
- [64] Ramírez-Niño J, Mendoza D and Castaño V M 1999 Design and fabrication of an optical dosimeter for UV and gamma irradiation *Radiation Measurements* **30** 181–187

- [65] Ramírez-Niño, José & PEREZ-ABAD, C & Rodriguez, Joaquin & GARCIA, J & CASTANO, M & Castaño V 1997 Optical properties of chlorophyll-doped silica gels *Journal of Materials Science: Materials in Electronics* **8**, 1-5
- [66] Nouh S A and Abutalib M M 2011 A comparative study of the effect of gamma and electron beam irradiation on the optical and structural properties of polyurethane *Radiation Effects and Defects in Solids* **166** 165–77
- [67] Abdelrazek E M, el Damrawi G, Elashmawi I S and El-Shahawy A 2010 The influence of γ -irradiation on some physical properties of chlorophyll/PMMA films *Applied Surface Science* **256** 2711–8
- [68] Hassan G M, Sokker H H, Lotfy S and City N 2011 Studying the dosimetric properties of γ -rays irradiated chlorophyll polyvinyl alcohol *Isotope and Radiation Research*
- [69] Chow W S 2014 Photosynthesis : From Natural Towards Artificial *Journal of Biological Physics* **29** 447–59

Chapter 2

Methodology

2.1 Introduction

The current research work is based on the development of the chlorophyll molecule as a radiation dosimeter for measurement of radiation dose delivered by therapeutic x-rays and electron beam radiations. The dosimeter has been prepared from the chlorophyll extracted from plants. The radiometric analysis has been done under the x-rays and electron beam radiation from a medical linac. A detailed methodology has been established for this work. The process of making a chlorophyll solution includes the selection of plant and solvent and a suitable method of chlorophyll extraction. A detailed process for the preparation of chlorophyll polymer films has been given and the characterization of these films has been performed. The radiometric analysis of the chlorophyll solution and the copolymer films has been presented.

A Monte Carlo simulation technique has also been applied for the determination of the correction factors for non-water equivalence of the vessel wall, volume averaging, and non-water equivalence of the dosimeter material (chlorophyll). The chlorophylls are present in several different forms as has been elaborated in chapter 1. These chlorophylls are commonly found in higher vascular plants. In the present study, the *chl-a* molecule has been studied for its radiation dosimetric properties. The detailed process of preparation of radiation dosimeter has been presented in the following sections:

2.2 Extraction of chlorophylls

chlorophyll extraction has been a very wide subject and several processes have been studied for chlorophyll extraction from different plant species. In the present study, based on the selected plant species and available resources, solvent extraction techniques have been employed for chlorophyll extraction. These techniques require conventionally used lab reagents and follow a very simple methodology and reduce the financial burden too. The first objective of the present study was to determine the optimal combination of plants

and solvents which yield maximum chlorophyll content to carry out the process further. The consideration has been given to its consistency and availability throughout the year.

2.2.1 Selection and preparation of leaves

The process of leaf selection has been based on a well-defined methodology [1]. Four plants namely *Mangifera Indica* (mango), *Hibiscus*, *Pinus* (pine), and *Spinacia Oleracea* (spinach) have been selected based on their availability and diversity. The leaves have been selected considering the amount of sunlight it receives, location in the plant, and age of the leaves. The selected plants were all dioicous except mango, which is monoicous. These plants were easily available in this region and rich sources of *chl-a* and *chl-b*. The plants from a sunny environment have been selected. Relatively young leaves of the plants have been selected from the central part of the plants. The leaves of the nearly the same size from one single plant of each mentioned species have been obtained.

The selected leaves have been washed under running tap water to remove dust and other external factors present on their surface. The leaves have been dried with paper wipes and kept in aluminium foil at 4°C until required for chlorophyll extraction. The leaves have been cut into small pieces of almost equal size and processed for chlorophyll extraction as per the methods described in the proceeding sections.

2.2.2 Selection of chemicals

The chlorophyll molecule is non-polar and hydrophobic in nature and needs very less or nearly non-polar solvent for its extraction from the thylakoid membrane of the leaves. Less polar solvents like acetone, Dimethyl sulfoxide (DMSO), N, N Dimethylformamide (DMF), ethanol, methanol, and petroleum ether, etc. have been widely used for the extraction of these pigments. This observation has been considered for the selection of the solvents.

Four organic solvents viz. acetone, DMSO, DMF, and ethanol have been selected. Ethanol is a polar protic solvent while the other three are polar aprotic solvents. Acetone has been diluted by v/v addition of 20% water to obtain acetone (80%). The ethanol has the highest polarity followed by acetone, DMSO and DMF respectively. The CaCO₃ has

been used to neutralize the acidity of acetone and DMF and hence to prevent the acid-induced degradation of the chlorophylls in the solution [2]. All the chemicals have been obtained from Loba Chemicals, Chennai, India. The reverse osmosis (RO) treated water with total dissolved solids less than 3 ppm has been obtained from the local laboratory.

2.2.3 Extraction in acetone (80%) and DMF

The extraction of chlorophyll in acetone (80%) and DMF has been carried out by following the technique of Porra et al., [3]. 100 mg of leaf pieces with 10 mg of CaCO₃ have been ground in a mortar pestle grinder with dropwise addition of the solvent (acetone / DMF). The grinder has been immersed in a dish containing ice to prevent thermal degradation during extraction. The slurry has been obtained and filtered through Whatman number 1 filter paper; the residue is then discarded. The total volume of the solution has been made to 10 ml by adding the solvent. The filtrate thus obtained has been centrifuged under temperature-controlled conditions at 4 °C at 5000 rpm. The samples obtained have been stored at 4 °C in the darkness until analysed.

2.2.4 Extraction in DMSO

The chlorophyll extraction in DMSO has been carried out by following the strategy of Barnes et al., [4]. 100 mg of leaf pieces have been immersed in 10 ml DMSO and kept in an oven maintained at 65 °C for variable time till full discolouration of the leaves has been obtained. The full decolourization has been obtained within 1 h for hibiscus and spinach while it took around 3 hr for mango and pine leaves. The solution has been filtered through Whatman number 1 filter paper. The solution has been kept at room temperature considering the freezing point of DMSO, in the dark until analysed.

2.2.5 Extraction in ethanol

In ethanol, chlorophyll extraction has been done by following the methodology of Ritchie et al., [5]. 100 mg of leaf pieces have been immersed in ethanol and kept at normal room temperature until the full discolouration of the leaves has achieved. The solution has been filtered through Whatman number 1 filter paper and stored at 4 °C until required for analysis. The time for full decolourization has varied from 1 h to 4 h depending on leaf

thickness and hardness. The concentrations of *chl-a* and *chl-b* have been determined by the equations given by respective research groups.



Figure 2.1 The process of chlorophyll extraction from the leaves.

2.2.6 Sample analysis

2.2.6.1 UV-Vis spectrophotometry

Ultraviolet-Visible (UV-Vis) absorption spectroscopy has been the technique used for qualitative and quantitative analysis of chemical species. The process involves the

excitation of the bound electrons of the chemical entity and the wavelength absorption maxima peak can be correlated with the presence of any functional group. The electronic transitions may involve the π , σ and n electrons, depending upon the type of chemical species. The analytical range of wavelength lies in the region between 150 – 1000 nm in different techniques of UV-Vis absorption spectroscopy. It has numerous applications in chemical analysis both quantitatively as well as qualitatively.

In the present study, the extracts have been analysed by UV-Vis spectrophotometry using Shimadzu 1800 spectrophotometer (Shimadzu corp., Kyoto, Japan). The scanning range of 400 – 750 nm with 0.5 nm pitch has been set on the instrument. The data have been analysed in UV Probe software (v 4.2; Shimadzu corp., Kyoto, Japan). The equations given by different researchers have been used for the determination of chlorophyll contents in these solvents (Table 3.1). Analysis has been performed to obtain an optimum pair of plant and solvent that yield maximum chlorophyll content and shows consistent results.



Figure 2.2 The UV 1800 UV-Vis spectrophotometer used in this study.

The data of chlorophyll concentrations has been tested for two-way analysis of variance (ANOVA) for the null hypothesis that there is no statistically significant difference between the combinations of plant species and solvents for chlorophyll extraction. Also, the absorption spectra of chlorophyll extracts have been analysed and interpreted so that the absorption pattern can be used as a base to determine any radiation-induced changes in the chlorophyll solution.

Table 2.1 The equations used to determine the chlorophyll concentrations in-vitro.

Solvent	Equation (concentrations/ $\mu\text{g/ml}$)	Reference
Acetone (80%)	Chl-a = 12.25 A (663.6) - 2.55 A(646.6) Chl-b = 20.31 A (646.6) - 4.91 A (663.6) Chl-tot = 17.76 A (646.6) + 7.34 A (663.6)	Porra et al., (1989) [3]
DMF	Chl-a = 12.0 A (663.8) - 3.11 A (646.8) Chl-b = 20.78 A (646.8) - 4.88 A (663.8) Chl-tot = 17.67 A (646.8) + 7.12 A (663.8)	Porra et al., (1989) [3]
DMSO	Chl-a = 14.85A(664.9) - 5.14 A (648.2) Chl-b = 25.8 A (648.2) - 7.36 A (664.9) Chl-tot = 7.49 A (664.9) + 20.34 A (648.2)	Barnes et al., (1992) [4]
Ethanol	Chl-a = 13.70 A (665) - 5.76 A (649) Chl-b = 25.8 A (649) - 7.60 A (665) Chl-tot = Ca + Cb	Ritchie et al., (2006) [6]

* A = Absorbance at respective wavelengths given in the brackets.

2.2.6.2 FTIR spectroscopy

The Fourier transformation infra-red (FTIR) spectroscopy is a characterization technique used to determine the presence of various functional groups present in the sample. The technique has been used for qualitative as well as quantitative analysis of various chemical samples. The IR radiations are directed at the samples that produce atomic vibrations of molecule group-specific wavelengths of the IR spectra. The transmitted radiation is detected by an interferometer as a function of time. This data is then fed to the computer. The Fourier transform is applied to this data to transform it from the time domain to the frequency domain. The transformed data is plotted as a spectrum of

absorbance or transmittance versus wavenumber and shows peaks corresponding to the functional groups present in the sample under examination.

The characterization in FTIR is done in the range of wavelengths from 0.78 to 100 μm or 12800 to 10 cm^{-1} wave number. However, the most useful range is between 4000 and 600 cm^{-1} . IR spectroscopy is used for elucidation of compounds and quantification analysis. The IR is only possible in the species where a difference in energy due to the vibrational and rotational states is present allowing IR radiation absorption. The IR absorption causes vibrations in specific molecular bonds, this absorbed energy is consumed and hence missing from the spectra and gives the corresponding peaks.



Figure 2.3 The Shimadzu 8400 S FTIR spectrometer used in this study.

The FTIR spectroscopy of samples obtained from the optimum pair of plant and solvent has been performed in the present study. Shimadzu 8400S FTIR spectrometer (Shimadzu corp., Kyoto, Japan) has been used in this study. The liquid samples have been analysed against air reference in a range of wavenumbers from 4000 cm^{-1} to 600 cm^{-1} .

2.3 Preparation of polymer films

2.3.1 Selection of polymer

The selection of the polymer has been based on its density, cost, preparation procedure, miscibility with chlorophyll acetone (80%) solution and oxygen barrier properties. Polyvinyl alcohol (PVA) is nearly equivalent to human tissues, less expansive and miscible with acetone. Hence, it has been selected for the preparation of the copolymer composite with chlorophyll. It is a synthetic chain polymer of cross-linked carbons. It is water-soluble in nature having the chemical formula $[\text{CH}_2\text{CH}(\text{OH})]_n$. Polymerization of polyvinyl acetate forms this polymer, which is followed by partial hydrolysis of the ester in the presence of an alkaline catalyst. It is colourless and odourless in nature.

In the present study, the PVA has been obtained from Loba Chemicals, Chennai, India. A white crystalline powder is obtained with a degree of polymerization of 1700-1800 and viscosity of 25-32 cps. The polymer has a density of 1.19 g/cm^3 .

2.3.2 Preparation of chlorophyll polymer composite

The polymer solution has been prepared in RO-treated deionized water. 200 ml water has been heated up to $60 \text{ }^\circ\text{C}$ in a glass beaker on a heating plate. 50 mg of the PVA powder has been added slowly with continuous stirring on a magnetic stirrer to avoid the formation of lumps. The temperature during the stirring has been set in a range from 93 to $97 \text{ }^\circ\text{C}$ for about 5 h until it became clear.

The solution has been allowed to cool to room temperature. 10 ml $1 \text{ nmol chl-}a$ solution has been added to 10 ml of the polymer solution and stirred continuously at the room temperature. The stirring has been performed to prepare a homogenous mixture. The casting method with freezing and thawing cycles has been employed to prepare the composite films. The technique has been reported to produce films of optimal quality and strength [7]. 10 ml volume of the mixture has been poured into glass dishes of equal diameter. In this way the thickness of the films has been regulated. The plates have been placed on a uniformly levelled flat surface to allow uniform distribution and settlement of the solution.

Several cycles of freezing at -15°C and thawing at room temperature (20°C) have been applied to form the composite. The composites have been kept in a refrigerator in absolute darkness for freezing. The thawing has also been performed in absolute darkness at room temperature. In this way, the effect of light has been controlled.

2.3.3 Characterization of the copolymer films

Along with the UV-Vis and FTIR spectroscopy, the following methods have been applied for the characterization of the copolymer films.

2.3.3.1 Flatbed scanning

The flatbed scanner is a simple office scanner containing a source of white light, a reflection plate covering the scanner bed. The flatbed scanning is based on the principle of measurement of the transmitted light. A light source is used to flash the sample and the reflected light is directed through an arrangement of mirrors to a lens. This lens splits the light into three components. These components are further detected by a charged coupling device (CCD). The CCDs convert the light signal into electrical charges. The electrical charges corresponding to each colour component are further processed to obtain the final image. This technique is applicable for two-dimensional samples e.g., thin films such as radiographic and radio-chromic films used in radiology and radiotherapy [3,8].

In the present study, an EPSON 12000XL flatbed scanner has been used. It is an A3 flatbed colour scanner. It has a resolution of 6400 dpi and a colour depth of 16 bits per pixel. The scanner has a colour CCD line sensor to detect the light and convert it to an electrical signal. The scans of the *chl-PVA* films have been acquired at 240 dpi resolution in reflection mode. The images have been processed in the ImageJ software (National Institute of Health, USA), which is open-source software for various types of image analysis. Enhance Local Contrast filter has been applied over the central region of the interest of the image. The RGB analysis has been performed over this region. The RGB data has been used to determine the luminescence and grayscale values.



Figure 2.4 The EPSON 12000XL flatbed scanner used in this study.

2.3.3.2. Photoluminescence (PL) spectroscopy

PL spectroscopy has widely been used to determine the absorption and emission behaviour of chemical compounds. The PL spectroscopy consists of the measurement of emission and absorption (excitation) spectra of any sample. The basic principle of PL is photon stimulated emission of other photons from any matter. The process is a non-destructive and non-contact method of characterization. In this method, the molecule is excited from its ground state (E_0) to the excitation states E_1 , E_2 etc. E_1 further consists of several vibrational and rotational energy states. The transition from higher vibrational energy states to the E_1 is non-radiative, while the deexcitation from E_1 to E_0 is radiative, emitting energy corresponding to the fluorescence energy of the molecule.

The excitation spectrum is recorded for any fixed wavelength corresponding to the maximum emission intensity in the emission spectra. The spectrum is recorded over a range of excitation wavelengths. It shows that at the excitation peak, the emission maxima have maximum intensity. On the other hand, the emission spectrum is recorded over a range of emission wavelengths keeping the excitation wavelength fixed at the value yielding the highest emission.

In the present study, the modifications in photoluminescent properties of PVA films with chlorophyll solution have been studied. Perkins Elmer LS55 (Xe source) luminescence spectrophotometer (PerkinElmer, Inc., USA) has been utilized in the present study. The emission spectra have been acquired in the range of 400 – 800 nm at an excitation wavelength of 320 nm. The excitation spectra have been recorded over a range of 200 – 450 nm for an emission wavelength of 550 nm.

2.3.3.3. X-ray diffraction (XRD) spectroscopy for crystallographic study

XRD is one of the most employed characterization techniques for studying the crystallinity of the samples. It is employed for several different forms of samples. The x-rays in the range 0.1 – 2.5 Å are employed in XRD. These x-rays undergo coherent interaction with the matter. The technique is based on the principle of constructive interference of monochromatic x-ray after interaction with the crystalline samples. The coherent scattering of the x-rays diffracted from the sample is recorded for structural analysis. In this technique, for the desired diffraction of the x-rays, it is required that the size of the object is in the range of the wavelength of the x-rays. The technique is based on Bragg's law for the determination of the crystalline properties of the sample.

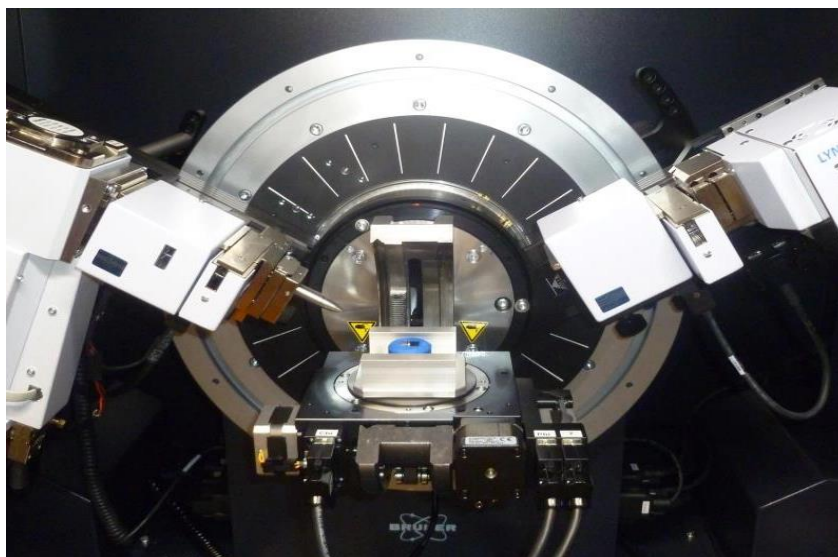


Figure 2.5 The Bruker x-ray diffractometer utilised for XRD analysis of the samples.

In the present study, the Bruker XR diffractometer (Bruker UK limited, UK) has been used to determine the crystalline properties of the *chl-PVA* composite films. The films have been exposed to the monochromatic x-ray of 1.5406 Å wavelength from the Cu K α 1 filter. The diffraction data have been obtained in a range of 2θ from 10° to 80°.

2.3.3.4. Scanning electron microscopy (SEM) for morphological study

The SEM works on the principle of electron interactions, scattering and backscattering of the electrons on the surface of the samples. After interaction of the primary electron beam, the secondary electrons, diffracted electrons, and backscattered electrons are produced. These electrons are utilised for the visualisation of the samples under investigation. The secondary electrons are used for image formation and detection of morphology and topography, while the backscattered electrons are useful in producing contrast in the composition of elements in the sample. It is a destructive method of sample analysis.



Figure 2.6 The JOEL SEM equipment utilised for sample analysis.

In the present study the SE microscopy of the *chl-PVA* films has been performed using a JEOL FESE microscope (JEOL USA). The energy dispersive x-ray spectrometry (EDX) has been performed for elemental analysis for all the sample on this instrument. The samples have been gold coated before spectroscopic analysis.

2.4 Radiometric analysis

2.4.1 Dose calculation system

Monaco treatment planning system (TPS) (Elekta AB, Stockholm, Sweden; Version 5.11) has been used for calculation of radiation dose for the setup utilized for irradiation. The radiation dosimetry for all the x-ray beams has been performed at 95 cm SSD, 5 cm depth for a 10×10 cm² field size. The computed tomography (CT) scan images of the slab phantom (PTW dosimetry, GmbH, Germany) have been acquired on Optima 580 W CT simulator (Wipro GE Healthcare, USA). The phantom has a slot for placement of the chlorophyll dosimeter ampules. The CT data has been assigned a CT number to relative electron density (RED) calibration to make the dosimetric calculations more accurate in the regions of inhomogeneity and mediums of density other than water.

The monitor units (MU) corresponding to different doses have been calculated on this phantom in the TPS. The dose calculations have been performed by the Monte Carlo dose calculation algorithm with a standard uncertainty of 0.25 per calculation. The MU obtained have been delivered to the dosimeter on the linac. For electron beams, the dose calculation has been performed at 95 cm SSD, 1.5 cm depth for a 10×10 cm² applicator in the slab phantom.

2.4.2 Radiation delivery system

The radiometric analysis of the chlorophyll solution has been done on VersaHD medical linear accelerator (Elekta AB, Stockholm, Sweden). This linear accelerator (linac) is installed in the department of radiotherapy at Dr Rajendra Prasad Government Medical College Kangra at Tanda, Himachal Pradesh, India. The accelerator is a “C” arm geometry capable of delivering high-energy x-ray and electron radiations. The x-ray energies with

flattened (FF) beams of 6, 10 and 15 MV and the flattening filter-free (FFF) beams of 6 MV and 10 MV are available in this accelerator.

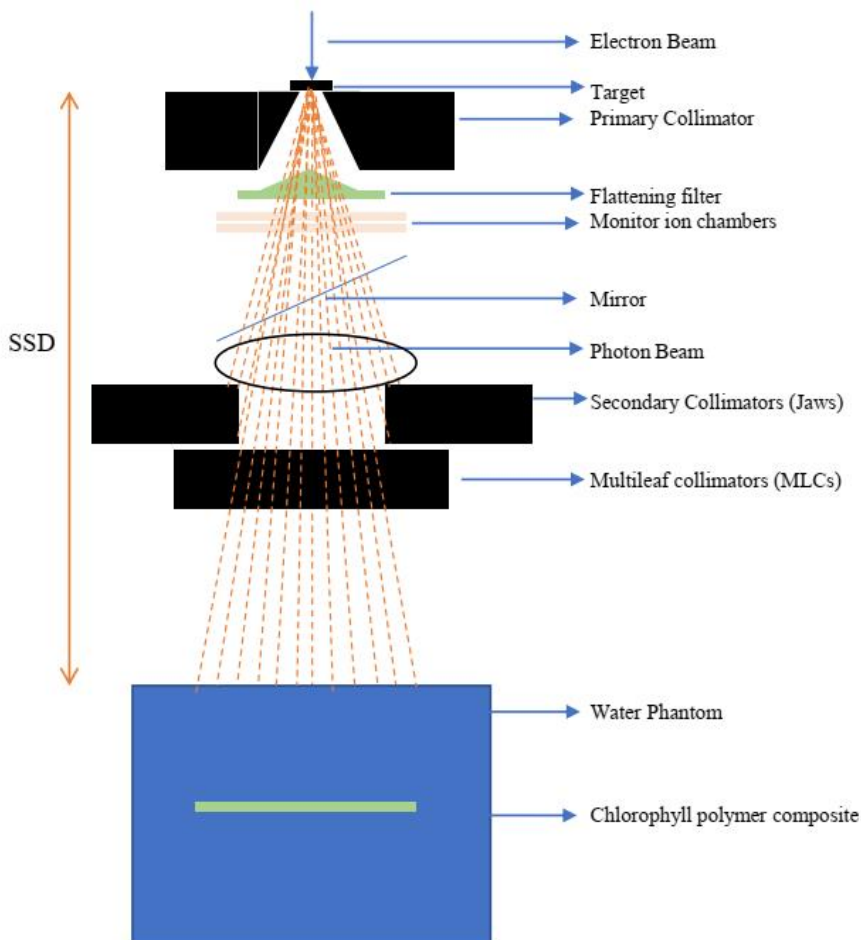


Figure 2.7 Setup conditions for irradiation of chlorophyll and chlorophyll-based polymer composite films dosimeter under x-ray beams from a medical linear accelerator.

The x-ray beams have been calibrated for a dose of 1 cGy for 1 MU at the depth of maximum dose at 100 cm SSD and $10 \times 10 \text{ cm}^2$ field size. For electron beams the calibration has been performed for a dose of 1 cGy for 1 MU at a reference depth calculated as per the protocol of IAEA TRS 398. The maximum dose rate for the flattened beams is 600 cGy/min, for 6 MV FFF is 1400 cGy/min and for 10 MV FFF is 2200 cGy/min. The dose

rates are variable from 50 cGy/min to the maximum values. This linac is also capable of delivering electron radiations of energy 4, 6, 8, 10, 12 and 15 MeV. The maximum dose rate for electron beams is 600 cGy/min.

2.4.3 Irradiation setup

2.4.3.1 X-ray beams

The radiation dosimetry of x-ray beams has been performed in the source to axis distance (SAD) setup. The source to surface distance (SSD) has been kept at 95 cm and a field size of 10×10 cm² was formed by a pair of jaws and multileaf collimators (MLCs). The depth of measurement has been kept at 5 cm. All the measurements have been performed in a solid water slab phantom (figure 2.8 a). The therapeutic range of x-rays from 6 MV to 15 MV at a fixed dose rate of 600 cGy/min have been used for irradiation of the dosimeter in a range of therapeutic doses from 0.06 Gy to 32 Gy. The effect of dose, dose rate and energy on the dose-response has been studied.

2.4.3.2 Electron beams

The radiation dosimetry for electron beams has been performed in an SSD setup in a similar way as for x-ray beams. The field has been defined by an applicator of 10×10 cm². The electron beams have been operated at a 600 cGy/min dose rate to deliver a dose of 2 Gy. The irradiation has been performed at 95 cm SSD and 1.5 cm depth (figure 2.8 b).

2.4.4 Characterization of chlorophyll dosimeter

The properties of ideal dosimeters discussed in chapter 1 have been studied for chlorophyll dosimeters. The setup conditions and irradiation procedure has been discussed in the proceeding sections.

2.4.4.1 Accuracy and precision

The accuracy of a radiation dosimeter is paramount requirement in radiotherapy. The accuracy gives the tendency of the dosimeter to measure the radiation dose as it is. Since there is no standard of the chlorophyll dosimeter yet, therefore the present study has determined the accuracy and precision of this dosimeter. Ten samples have been irradiated to a 2 Gy dose. The precision has been determined by calculating the standard deviation of

the absorbance values. The average value with its standard deviations has been considered as the measure of accuracy and precision for this dosimeter respectively.

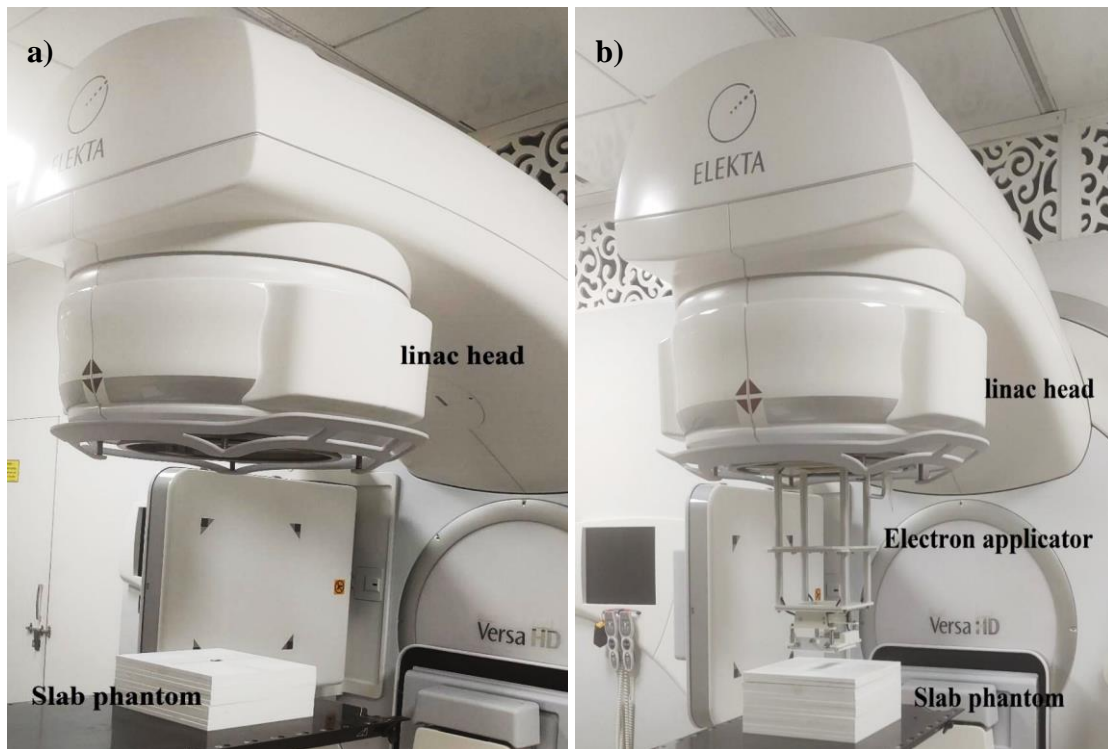


Figure 2.8 The irradiation setup for x-rays (a) and electron beam radiations (b).

2.4.4.2 Dose linearity

The dosimeter has been tested in a range of therapeutic doses from 0.12 Gy to 32 Gy in the geometric progression of number 2. 6 MV x-ray beams have been delivered to study the dose linearity. The dose range has been selected to incorporate the extremities of therapeutic doses. The Pearson correlation coefficient has been determined. The slab phantom has been used and setup conditions are maintained as $10 \times 10 \text{ cm}^2$ field size at 95 cm SSD and 5 cm depth.

2.4.4.3 Dose rate dependence

The dose rate dependence has been checked by measuring the absorbance at 664 nm at different dose rates. 2 Gy dose of 6 MV x-rays at different dose rates from 100 cGy/min to 600 cGy/min has been delivered.

2.4.4.4 Energy dependence

The energy dependence has been checked by measuring the absorbance at 664 nm at different beam qualities of x-ray and electron beams. 2 Gy dose of range of energies available in the linear accelerator has been delivered. The dose rate has been fixed at 600 cGy/min dose rate while checking the energy dependence.

2.5 Monte Carlo simulations

2.5.1 MC simulation of the linac

The Elekta VersaHD linac has been under investigation in the present study. The x-ray target has been made up of Tungsten (90%) and Rhodium (10%) of 0.01 cm thickness fitted on a copper plate. The Agility collimator head of the linac consists of a thick tungsten-made primary collimator, beam flattening filter, mirrors, eighty pairs of multileaf collimators (MLC) and a pair of independently moving jaws. These components have been simulated for a 6 MV x-ray beam. The simulation has been done using the BEAMnrc (National Research Centre, Canada) [9] user code of the electron gamma shower (EGSnrc) toolkit. The simulation has been performed on a Dell Alienware 14 laptop.

2.5.2 MC simulation of the chlorophyll dosimeter

To obtain accurate correction factors by MC, an accurate MC model of the radiation generator i.e., the linac and the radiation dosimeter must be achieved. Similarly, the dosimetry vessel has been modelled in the DOSXYZnrc code. Appropriate densities have been given to different regions of the dosimeter, modelled in a water phantom. The simulations have been performed to determine the correction factors for volume averaging and non-water equivalence of the dosimeter vessel wall and the dosimetry material.

Bibliography

- [1] Porra R J and Scheer H 2019 Towards a more accurate future for chlorophyll a and b determinations: the inaccuracies of Daniel Arnon's assay *Photosynthesis Research* **140** 215–9
- [2] Arnon D I 1949 Copper Enzymes in Isolated Chloroplasts. Polyphenoloxidase In Beta Vulgaris. *Plant Physiology* **24** 1–15
- [3] Porra R J, Thompson W A and Kriedemann P E 1989 Determination of accurate extinction coefficients and simultaneous equations for assaying chlorophylls a and b extracted with four different solvents: verification of the concentration of chlorophyll standards by atomic absorption spectroscopy *Biochimica et Biophysica Acta (BBA) - Bioenergetics* **975** 384–94
- [4] Barnes J D, Balaguer L, Manrique E, Elvira S and Davison A W 1992 A reappraisal of the use of DMSO for the extraction and determination of chlorophylls a and b in lichens and higher plants *Environmental and Experimental Botany* **32** 85–100
- [5] Ritchie R J 2008 Universal chlorophyll equations for estimating chlorophylls a, b, c, and d and total chlorophylls in natural assemblages of photosynthetic organisms using acetone, methanol, or ethanol solvents *Photosynthetica* **46** 115–26
- [6] Ritchie R J 2006 Consistent sets of spectrophotometric chlorophyll equations for acetone, methanol and ethanol solvents *Photosynthesis Research* **89** 27–41
- [7] Surkatti R, El-Naas M H, van Loosdrecht M C M, Al-Naemi F and Onwusogh U 2019 Improvement of PVA gel properties for cell immobilization *Proceedings of the World Congress on Mechanical, Chemical, and Material Engineering* (Avestia Publishing)
- [8] Devic S 2011 Radiochromic film dosimetry: Past, present, and future *Physica Medica* **27** 122–34
- [9] Rogers D W O, Walters B and Kawrakow I 2015 *BEAMnrc Users Manual*

Chapter 3

Analysis of Chlorophyll extraction and storage conditions

3.1 Introduction

The chlorophylls have been extracted from four different plant species using four solvents of varying polarities. A total of sixteen combinations of plant and solvents yielding the chlorophylls have been tested for consistent and higher yields of *chl-a* and *chl-b*. A feasibility study on the seasonal availability of selected plant species and ease of handling of the solvents has also been studied. The chlorophylls have been quantified by UV-Vis absorption spectroscopy. The absorbance spectra have also been studied and compared among different combinations of plant species and solvents. FTIR spectra of the chlorophyll samples from different plants have also been analysed to confirm the presence of pigments in the solution.

Literature [1] shows that chlorophylls are affected by the storage conditions of temperature and light. The thermal degradation and photodegradation have been studied and quantified by measuring the chlorophyll concentrations over a period of one month under different conditions of light and temperature. A comparative analysis of the absorption spectra has also been presented.

3.2 Analysis of chlorophyll extraction

The *chl-a* and *chl-b* has been obtained in the range of 0.574 $\mu\text{g}/\text{mg}$ – 7.338 $\mu\text{g}/\text{mg}$ and 0.122 $\mu\text{g}/\text{mg}$ – 2.915 $\mu\text{g}/\text{mg}$ respectively. The highest amount of *chl-a* was obtained from pine in acetone (80%), while the highest amount of *chl-b* was from mango leaves in ethanol. Table 3.1 gives the detailed results of chlorophyll concentrations while figure 3.1 presents the comparative analysis of chlorophyll extraction.

Table 3.1 Chlorophyll concentrations $\mu\text{g}/\text{mg}$ (of fresh leaves' weight) were obtained in different solvents from selected plants.

		<i>chl-a</i>	<i>chl-b</i>	<i>chl-tot</i>	<i>chl-a/b</i>
Acetone (80 %)	Mango	6.562	2.161	8.723	3.037
	Pine	7.338	2.223	9.561	3.301
	Spinach	5.586	1.707	7.293	3.272
	Hibiscus	3.887	1.567	5.453	2.481
DMSO	Mango	4.157	1.205	5.362	2.777
	Pine	1.513	0.399	1.912	3.794
	Spinach	2.973	1.053	4.026	2.824
	Hibiscus	3.786	1.518	5.304	2.494
Ethanol	Mango	6.162	2.915	9.078	3.460
	Pine	0.724	0.344	1.068	2.837
	Spinach	5.307	2.707	8.014	3.481
	Hibiscus	2.348	0.857	3.205	2.738
DMF	Mango	2.663	0.751	3.414	3.546
	Pine	3.819	1.040	4.860	3.672
	Spinach	2.957	1.160	4.117	2.550
	Hibiscus	0.574	0.122	0.696	3.105

The *chl-a* content from mango and spinach in acetone (80%) and ethanol and that in DMSO and DMF respectively was comparable. The *chl-a* from hibiscus leaves in acetone (80%) and DMSO were comparable while the same from spinach was in similar ranges in DMSO and DMF. Also, a significantly similar amount of *chl-b* was obtained from pine and mango in acetone (80%) while that in ethanol from mango and spinach was also in similar ranges.

The *chl-a/b* ratio has been obtained in the range of 2.481 – 3.794, with the highest value for pine in DMSO and the lowest for hibiscus in acetone (80%). Fig. 3.2 gives the variations of the *chl-a/b* ratio with solvent polarity. There was no clear trend of *chl-a/b* variations with solvent polarity. Table 3.1 gives the *chl-a/b* values for the extractions obtained in this study. It can be deduced that the *chl-a/b* ratio is highest for pine in all solvents except in ethanol and lowest for hibiscus in all solvents except in DMF showing that plants grown under similar natural conditions can have variable chlorophyll fractions.

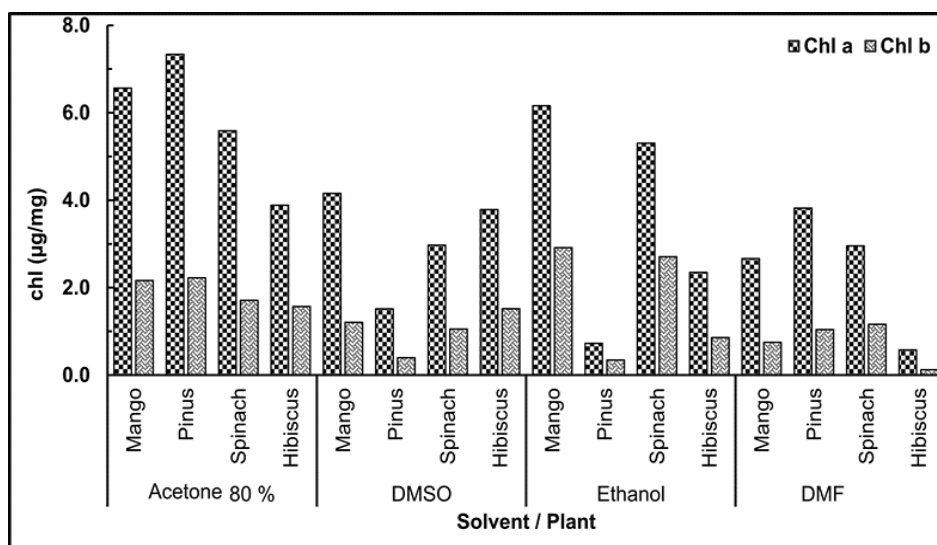


Figure 3.1 The comparative analysis of the chlorophyll extraction from different plants in different solvents.

3.2.1 Spectrum Parameters

The UV-Vis absorbance spectra of all the tested combinations have been obtained and analysed. Irrespective of the plant species and the solvent, all the spectra show some common features and characteristics of the mixture of pigments in the solution. The spectra show absorption beaks in the blue and red regions around 434 nm and 664 nm respectively. These peaks are the result of the delocalised π electron system in the chlorophyll

macrocycle [2]. The red and blue absorption peaks called Q band and B band/Soret band respectively are characteristics of *chl-a*, the absorption of *chl-b* is obtained around 647 nm and 660 nm and gets merged in the spectra due to the higher concentration of *chl-a*. Other than the absorption peaks in the red and blue regions, small absorption in the yellow-green region has also been observed. This absorption indicates the presence of xanthophylls and pheophytins in the solution [3] However, the absorption values have been less than 10 % of the red maxima absorption, indicating the insignificant effect of these pigments on the overall spectra [4,5].

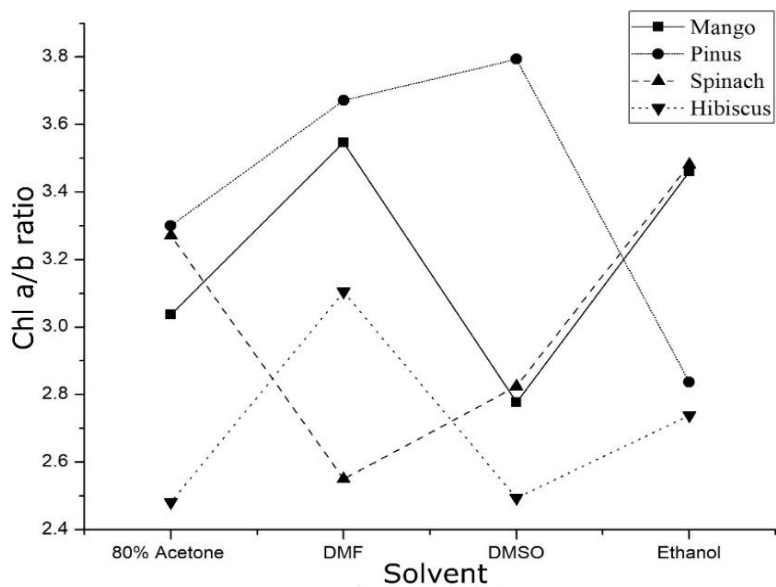


Figure 3.2 Variations of *chl-a/b* ratio with solvent polarity. The connecting lines are for representations only not as a trendline.

The variation of the spread of the absorption peak in the red region with solvent polarity has also been studied. The highest value of full width at half the maxima (FWHM) of the red absorption peak has been obtained in ethanol followed by that in DMSO. In acetone (80%) and DMF, the values are relatively smaller indicating a more sharply peaked

spectrum of the chlorophylls. The FWHM values have been observed to be dependent on the solvent polarity, with a more polar solvent such as ethanol having a broader peak. The findings are supported by similar trends reported by other investigators [4,6].

The ratio of the Soret band to the *Q* band called the soret ratio has also been analysed. The soret ratio has been found in the range of 1.683 – 2.249 in acetone (80%), 1.950 - 2.063 in DMSO, 1.719 - 2.125 in ethanol and 1.734 - 2.047 in DMF. The lowest value was 1.683 for pine in acetone (80%) while the highest was 2.738 for hibiscus in DMSO. However, there has not been any clear trend, the soret ratio has been found to increase with increasing polarity except for higher polarity in ethanol extractants. Table 3.2 shows these variations.

Table 3.2 The solvent and plant-wise values of chlorophyll spectrum characterization by soret ratio and FWHM of the red peak absorption.

Solvent	Soret ratio				FWHM			
	Mango	Pinus	Spinach	Hibiscus	Mango	Pinus	Spinach	Hibiscus
acetone (80%)	1.900	1.683	1.704	2.249	23.85	23.32	23.44	25.27
DMF	2.009	1.734	1.798	2.047	22.10	22.24	24.58	21.03
DMSO	2.063	1.979	1.950	1.978	27.78	27.33	27.31	29.58
ethanol	1.951	1.719	1.904	2.125	29.83	30.01	27.31	29.91

3.2.3 Choice of Solvent and Plant Species

From the ANOVA results we observed that the differences concerning varieties of solvents for extraction of *chl-a* are insignificant at the 5% level as the calculated F-ratio of 2.542 is less than the F-critical value of 3.863. Similarly, a difference for varieties of plants on chlorophyll extraction is also insignificant as the calculated F-ratio of 2.310 is smaller than the F-critical value of 3.863. Similarly, for *chl-b* extraction, the differences for the varieties of solvents are insignificant with the calculated F-ratio of 2.241 less than the F-critical value of 3.863 and for the varieties of plant species, the F-ratio of 1.260 is smaller

than the F-critical value of 3.863 showing insignificant differences. The ANOVA results are presented in table 3.3.

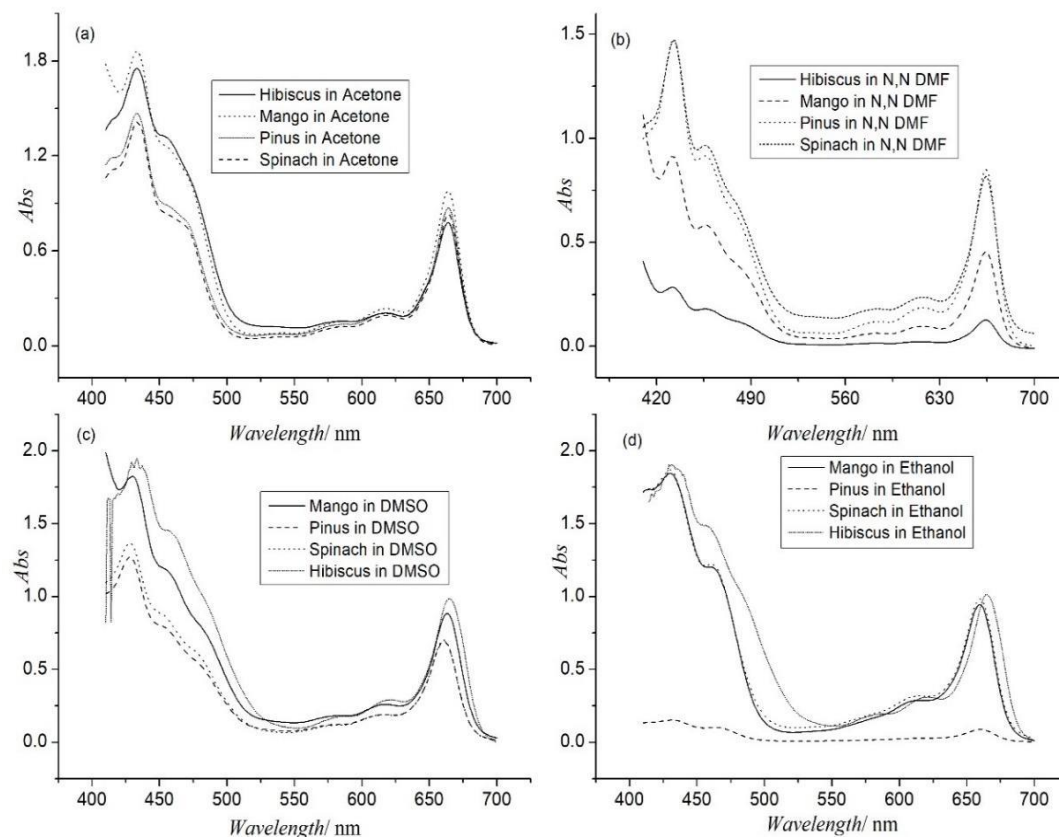


Figure 3.3 The UV-Vis absorption spectra of the chlorophyll solution from different plants in different solvents.

From table 3.1, however, pine has yielded the highest amounts of chlorophylls in acetone (80%), but table 3.3 shows that its results are not consistent throughout the range of solvents used. Also, it is evident that spinach and mango show comparatively similar amounts of chlorophylls in the range of solvents used in this study. The spinach leaves have the minimum variations of chlorophyll contents among the selected plants. To obtain the chlorophylls throughout the year from the same species, the seasonal availability of the leaves must also be ensured.

In this study, higher chlorophyll contents have been obtained in acetone (80%), and mango leaves have yielded consistently higher amounts of chlorophylls in all the solvents. The selection has been based on the availability of mango leaves throughout the year. Hence, the combination of acetone (80%) and mango has been selected for all further experiments of chlorophyll dosimetry.

Table 3.3 (a) ANOVA results comparing selected plant species and solvents for extraction of chlorophylls.

	Plant Species							
	Mango		Pinus		Spinach		Hibiscus	
Pigment	<i>chl-a</i>	<i>chl-b</i>	<i>chl-a</i>	<i>chl-b</i>	<i>chl-a</i>	<i>chl-b</i>	<i>chl-a</i>	<i>chl-b</i>
Sum	19.544	7.033	10.300	4.006	20.235	6.627	10.135	4.064
Average	4.886	1.758	2.575	1.002	5.059	1.657	2.534	1.016
Variance	3.304	0.941	10.221	0.763	2.135	0.573	3.094	0.460
Standard Error	0.909	0.485	1.599	0.437	0.731	0.378	0.880	0.339

Table 3.3 (b) ANOVA results comparing se selected solvents for chlorophyll extraction.

	Solvents							
	acetone (80%)		DMSO		ethanol		DMF	
Pigment	<i>chl-a</i>	<i>chl-b</i>	<i>chl-a</i>	<i>chl-b</i>	<i>chl-a</i>	<i>chl-b</i>	<i>chl-a</i>	<i>chl-b</i>
Sum	23.373	7.658	12.429	4.175	14.542	6.824	9.871	3.073
Average	5.843	1.915	3.107	1.044	3.635	1.706	2.468	0.768
Variance	2.215	0.107	1.374	0.222	6.437	1.680	7.944	0.215
Standard Error	0.744	0.163	0.586	0.236	1.269	0.648	1.409	0.232

3.2.4 Analysis of the FTIR spectra of chlorophyll solution

The FTIR spectra of mango, pine, hibiscus, and spinach leaf extracts in acetone (80%) have been acquired with reference to air blank. The spectra are presented in figure 3.3. several peaks in the functional group and fingerprint regions have been obtained corresponding to different chemical functional groups present in the solution. Figure 3.3 shows the details of the peaks and corresponding functional groups.

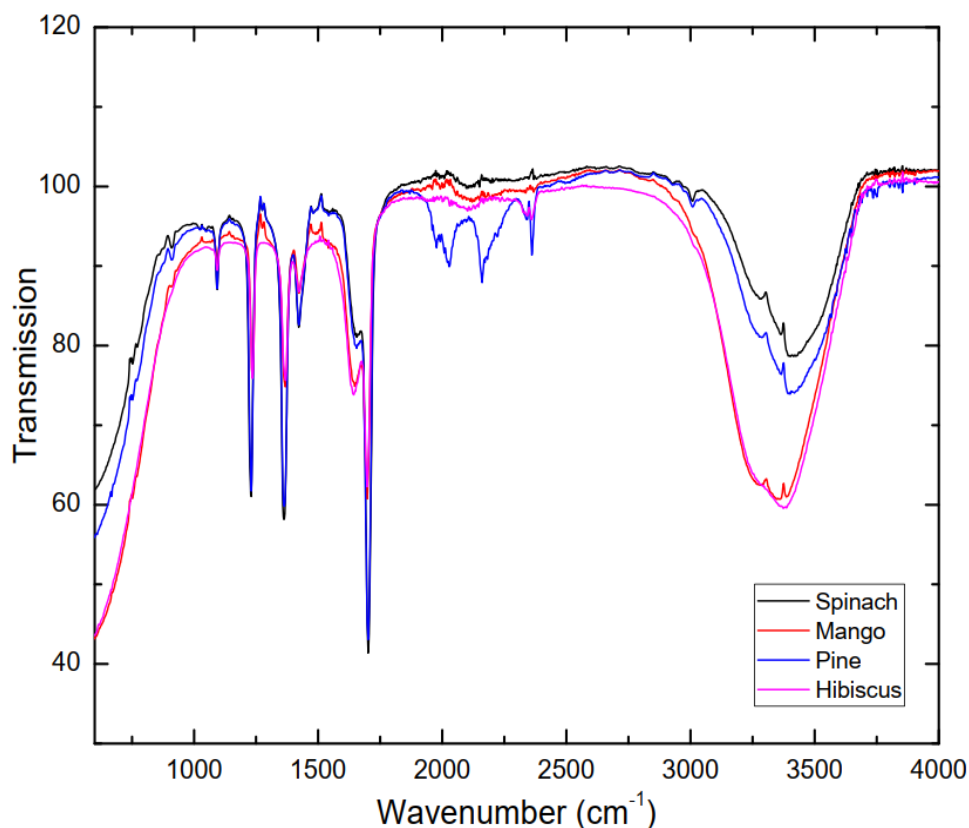


Figure 3.4 The FTIR spectra of leaf extracts obtained from different plant species in acetone (80%).

All these functional groups have been found to be present in the chlorophyll molecules. The presence of these functional groups in the FTIR spectra confirms the

presence of the chlorophylls in the solution obtained from different plant species in acetone (80%). Similar observations have been made by Li et al., [7] in determining the chlorophylls and pheophytins in commercial green tea samples. Similarly, Munawaroh et al., [8] have also observed the same for the chlorophyll extracts from *Spirulina* species. These researchers have identified the functional groups in the single bond, double bond and fingerprint regions that correspond to the same regions as observed in the present study.

In another study by Chang et al., [9] the chlorophyll extracts from wormwood and purple cabbage for the dye-sensitized solar cells have been investigated. The study has shown that different functional groups characterizing the chlorophylls can be observed at 3425 cm^{-1} , 2930 cm^{-1} , 1721 cm^{-1} , 1644 cm^{-1} , 1450 cm^{-1} , 1261 cm^{-1} , and 1045 cm^{-1} corresponding to the same set of functional groups as observed in this study. The FTIR of the samples confirms and characterizes the presence of the chlorophylls obtained from different plants in the solution.

3.3 Analysis of storage conditions

The chlorophylls are highly sensitive to thermal and photodegradation and hence demand careful handling. The determination of correction factors for the effect of light and temperature on chlorophylls is important, otherwise, it may affect the results of radiation-induced chlorophyll degradation. The mango leaves and 80 % acetone have been selected for the analysis of the effects of light and temperature on chlorophyll degradation. This selection has been based on the results of section 3.2.

The chlorophyll has been extracted from mango leaves in acetone (80%) following the method explained in chapter 2. The extracted chlorophyll has been stored in four different conditions i.e. In low temperature, room temperature, dark and ambient light. The room temperature and the low temperature have been set at $20\pm 0.5\text{ }^{\circ}\text{C}$ and $5\pm 0.5\text{ }^{\circ}\text{C}$ respectively. Ambient light condition is obtained by scattered and shady sunlight entering the room from windows. For dark conditions, the chlorophyll solution has been stored in light opaque polypropylene vials.

The chlorophyll concentrations have been analysed for a period of one month. The degradation of the chlorophylls has been found to follow the first-order thermal kinetics [10–12]. The thermal and photo degradation rate constants (k) have been determined using the Arrhenius equations of first-order thermal kinetics [13]. The activation energy (E_a) has also been determined from the Arrhenius plot. The following equations have been used.

$$\frac{dC}{dt} = -kC \quad (3.1)$$

Integrating equation (3.1)

$$\ln\left(\frac{C}{C_o}\right) = -kt \quad (3.2)$$

Here, C is the concentration of the chlorophyll at any time t , C_o is the initial concentration. The degradation rate constant k has been determined from the slope of $\ln(C/C_o)$ vs t graph. The activation energy (E_a) corresponding to the difference of the two temperatures has been determined from the Arrhenius plot. The half-life of the chlorophylls in the chemical reaction has also been determined. The half-life equation for the first-order kinetics has been used as follows:

$$t_{\frac{1}{2}} = \frac{\ln(2)}{k} \quad (3.3)$$

The chlorophylls have been found to degrade under the effect of temperature and light. Such degradations affect the chlorophyll content and produce a change in UV-Vis absorbance spectra. The x-rays are also associated with the production of chlorophyll by-products after irradiation. In such a case, the presence of any temperature and light-induced degradation products may produce errors in the quantification of radiation-induced changes in the chlorophyll dosimeter. Hence, the thermal and photodegradation kinetics of the chlorophylls have been studied to determine an optimal storage condition for the long shelf life of the chlorophyll extracts.

3.3.1 Temporal analysis of chlorophyll contents

The effect of temperature on the degradation of chlorophyll extracts over a storage duration of 720 h (one month) has been investigated. The initial concentrations of *chl-a* and *chl-b* at different storage conditions have been obtained to be within 1.2 % and 0.5 % of the mean values, respectively. The degradation of chlorophylls in samples exposed to ambient light has been found to be higher than those in the dark. Similarly, the samples at ambient temperature have degraded by larger amounts than those stored at low temperature. The chlorophyll concentrations of the samples stored at low temperature in dark have been found most stable over the observation period of 720 h.

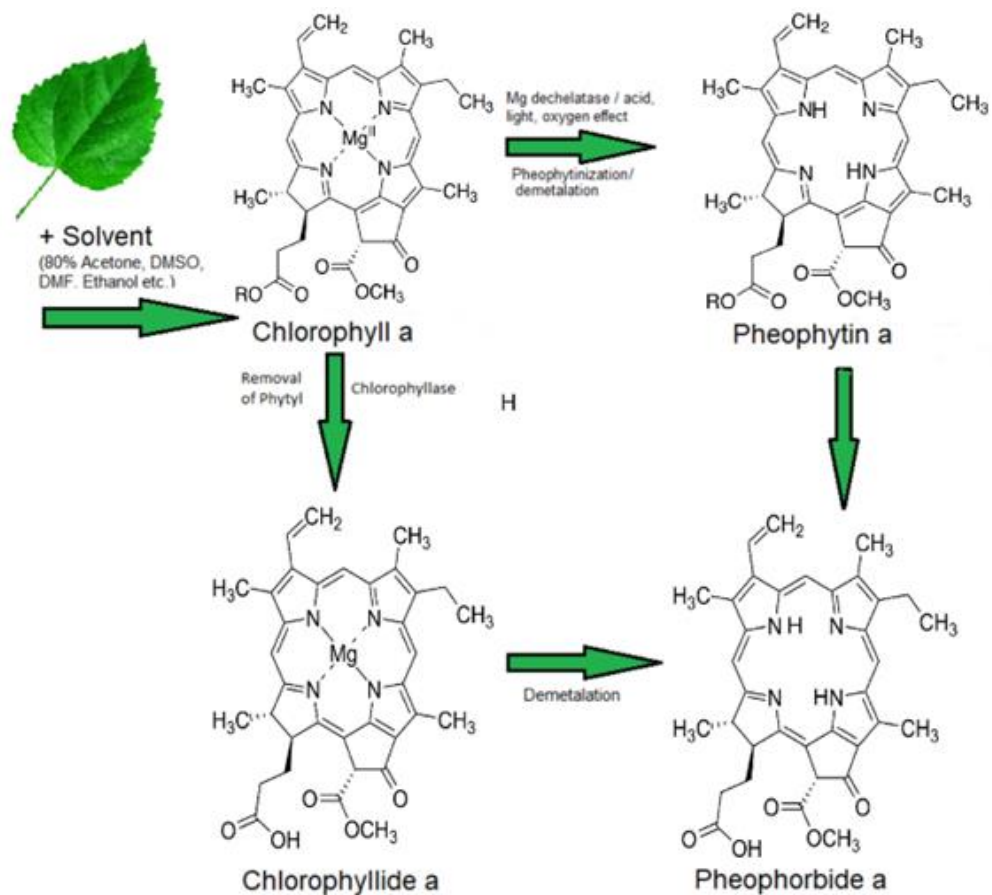


Figure 3.5 The degradation pathways of chlorophyll in vitro under the effect of different biochemical and physical conditions.

The samples stored at ambient temperature in dark were relatively stable as indicated in figure 3.6. The catalytic action of light has been observed in speeding up the degradation reaction manifolds. The spectra have been found to be dependent on the storage conditions with observable spectral changes over the temporal range. The chlorophyll concentrations have been analysed temporally by taking the chlorophyll concentrations obtained after 12 h of extraction as base values. For one month of storage, *chl-a* and *chl-b* contents have been varied maximum by 8% and 0.9% respectively for samples stored at 5 °C in darkness. Maximum degradation has been found to occur at 20 °C in ambient light. For the samples stored at 20 °C in dark, the maximum content degradation has been found to be 20% and 35.8% for *chl-a* and *chl-b* respectively.

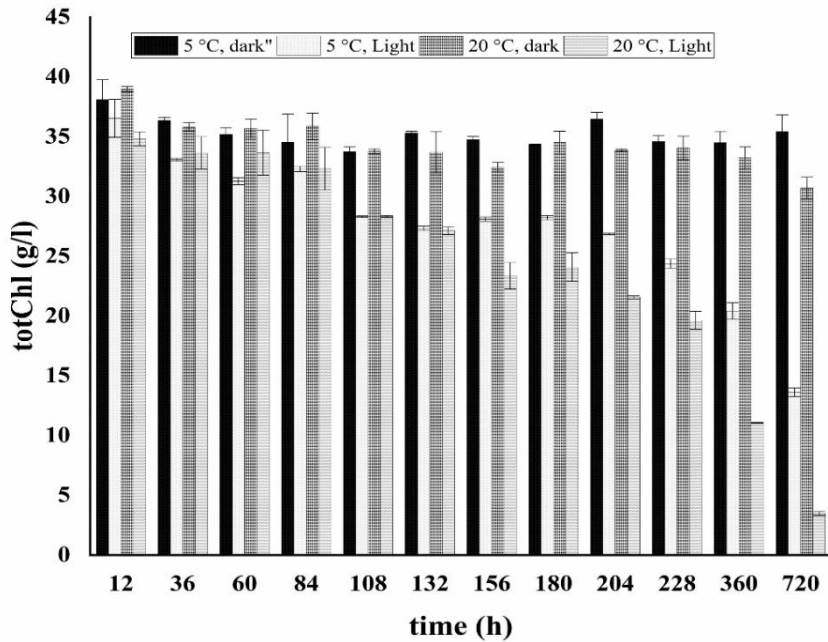


Figure 3.6 The temporal variations of total chlorophyll concentration stored at different conditions of light and temperature.

For samples stored in light, at 5 °C the degradation was rapid, and the maximum content decrease of *chl-a* and *b* was 67.5% and 51.3 % respectively at 720th h. At 20 °C in

light, the degradation was maximum of all the conditions, and the contents decreased by 90 % and 90.4 % respectively for *chl-a* and *chl-b*. It has been observed that light acts as a catalyst by initiating the photodegradation reaction of the chlorophylls that adds to the thermal degradation. A change in colour in both the samples kept in light was observed from initial bright green to olive (intermediate) and brown (at 720 h) as shown in figure 3.7.

3.3.2 Spectral analysis

The spectra of all the samples stored under different conditions have been analysed for differential absorbances at discrete locations of the visible spectrum. The red maximum absorbance peak has been obtained at 664 nm. The spectrum was gradually raising at the lower wavelength side of the spectral peak and rapidly falling to the higher wavelength side. An increase in the blue region around 434 nm has been observed. These two peaks in the red and blue region are attributed to the delocalization of the π electron cloud of the chlorophyll macrocycle. A shift in the peak location from 434 nm to 414 nm has been observed with chlorophyll degradation.

The absorbance at 414 nm increased gradually with time, which indicates the presence of chlorophyll degradation products like pheophytins and chlorophyllides. In the region between 500 – 560 nm, the absorbance was nearly 10 % of the absorbance of major red peak of the spectrum. The absorbance values in this region increased with time and were more than 10 % and a small peak was observed at 535 nm at 720 h. These changes have been attributed to the presence of xanthophyll in the solution. The small peak around 457 nm due to *chl-b*, has been found to shift towards the lower wavelength side after 12 h for the samples stored at 20 °C in light. This change has been associated with the presence of *chl-b* degradation products.

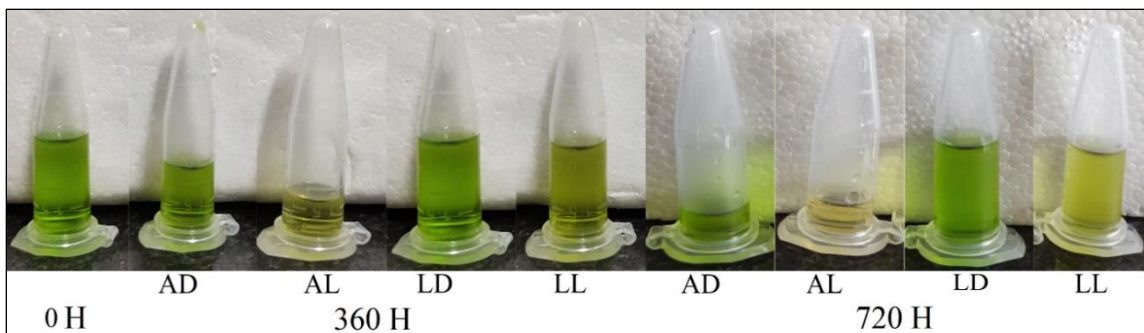


Figure 3.7 Trend of the change in colour of chlorophyll solution over one month time.

The samples stored at 20 °C and light have been found to degrade rapidly. The spectra reflected those changes over the period. The absorbance in the region between 500-560 nm shows the absorbance of less than 10 % up to 36 h, however, a gradual increase in absorbance values in this region of the spectra has been observed after that period as shown in figure 3.8. A change in the sample colours from green to olive was noted after 36 h of storage in the samples stored at 20 °C in light (figure 3.7). The absorbance in the blue region around 414 nm increased very rapidly after 36 h of storage in these samples. At 720 h the blue peaks had completely disappeared, and a region of continuous high absorbance was formed indicating complete degradation of chlorophylls of these samples. This observation has been supported by the change of the colour of the solution from initial green to brown at the end of the study.

The samples stored at 5°C temperature and dark have shown the highest stability. The spectra of these samples after 12 h of preparation have shown absorbance in the blue region around 414 nm and 434 nm which then varied by very small fractions throughout this study. The absorbance peak at 414 nm has low absorbance as compared to that at 434 nm. The absorbance in the green-yellow region was less than 10 % of the red maxima and the peak at 462 nm was stable. The increased absorbance at 414 nm predicts rapid degradation of *chl-a* as compared to *chl-b* due to the presence of the electron-withdrawing CHO group at the C7 location in *chl-b* [14,15].

The samples stored in the darkness in both temperature conditions retained their green colour throughout the experiment. The colour change is attributed to the replacement of the central Mg^{2+} atom with an H atom, also, the colour change follows the first-order kinetics and is found to be dependent on pH values [10,16].

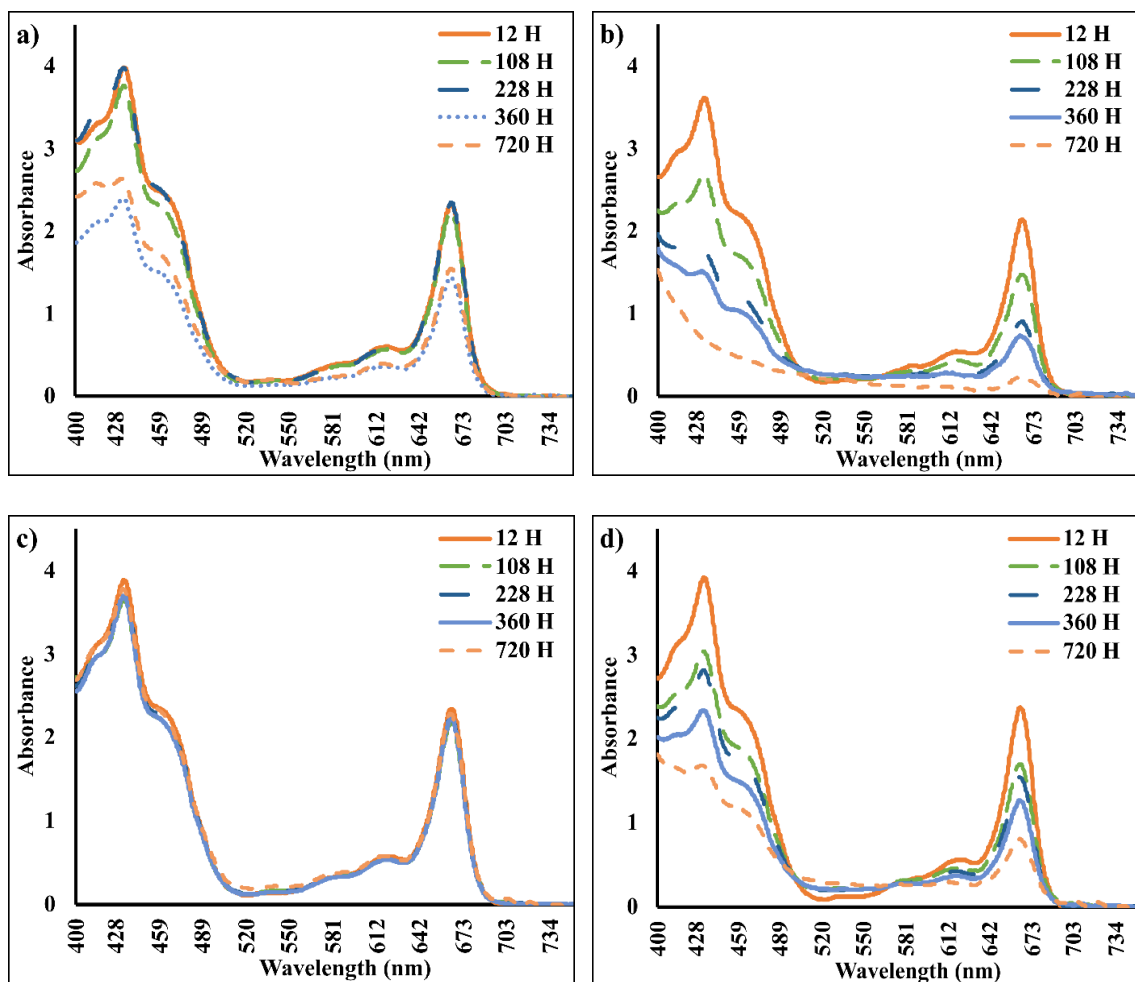


Figure 3.8 Variations observed in the UV-VIS absorbance spectra of chlorophyll samples over a period of one month at 20°C in the dark (a), 20°C in light (b), 5°C in dark (c) and 5°C in light (d) storage conditions.

3.3.3 Kinetic Analysis

The kinetic analysis of chlorophyll samples has been carried out to determine the rate constants, activation energy, temperature quotient and half-lives. The linear regression of equation (3.2) has been performed by using the least square method. The k and coefficient of determination (R^2) have been deduced from the degradation data. The representative curves for *chl-a* and *chl-b* are presented in Figures 3.9 a, b respectively. The plots have shown a good agreement between experimental and model parameters for samples stored in the light as determined by the range of R^2 values between 0.933 and 0.991. However, for the samples stored in dark, the R^2 values were less indicating that the chlorophyll concentrations are affected by very small amounts in the samples stored at 5 °C in darkness. The R^2 values for the samples stored at 20 °C in light were higher than those at 20 °C in dark indicating that the first-order kinetics of the thermal degradation is catalysed by light.

The E_a values for 5 °C to 20 °C temperature gradient in dark and in the presence of ambient light have been determined from the Arrhenius plots. The values of E_a for *chl-a* are 60.242 kJ/mol and 36.174 kJ/mol respectively in the dark and light, the corresponding values for *chl-b* were 110.909 kJ/mol and 53.937 kJ/mol. This indicates that the degradation of *chl-b* requires as much as twice the activation energy of *chl-a* when storage temperature changes from 5 °C to 20 °C in the dark. The results of the present study have shown that the *chl-a* degrades more rapidly than *chl-b* under the effect of temperature and light, but it has also been noted that the effect of light on *chl-b* degradation is relatively higher. [17]

The k values of 6.41×10^{-5} , and 1.55×10^{-3} for *chl-a* at 5 °C in dark and light respectively have been obtained. These values represent a slow reaction rate for the samples stored in dark. A similar effect of light has been observed for *chl-b*. The k value of 2.430×10^{-4} for *chl-a* sample stored at 20 °C in dark and respective value of 1.760×10^{-4} for *chl-b* shows that the degradation of *chl-b* is slower than that of *chl-a*. Table 3.4 presents all the kinetic analysis factors calculated for the dataset. These observations are supported

by the change in the UV-Vis absorbance spectra over the time and changes in sample colour.

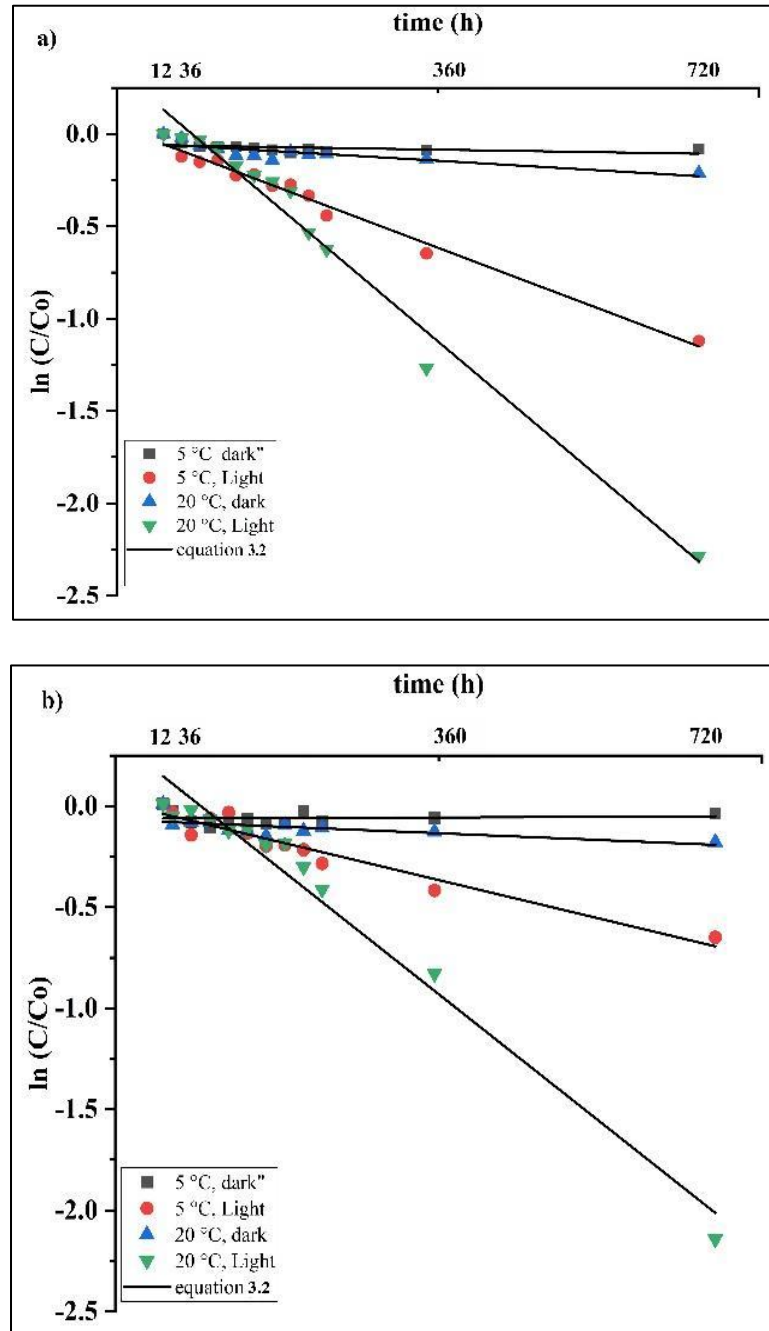


Figure 3.9 Thermal and photodegradation kinetics of *chl-a* and (a), *chl-b* (b) under different storage conditions.

The chemical half-life of these molecules had been determined in the solution stored under different conditions. The highest half-life of 45782.510 h has been obtained for *chl-b* at 5 °C in dark, followed by 10811.840 h for *chl-a* at 5 °C in dark. The lowest half-life values have been observed for the solution stored at 20 °C in light. The values are suggestive of a shelf time of at least six months under the storage condition of 5 °C in dark. The degradation of chlorophylls is affected by temperature and light. Light acts as a reaction catalyst in thermal degradation. The samples stored at ambient temperature in light have shown a maximum variation of Chl concentration over the observation period, followed by samples stored at low temperature in light. The degradation of chlorophyll with temperature follows first-order kinetics and *chl-b* is more stable than *chl-a* towards the thermal changes [13, 18].

Based on the results of kinetic analysis, it has been concluded that the low-temperature storage in dark keeps the chlorophyll concentrations most stable. Other researchers have also suggested low-temperature storage for the longer shelf life of leaf extracts [19]. Researchers [20] have compared different extraction methods and suggested temperature storage of 4 °C for least chlorophyll changes up to 21 days. Similar conditions have also been suggested for the storage of chlorophyll extracts in dimethyl sulfoxide solution [5]. Hence, the present study suggests a storage condition of 5 °C in dark for the chlorophyll extracts and other related products.

Table 3.4 The rate constants k ($\times 10^{-3}$; h^{-1}) and coefficients of determination (R^2) for photo and thermal degradation of chlorophyll in mango leaves, obtained from chemical analysis and plot of $\ln(C/C_0)$ vs observation time are given along with E_a and $t_{1/2}$.

Storage condition	<i>chl-a</i>				<i>chl-b</i>			
	k ($\times 10^{-3}$; h^{-1})	R^2	E_a (kJ/mol)	$t_{1/2}$ (h)	k ($\times 10^{-3}$; h^{-1})	R^2	E_a (kJ/mol)	$t_{1/2}$ (h)
5°C, dark	0.064 ± 0.039	0.205	60.242	10811.84	$0.015 \pm 0.058^*$	0.007	110.909	45782.51
20°C, dark	0.243 ± 0.049	0.707		2852.458	0.176 ± 0.059	0.828		3938.336
5°C, Light	1.550 ± 0.059	0.985	36.174	447.192	1.010 ± 0.085	0.933	53.937	686.284
20°C, Light	3.450 ± 0.156	0.979		200.912	3.33 ± 0.182	0.971		208.152

3.4 Conclusion

The analysis of chlorophyll extraction from four different plants has been achieved in four different solvents. These comprise a combination of polar protic and aprotic solvents. All the solvents have been capable of extracting chlorophylls from the selected plant species. An optimum pair of solvent and plant has been chosen based on the chlorophyll extraction efficiency and the availability of plant species throughout the year. The ANOVA results have shown the statistically insignificant effect of different solvents and plants in yielding *chl-a* and *chl-b*. A combination of mango and acetone (80%) has been found most suitable for the purpose of this study as acetone (80%) is highly efficient in chlorophyll extraction and mango leaves are available throughout the year. The variation of soret ratio and the FWHM of the absorbance peak in red region of the spectra with peak corresponding to 664 nm has been observed to increase with increasing solvent polarity. These parameters have been found to increase with increasing solvent polarity. Further, the optimal storage conditions have been tested for the chlorophyll extracted from mango leaves in acetone (80%). It has been found that storage at the low temperature of 5 °C in absolute darkness is most suitable for stable chlorophylls for up to six months.

Bibliography

- [1] Viera I, Pérez-Gálvez A, Roca M, Viera I, Pérez-Gálvez A and Roca M 2019 Green Natural Colorants *Molecules* **24** 154
- [2] Buscemi G, Vona D, Trotta M, Milano F and Farinola G M 2022 Chlorophylls as Molecular Semiconductors: Introduction and State of Art *Advanced Materials Technologies* **7** 2100245
- [3] Sanja M. Milenković, Jelena B. Zvezdanović, Tatjana D. Anđelković D Z M 2012 The Identification of Chlorophyll and its Derivatives in the Pigment Mixtures: HPLC-Chromatography, Visible and Mass Spectroscopy Studies *Advanced Technologies* **1** 16–24

- [4] Lichtenthaler H K 1987 Chlorophylls Carotenoids *Chlorophylls and Carotenoids: Pigments of Photosynthetic Biomembranes* **148** 350–82
- [5] Barnes J D, Balaguer L, Manrique E, Elvira S and Davison A W 1992 A reappraisal of the use of DMSO for the extraction and determination of chlorophylls a and b in lichens and higher plants *Environmental and Experimental Botany* **32** 85–100
- [6] Lichtenthaler H K and Buschmann C 2001 Extraction of Photosynthetic Tissues: Chlorophylls and Carotenoids *Current Protocols in Food Analytical Chemistry* **1** F4.2.1-F4.2.6
- [7] Li X, Zhou R, Xu K, Xu J, Jin J, Fang H and He Y 2018 Rapid Determination of Chlorophyll and Pheophytin in Green Tea Using Fourier Transform Infrared Spectroscopy *Molecules* **23** 1010
- [8] Munawaroh H S H, Fathur R M, Gumilar G, Aisyah S, Yuliani G, Mudzakir A and Wulandari A P 2019 Characterization and physicochemical properties of chlorophyll extract from *Spirulina* sp. *Journal of Physics: Conference Series* **1280** 022013
- [9] Chang H, Kao M J, Chen T L, Chen C H, Cho K C and Lai X R 2013 Characterization of natural dye extracted from wormwood and purple cabbage for dye-sensitized solar cells *International Journal of Photoenergy*
- [10] Koca N, Karadeniz F and Selen Burdurlu H 2007 Effect of pH on chlorophyll degradation and colour loss in blanched green peas *Food Chemistry* **100** 607–15
- [11] Sonar C R, Rasco B, Tang J and Sablani S S 2019 Natural color pigments: oxidative stability and degradation kinetics during storage in thermally pasteurized vegetable purees *Journal of the Science of Food and Agriculture* **99** 5934–45
- [12] Jinasena M A M, Amarasinghe A D U S, Marasinghe B M W P K and Prashantha M A B 2016 Extraction and degradation of chlorophyll a and b from *Alternanthera sessilis* *J Natl Sci Found* **44** 11–21

- [13] Gaur S, Shivhare U S, Sarkar B C and Ahmed J 2007 Thermal chlorophyll degradation kinetics of mint leaves puree *International Journal of Food Properties* **10** 853–65
- [14] JEN J J and MACKINNEY G 1970 on the Photodecomposition of Chlorophyll in Vitro-ii. Intermediates and Breakdown Products *Photochemistry and Photobiology* **11** 303–8
- [15] Saga Y and Tamiaki H 2012 Demetalation of chlorophyll pigments *Chemistry and Biodiversity* **9** 1659–83
- [16] Weemaes C A, Ooms V, van Loey A M and Hendrickx M E 1999 Kinetics of chlorophyll degradation and color loss in heated broccoli juice *Journal of Agricultural and Food Chemistry* **47** 2404–9
- [17] Lee E, Ahn H and Choe E 2014 Effects of light and lipids on chlorophyll degradation *Food Science and Biotechnology* **23** 1061–5
- [18] Petrović S, Zvezdanović J and Marković D 2017 Chlorophyll degradation in aqueous mediums induced by light and UV-B irradiation: An UHPLC-ESI-MS study *Radiation Physics and Chemistry* **141** 8–16
- [19] Porra R J and Scheer H 2019 Towards a more accurate future for chlorophyll a and b determinations: the inaccuracies of Daniel Arnon's assay *Photosynthesis Research* **140** 215–9
- [20] Lefebvre T, Destandau E and Lesellier E 2020 Evaluation of the extraction and stability of chlorophyll-rich extracts by supercritical fluid chromatography *Analytical and Bioanalytical Chemistry* **412** 7263–73

Chapter 4

Synthesis and characterization of the chlorophyll-PVA composite films

4.1 Introduction

Measurement of the radiation dose in two dimensions requires a planar dosimeter. For this purpose, the film dosimeters have been found efficient detectors with good sensitivity and the highest resolution. The film dosimeters based on inorganic detectors such as Silver Iodide (AgI) and some leuco dyes have been used widely in medical imaging and dosimetry [1]. In the present study, a chlorophyll-based liquid dosimeter has been developed for point dosimetry of the therapeutic x-rays. A free-standing thin film of chlorophyll with PVA (*chl-PVA*) for measuring the radiation dose in a two-dimensional plane has been prepared. The preparation methods employ different conditions of heat, temperature, and humidity. The method for film preparation has been explained in chapter 2. Various characterization techniques have been employed to study the different properties of these films. The presence of chlorophylls, morphology and physical properties of *chl-PVA* composite films have been determined by UV-Vis, PL, flatbed scanning, SEM, and XRD analysis. This chapter presents the characterization of the *chl-PVA* thin films.

4.2 Preparation of composite films

The free-standing thin films of *chl-PVA* have been prepared by the casting technique. The freezing and thawing cycles of 12 hours and 30 minutes respectively have been applied. Freezing at -15 °C and thawing at 20 °C have been performed. The films prepared by this technique have been found to have significant improvement in the mechanical properties of PVA composites [2]. The reproducibility of the preparation procedure has been checked over time by preparing samples at different times using same methodology. These films have been packed in light-tight aluminium foil to prevent any light-induced chemical changes in the film. However, it has been shown by other investigators that the composites of chlorophyll with PVA form a stable product and can

be kept photostable for up to six months [3]. The films have been stored at temperatures less than 5°C in darkness until required for irradiation and analysis. The films have been characterized for the confirmation of preparation and identification of the nanoparticles and functional groups in them. The composite film obtained in this study is shown in figure 4.1 below.

The *chl-PVA* film has been a mixture of *chl-a* and PVA. The density of *chl-a* is 1.079 g/cm³ and the density of PVA is 1.19 g/cm³. Since the amount of *chl-a* in the film is in the range of nmol, hence the effective density of the films is nearly the same as that of PVA. This density value is in the range of most of the human tissue substitutes used in radiation dosimetry applications. The ICRU [4] has proposed the use of a wide range of such substitutes for these applications. It is expected that the radiological properties of the film shall be like that of soft tissues in the therapeutic range of radiations where the major mode of photon interactions is Compton scattering [5].

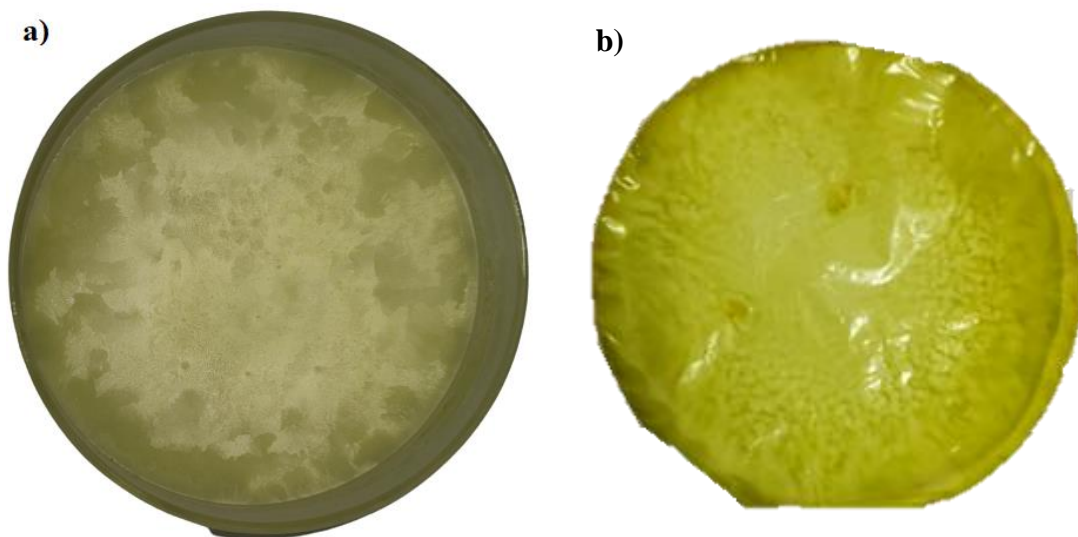


Figure 4.1 The *chl-PVA* composite film during the freeze and thaw cycles (a) and the dried films (b).

4.3 Analysis of UV-Vis absorbance

UV-Vis spectroscopy is a very useful technique as it provides the information of absorbance, transmittance, and reflectance of the polymer materials. The UV-Vis spectrophotometry of the free-standing thin films has been performed on a UV-2600 spectrophotometer (Shimadzu Corporation, Japan). The scanning range has been set from 200 nm to 900 nm at a resolution of 1 nm. PVA due to its distinct physical and optical properties is an important polymer. Researchers have obtained a characteristic absorbance peak at 194 nm in the UV-Vis spectra of the PVA water solution [6]. The peak has been attributed to the carbonyl groups (C=O) of PVA. In the present study, due to technical limitations, the spectra have been acquired from 200 nm to 750 nm. However, the falling tail of the peak can be seen in the UV-Vis absorbance spectrum of PVA film. The absorbance spectra are presented in figure 4.2.

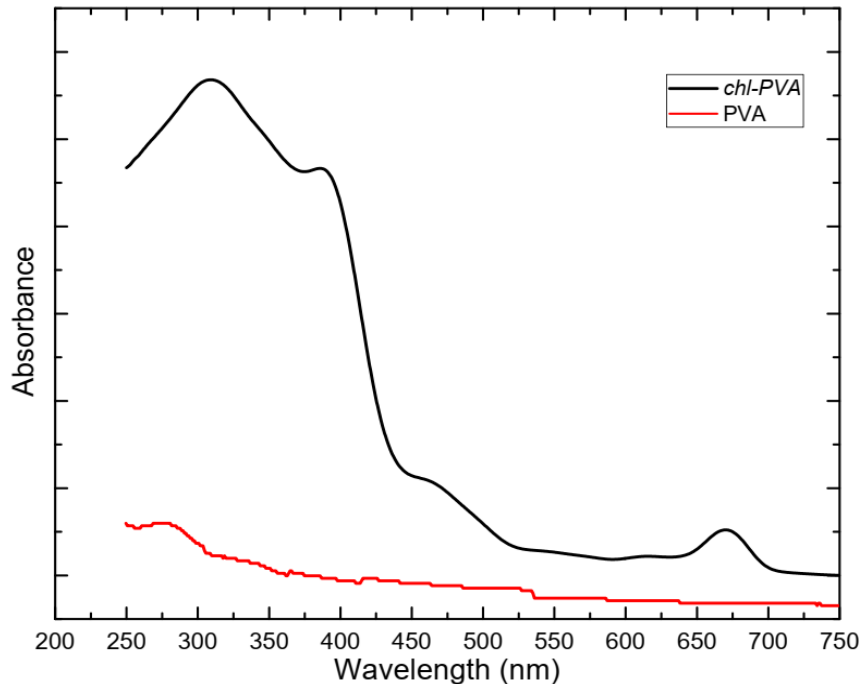


Figure 4.2 The UV-Vis absorption spectra of PVA film and *chl-PVA* composite film.

The absorbance spectra for *chl-PVA* composite films show absorbance in the red region around 670 nm. The spectrum is characterised by the solet peaks in the blue region around 400 nm. The hypsochromic shift of the solet peak and a bathochromic shift of the red absorbance peak have been noted in the spectrum as compared to that in the acetone (80%) solution reported in chapter 3. The peak indicates the presence of the *chl-a* molecules in the films. Similar observations have been reported for chl-PMMA [7], *chl-PVA* [3,8] and PVC-PANI composite films [9]. The presence of distinct absorption bands in the UV-Vis spectra of the composite films confirms the structural modifications in the PVA matrix on the incorporation of chlorophyll. This further insists that the addition of chlorophylls does not result in changing the optical band gap of PVA, rather it creates new inter-band levels. Researchers [10] have studied the chlorophyll-doped ethylene-vinyl alcohol composite films. They observed a pattern like that obtained in the present study. Distinct absorption peaks have been reported for the composite at 615, 540, 510, 460 and 300 nm.

Observations have been made for the *chl-a* chitosan composite films and the effect has been attributed to the presence of two different conformations of *chl-a* in the film [11]. Further, the authors [11] have suggested different interactions amongst *chl-a*, chitosan composite films that involved a change in the coordination of chitosan chains due to the symmetry of the porphyrin ring of *chl-a* in the films [12]. The shift in absorbance maxima at 670 nm can be attributed mainly to two factors; 1. The formation of *chl-PVA* conjugate resulting the close interactions of chlorophyll with PVA and a reduction in chlorophyll chain length [3], 2. The absorbance maxima in the red region are due to π - π^* transitions and shifts to higher wavelengths with increasing solvent polarity [13,14]. As the polarity of PVA prepared in water is higher than that of acetone (80%) hence the shift in peak location is obtained.

Another absorbance peak has been obtained at around 459 nm. This peak has been attributed to the presence of xanthophylls and *chl-b* in the film [13,15]. A small peak has been observed in the green-yellow region of the spectrum around 540 nm. Further, the solet

ratio for the film is in the range of 1.2- 1.5, the values are an indicator of the conversion of the *chl-a* to pheophytin-a in the film system. Similar observations have been reported by Hata et al., [16] for photosynthetic pigment-doped silica-surfactant nanocomposites. The authors further suggested that the pheophytin-a should be used as a photosensitizer due to its higher positive redox potential. Researchers have confirmed such conversions of chlorophylls to pheophytins under the effect of temperature and oxygen [17,18].

4.4 Analysis of FTIR spectra

The FTIR spectroscopy of the samples has been performed to study the formulation of the composite film and to understand the interactions between PVA and chlorophyll. The FTIR has been performed on Shimadzu IR 8400 FTIR spectrometer (Shimadzu corp., Kyoto, Japan). The spectra show peaks at different locations in the single bond, double bond, and fingerprint regions. The spectra have been dominated by the presence of the functional groups occurring in the PVA films. Figure 4.3 presents the FTIR spectra of pure PVA film and *chl-PVA* composite film.

Characteristic peaks have been obtained at 3267 cm^{-1} due to OH stretching confirming the presence of hydroxyl in the sample, 2935 cm^{-1} due to symmetric and asymmetric stretching of C-H bond, 1660 cm^{-1} due to C=O stretching, 1538 cm^{-1} due to stretching amide (NH), 1426 cm^{-1} due to CH_2 bending, 1328 cm^{-1} due to CH_3 bending vibrations, 1077 cm^{-1} is assigned to C=O stretching, 932 cm^{-1} due to CH_2 rocking and 827 due to C-C skeletal vibrations. The change in peak intensities indicates interactions between chlorophyll and PVA matrix. These interactions have caused a shift in the location of the C=O stretching peaks from 1660 cm^{-1} (PVA) to 1645 cm^{-1} (*chl-PVA*) because of the increased conjugation in the composite. The intensity of the peak at 827 cm^{-1} has been found reduced due to the overlapping of the C-C skeletal vibrations.

It is the intensity of the peaks that differentiate the addition of chlorophyll to the PVA film. Researchers [19–21] have confirmed the presence of chlorophylls by characteristics peaks at 1528 cm^{-1} , 1346 cm^{-1} , medium intensity peak at 1326 cm^{-1} and a low-intensity peak at 740 cm^{-1} . Li et al., [22] studied the FTIR of some commercial tea leaf

samples and Chang et al., [23] studied the natural dyes for application in dye-sensitised solar cells and obtained the bands around 1650, 1525, 1458, 1039 cm^{-1} assigned to similar functional groups as obtained in the present study. Broad and low-intensity bands in the region from 2500 to 2100 cm^{-1} have been observed in the present study, the investigators have assigned these bands to C=C stretching [24]. Hassan et al., [8] have evaluated the FTIR of *chl*-PVA composite films. They have assigned the bands at 1684 cm^{-1} to the C=O of the keto group, 1608 cm^{-1} to C=C or C=N and the band at 1632 cm^{-1} to macrocycle mode, indicating the 5 coordination of the central Mg atom. The presence of chlorophylls has been found to affect the spectra with small shifts in the peak locations. [7,25]

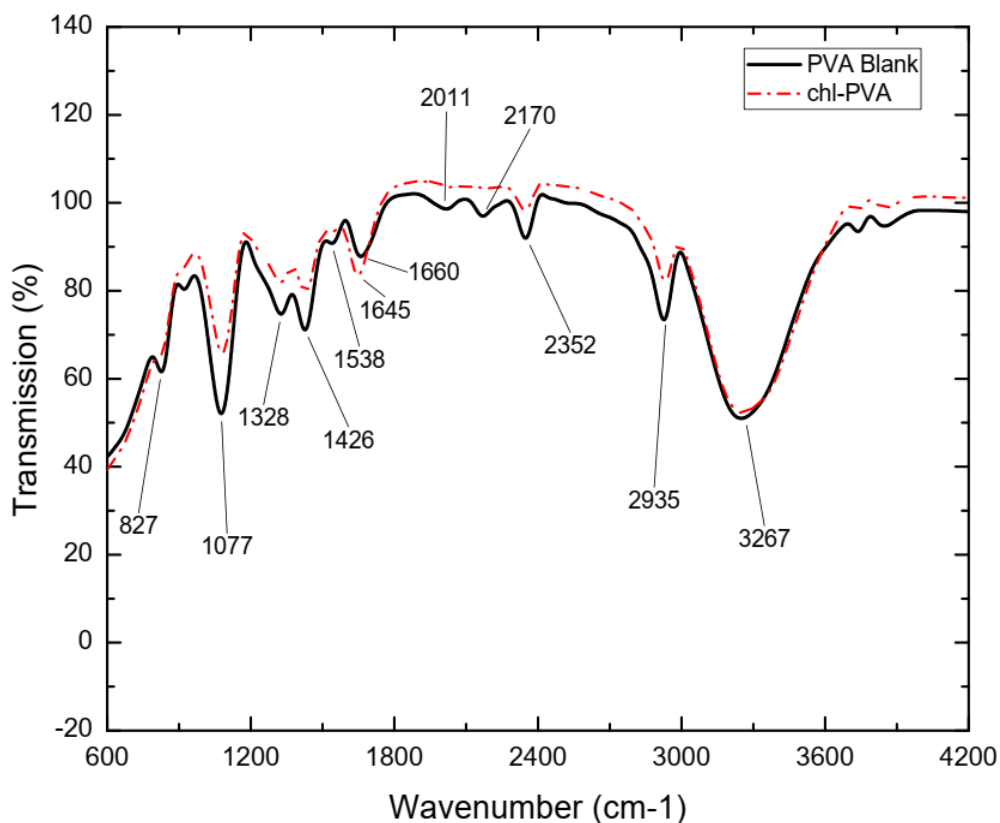


Figure 4.3 The FTIR spectra of pure PVA and chl-PVA composite thin film.

4.5 Analysis of PL spectra

Photoluminescent spectroscopy is the technique used to study the excitation and emission properties of composite films. The PL spectroscopy has been performed using a Perkin Elmer LS55 fluorescence spectrophotometer. Emission and excitation spectra of the composite films have been acquired. The emission spectra have been acquired in the range of wavelengths from 400 nm to 800 nm at an excitation wavelength of 320 nm. The excitation spectra have been acquired in the range of 200 to 450 nm at an emission wavelength of 550 nm. The emission spectra show peaks at 442 nm and 687 nm. In the excitation spectra, three peaks have been observed. The central peak has been at 400 nm while two small peaks at 235 and 266 nm have been observed. The peaks can be attributed to the *chl-a* present in the film. Figure 4.4 shows the photoluminescent (emission and excitation) spectra of *chl-PVA* composite films.

The trends from figure 4.4 indicate that there are strong interactions between chlorophylls and PVA. The addition of chlorophyll to PVA has resulted in the modification in the energy levels of the composite. The interactions resulted in the change in the electronic excitation and emission behaviour of PVA. There has been a shift in the emission maxima towards a higher wavelength as compared to that for pure chlorophyll. The emission peak at 688 nm has been attributed to the optical transitions of the first excitonic state of *chl-a* present in the PVA composite film. Abdelrazek et al., [7] have made similar observations for a chlorophyll PMMA polymer composite film. Soltaninejad et al., [26] have studied the bio composite properties of PVA/ZnO/AgI/chlorophyll nanocomposite films and reported that the addition of chlorophyll to these films resulted in shifting of the absorbance peak and a decrease in the peak intensity.

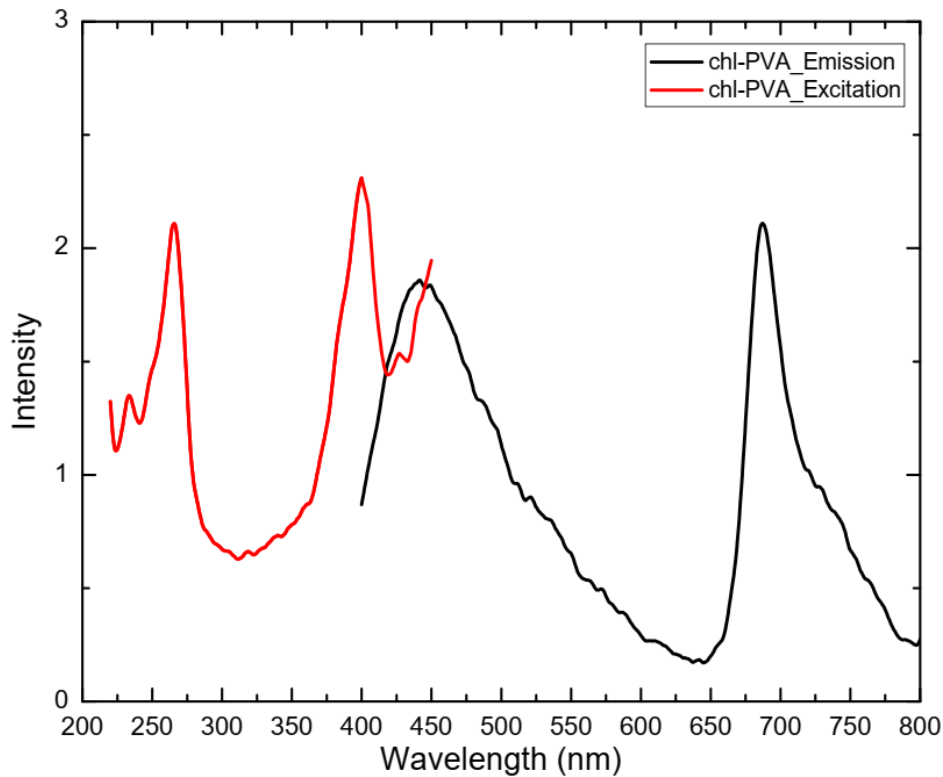


Figure 4.4 The photoluminescence spectrum of chl-PVA thin-film composites.

The researchers have analysed the PL spectra of pure chlorophylls [27]. They observed the emission for *chl-a* and *chl-b* at 670 nm and 650 nm respectively. The excitation maxima have been found at 440 nm and 460 nm respectively for *chl-a* and *chl-b*. However, due to the conjugate formation with PVA the emission and excitation peaks have been found to be shifted from these locations. The excitation maxima have been obtained at 400 nm for *chl-a* in the PVA matrix. Researchers have analysed the PL properties of pure PVA and its doping with some materials. Karthikeyan et al., [28] have observed the absorption and emission spectra of pure PVA and SiO₂ doped PVA composite. They reported a broad emission band from 360 to 480 nm centred at 410 nm for pure PVA. The addition of silica increases the spread of the peak and shifted it toward a higher wavelength side that corresponds to the characteristic peaks of silica. This effect

has been attributed to LUMO-HOMO transitions. In the present study, a similar effect has been observed.

4.6 Flatbed scanning

Flatbed scanning is a conventional technique of reading the radiation-induced colour changes in radio-chromic films. This technique is widely used for dose estimation and further analysis of the images for 2D dose determination. The flatbed scanning has been performed on an EPSON 12000 XL flatbed scanner. The resolution has been set to 256 dpi.

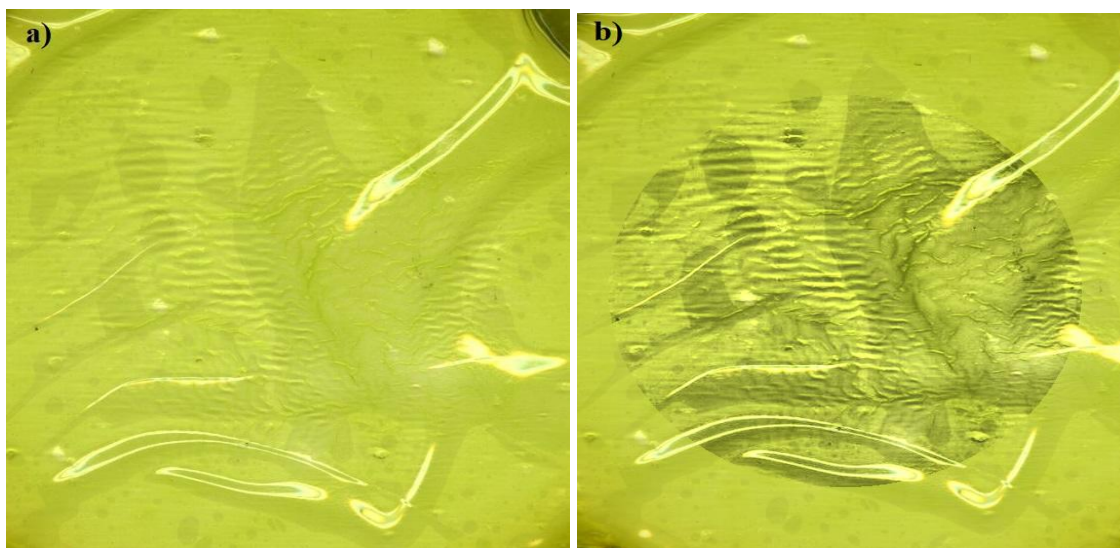


Figure 4.5 The flatbed scanning image of the *chl*-PVA composite film (a), and the region of interest chosen for RGB analysis in ImageJ (b).

The images of the films have been analysed in ImageJ software (NIH, USA). The RGB filter has been utilized to analyse the scanned images. The RGB analysis has been done in the central region of interest of the images. The intensity profiles have also been plotted along the central axis of the film. The RGB analysis shows the content of red, green, and blue colours in the film. The grayscale value of the image has been determined using the RGB values by the average method. Equation (4.1) gives the formula to determine the

image greyscale. Similarly, the RGB values have been used to determine the luminescence of the image using equation (4.2).

$$\text{Greyscale} = (R + G + B) / 3 \quad (4.1)$$

$$\text{luminescence} = 0.299R + 0.587G + 0.114B \quad (4.2)$$

The following RGB values of the *chl-PVA* composite film have been obtained.

Table 4.1 The RGB analysis of the composite film.

	Mean	Minimum	Maximum	Std. Dev
Red	185.0625	180.1072	189.7679	3.066903
Green	198.2119	194.0357	202.2679	2.477134
Blue	63.56456	56.9643	69.4286	3.93333
Grayscale	148.9463	143.7024	153.8214	3.150911
Luminescence	160.6092	156.4143	164.5997	2.511535

The values presented in table show that the film has the highest fraction of green colour followed by red and blue. This is due to the presence of green-coloured pigments i.e., *chl-a* and in the film.

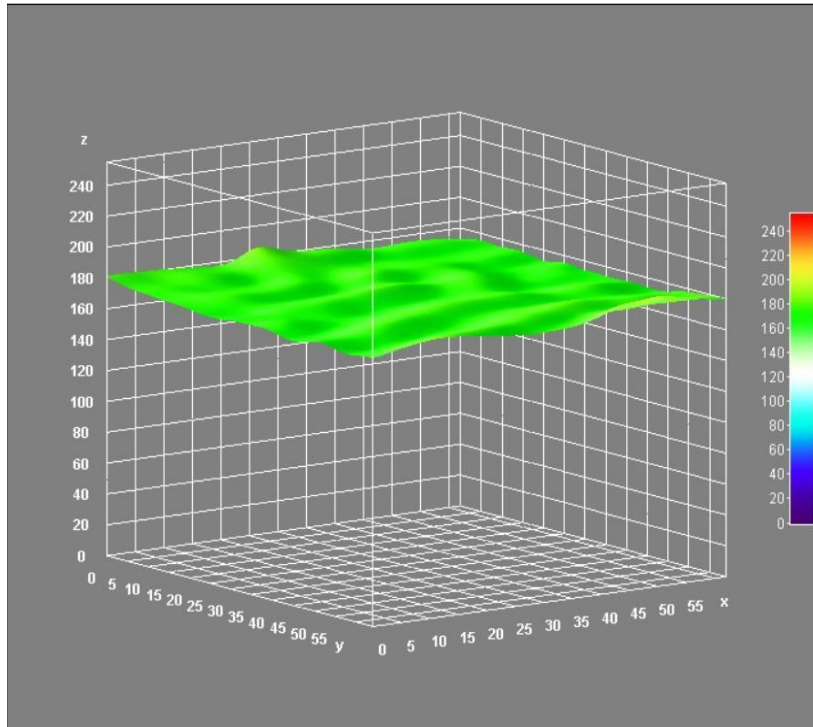


Figure 4.6 The 3D surface mapping of the RGB analysis of the ROI selected in the chl-PVA composite film.

4.7 Morphological study of the composite films using SEM

In general, the field emission scanning electron microscopy SEM gives information about the presence of voids, the presence of aggregate, the homogeneity of the composite, and the distribution of the nanoparticles within the matrix, and the possible orientation of nanoparticles [29]. The SEM has been performed to study morphology, presence, and distribution pattern of the nanoparticles i.e., chlorophyll molecules in the composite films. The SEM images of the pure PVA films exhibit a smooth and uniform surface. Small cracks and pores have been observed on the surface along with some protruding nodules. The composite film formed by the addition of the chlorophyll solution to the PVA solution has shown a rough and uneven surface. The chlorophylls have randomly distributed in the PVA matrix and caused changes in the morphology. The chlorophylls have been seen to enhance

the pores and cracks on the surface of the PVA matrix. The average size of the nanoparticles has been noted to be in the range of 100 nm.

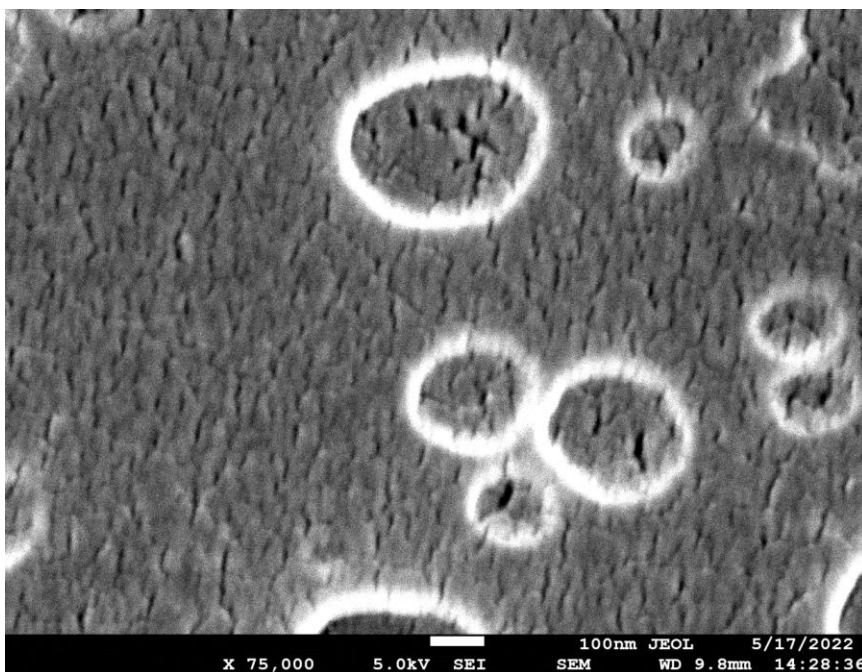
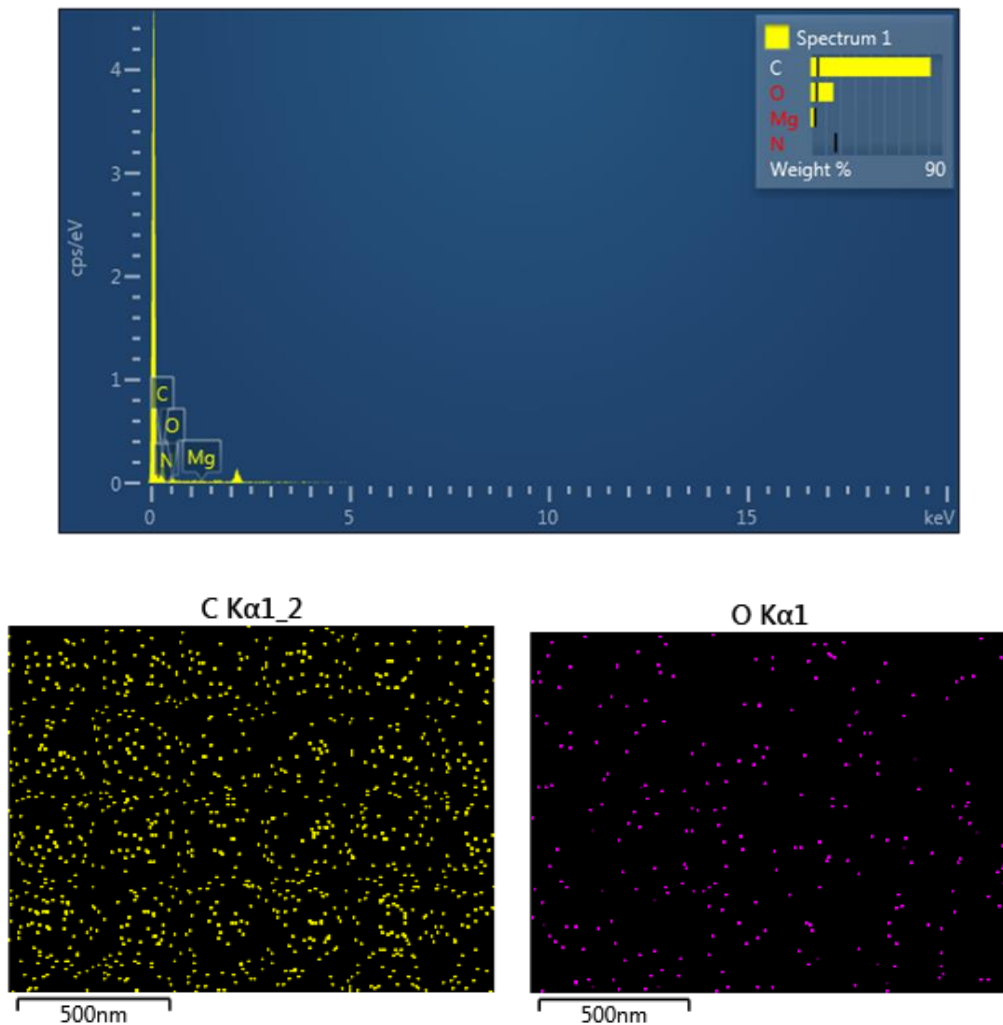


Figure 4.7 The SEM images of chl-PVA films ($\times 70000$) showing the chlorophyll distributed over the PVA matrix

The energy dispersive x-ray spectroscopy (EDS) of the pure and chlorophyll doped PVA film have also been performed. The EDS maps show the distribution of carbon (C) and oxygen (O) in the matrix. The EDS maps of the *chl-PVA* composite show uniform distribution of carbon (C), oxygen (O) and nitrogen (N) in the film. Based on the EDS spectra the elemental analysis has been carried out and the relative weight percentage of different elements has been determined in the composite. The composites contained C (81.95 %), N (0.00 %), O (15.29 %), and Mg (2.76 %).

4.8 Crystallographic study from XRD spectra

The x-ray diffraction (XRD) spectroscopy of the pure PVA and *chl*-PVA composite films has been performed to study their crystalline properties. The pure PVA films show a distinct peak at $2\theta = 19.9^\circ$. Two additional small intensity peaks at $2\theta = 29.01^\circ$ and 40.81° have been observed. The results are consistent with other researchers [25,30,31]. The side peaks at $2\theta = 29.01^\circ$ and 40.81° have been attributed to the diffraction profile of pure water as observed by investigators for biodegradable PVA [32].



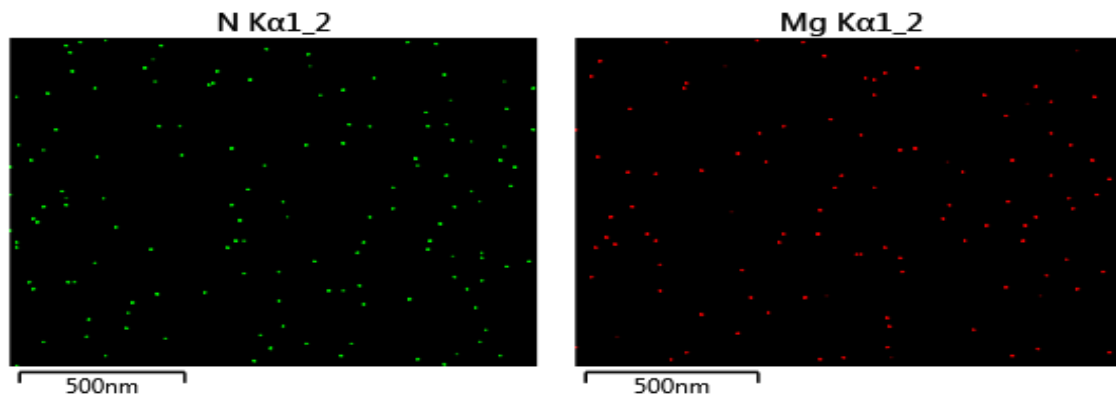


Figure 4.8 The EDS spectra and EDS mapping of the elements in the chl-PVA composite film.

The absence of any sharp peaks indicates the amorphous nature of pure PVA films. The addition of chlorophyll to PVA produces a shift in the major peak towards the lower 2θ side corresponding to a 2θ value of 19.3° . Two small peaks also appear at $2\theta = 17.2^\circ$ and $2\theta = 14.42^\circ$. The intensity of the central peak for *chl-PVA* at $2\theta = 19.3^\circ$ has a higher intensity than that for pure PVA at 19.9° . The peak full width at half maxima (FWHM) is also larger than that of pure PVA. The peak intensity and FWHM indicate the increase in amorphous nature of the films with the addition of chlorophyll solution [28].

The d-spacing corresponding to the characteristic peak of pure PVA at 19.9° has been 4.45, while that corresponding to the band at 29.01° has been 3.05. Such a pattern indicates a semi-crystalline nature of PVA. Researchers [33] have studied the XRD pattern of pure PVA and obtained a similar pattern. The peaks at 19.9° have been attributed to the reflections from (101) and $(10\bar{1})$ planes of PVA. Researchers [10] have studied the composite of ethylene-vinyl alcohol and chlorophyll and observed that the diffraction curves get shifted to the lower 2θ side with a broader peak indicating the amorphous nature of the composite.

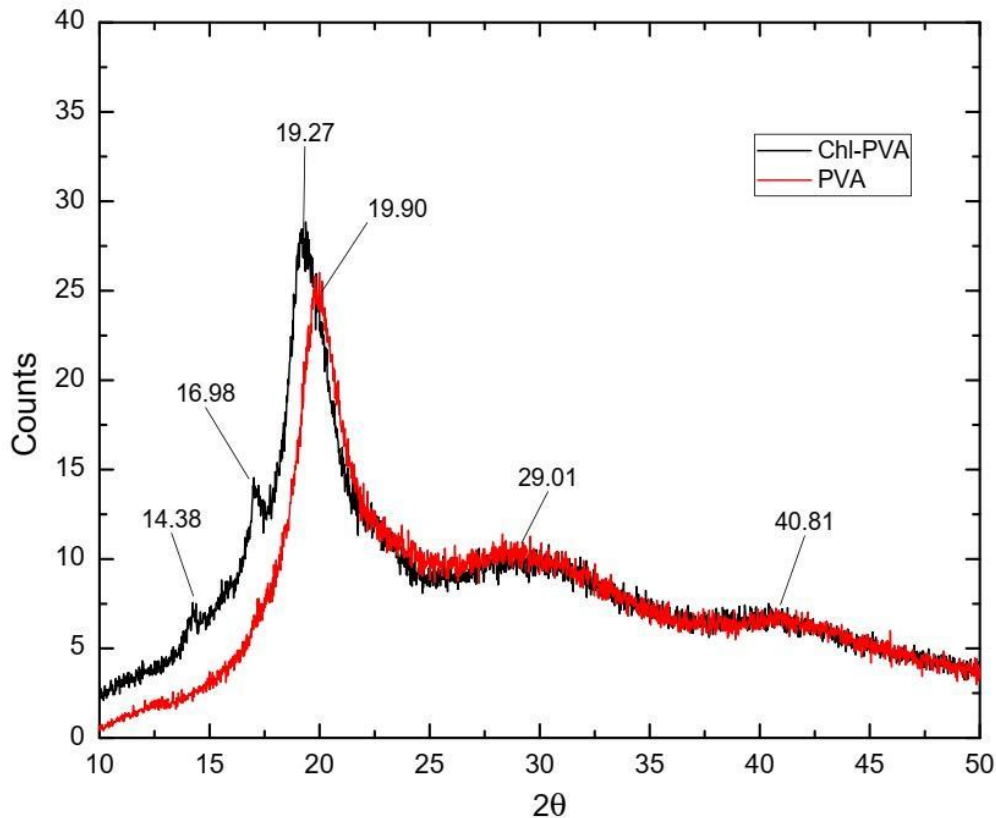


Figure 4.9 The XRD spectra of pure PVA and chl-PVA composite films. The values of 2θ corresponding to the peaks are indicated in the figure.

Recently researchers [34] have determined the impact of chlorophyll addition on wheat gluten films and shown that the chlorophyll addition reduces the crystalline nature of gluten films by broadening the peak. Similarly, [35] have studied the chlorophyll films from noni leaf and confirmed the presence of $Mg(N(CN_2)_2)$ from an intense peak around $2\theta = 28.7^\circ$.

4.9 Conclusion

The *chl-PVA* composite films have been prepared by casting method using freeze and thaw cycles. Six cycles of 12 h cooling at -15°C and 30-minute thawing at 20°C have resulted in the polymer composites being of optimal quality. The composite film has been

characterised by UV-Vis absorption spectroscopy, PL spectroscopy, FTIR spectroscopy, flatbed scanning, FE SEM analysis and XRD analysis techniques. The flatbed scanned images of the film have shown green coloured texture of the film with the distribution of chlorophylls in the PVA matrix. The green colour gives the primary presence of photosynthetic pigments. Further, the absorbance peaks at 670 nm and 460 nm confirm the presence of chlorophylls. The hypsochromic shift in the sorlet peak and bathochromic shift in the red peak of *chl-a* have been noted. The excitation spectra at an emission wavelength of 550 nm have shown a major peak at 400 nm and the emission spectra have shown a peak at 687 nm when excited by light of 320 nm wavelength. The spectra characterise the interactions of the *chl-PVA* matrix and resulting changes in the energy levels and band gap.

The FTIR spectra of pure PVA and *chl-PVA* composite film have shown almost similar peaks. However, there has been a difference in the peak intensities and location of peaks at 1683 nm (PVA-blank) and 1647 (*chl-PVA*). The SEM images of pure PVA show a uniform and smooth pattern with minor cracks on the surface. The Addition of chlorophyll solution has been non-uniform and aggregate formation has been observed. It indicates the physical interaction of chlorophyll molecules with the PVA matrix without the participation of hydrogen bonding. The XRD spectra show the semicrystalline of pure PVA with a broad peak corresponding to $2\theta = 19.9^\circ$. The addition of chlorophyll shifts the peak towards the lower 2θ with a broader peak. The addition of chlorophyll solution to PVA makes it more amorphous. The characterization of the composite film shows that the pure PVA film has been prepared and the incorporation of chlorophylls into PVA has been achieved.

Bibliography

- [1] Niroomand-Rad A, Blackwell C R, Coursey B M, Gall K P, Galvin J M, McLaughlin W L, Meigooni A S, Nath R, Rodgers J E and Soares C G 1998 Radiochromic film dosimetry: Recommendations of AAPM Radiation Therapy Committee Task Group 55 *Medical Physics* **25** 2093–115

- [2] Fukumori T and Nakaoki T 2013 Significant Improvement of Mechanical Properties for Polyvinyl Alcohol Film Prepared from Freeze/Thaw Cycled Gel *Open Journal of Organic Polymer Materials* **03** 110–6
- [3] Yang Y J, Hu B R, Liu Z M and Wu W J 2011 Preparation of Photostable Chlorophyll/PVA Film *Advanced Materials Research* **239–242** 2707–10
- [4] White D R, Booz J, Griffith R v., Spokas J J and Wilson I J 1989 Appendix A: Tissue Substitute Compositions *Reports of the International Commission on Radiation Units and Measurements* **os-23** 37–8
- [5] Gibbons J P and Khan F M 2020 *Khan's the physics of radiation therapy* ed J P Gibbons (Wolters Kluwer)
- [6] Deshmukh K, Ahamed M B, Deshmukh R R, Bhagat P R, Pasha S K K, Bhagat A, Shirbhate R, Telare F and Lakhani C 2016 Influence of K₂CrO₄ Doping on the Structural, Optical and Dielectric Properties of Polyvinyl Alcohol/K₂CrO₄ Composite Films *Polymer - Plastics Technology and Engineering* **55** 231–41
- [7] Abdelrazek E M, el Damrawi G, Elashmawi I S and El-Shahawy A 2010 The influence of γ -irradiation on some physical properties of chlorophyll/PMMA films *Applied Surface Science* **256** 2711–8
- [8] Hassan G M, Sokker H H, Lotfy S and City N 2011 Studying the dosimetric properties of γ -rays irradiated chlorophyll polyvinyl alcohol *Isotope and Radiation Research*
- [9] Sharma S, Prasher S, Singh K L and Kumar M 2020 Influence of gamma radiation on PVC/PANI composites *Journal of Physics: Conference Series* **1531**
- [10] Bakr N A and Ishra M 2002 Characterization of ethylene-vinylalcohol copolymer doped with chlorophyll *Polymer Testing* **21** 571–6
- [11] Rizzi V, Fini P, Fanelli F, Placido T, Semeraro P, Sibillano T, Fraix A, Sortino S, Agostiano A, Giannini C and Cosma P 2016 Molecular interactions, characterization and

- photoactivity of Chlorophyll a/chitosan/2-HP- β -cyclodextrin composite films as functional and active surfaces for ROS production *Food Hydrocolloids* **58** 98–112
- [12] Mandal P, Manna J S, Das D and Mitra M K 2015 Excitonic dynamics of Chlorophyll-a molecules in chitosan hydrogel scaffold *Photochemical & Photobiological Sciences* **14** 786–91
- [13] French C S 1960 The chlorophylls in vivo and in vitro *Die CO₂-Assimilation / The Assimilation of Carbon Dioxide* (Berlin, Heidelberg: Springer Berlin Heidelberg) pp 252–97
- [14] Itoh T, Yano K, Inada Y and Fukushima Y 2002 Photostabilized Chlorophyll *a* in Mesoporous Silica: Adsorption Properties and Photoreduction Activity of Chlorophyll *a* *J Am Chem Soc* **124** 13437–41
- [15] Porra R J, Thompson W A and Kriedemann P E 1989 Determination of accurate extinction coefficients and simultaneous equations for assaying chlorophylls a and b extracted with four different solvents: verification of the concentration of chlorophyll standards by atomic absorption spectroscopy *Biochimica et Biophysica Acta (BBA) - Bioenergetics* **975** 384–94
- [16] Hata H, Kimura T, Ogawa M, Sugahara Y and Kuroda K 2000 Immobilization of photosynthetic pigments into silica-surfactant nanocomposite films *Journal of Sol-Gel Science and Technology* **19** 543–7
- [17] Holt A S and Jacobs E E 1954 Spectroscopy of Plant Pigments. Ii. Methyl Bacteriochlorophyllide and Bacteriochlorophyll *American Journal of Botany* **41** 718–22
- [18] Petrovic S, Savic S, Markovic D and Petronijevic Z 2014 In vitro studies of temperature and pH influence on chlorophyll degradation by horseradish peroxidase: Spectroscopic and HPLC studies *Hem Ind* **68** 233–9
- [19] Mehraban Z, Farzaneh F and Shafiekhani A 2007 Synthesis and characterization of a new organic–inorganic hybrid NiO–chlorophyll-a as optical material *Opt Mater (Amst)* **29** 927–31

- [20] Masek A, Chrzescijanska E, Kosmalska A and Zaborski M 2014 Characteristics of compounds in hops using cyclic voltammetry, UV–VIS, FTIR and GC–MS analysis *Food Chemistry* **156** 353–61
- [21] Sravan Kumar S, Manoj P and Giridhar P 2015 Fourier transform infrared spectroscopy (FTIR) analysis, chlorophyll content and antioxidant properties of native and defatted foliage of green leafy vegetables *Journal of Food Science and Technology* **52** 8131–9
- [22] Li X, Zhou R, Xu K, Xu J, Jin J, Fang H and He Y 2018 Rapid Determination of Chlorophyll and Pheophytin in Green Tea Using Fourier Transform Infrared Spectroscopy *Molecules* 2018, Vol. 23, Page 1010 **23** 1010
- [23] Chang H, Kao M J, Chen T L, Chen C H, Cho K C and Lai X R 2013 Characterization of natural dye extracted from wormwood and purple cabbage for dye-sensitized solar cells *International Journal of Photoenergy* **2013**
- [24] Jeyaram S and Geethakrishnan T 2019 Linear and nonlinear optical properties of chlorophyll-a extracted from *Andrographis paniculata* leaves *Optics & Laser Technology* **116** 31–6
- [25] Sree K B, Kumar Y M, Gopal N O and Ramu C 2017 Preparation and characterization of pure and copper-doped PVC films *Journal of Polymer Engineering* **37** 83–92
- [26] Soltaninejad V, Ahghari M R, Taheri-Ledari R and Maleki A 2021 Bifunctional PVA/ZnO/AgI/Chlorophyll Nanocomposite Film: Enhanced Photocatalytic Activity for Degradation of Pollutants and Antimicrobial Property under Visible-Light Irradiation *Langmuir* **37** 4700–13
- [27] Israsena Na Ayudhya T, Posey F T, Tyus J C and Dingra N N 2015 Using a microscale approach to rapidly separate and characterize three photosynthetic pigment species from fern *Journal of Chemical Education* **92** 920–3

- [28] Karthikeyan B, Hariharan S, Sasidharan A, Gayathri V, Arun T, Akbari-Fakhrabadi A and Madhumitha C 2019 Optical, vibrational and fluorescence recombination pathway properties of nano SiO₂-PVA composite films *Opt Mater (Amst)* **90** 139–44
- [29] Choo K, Ching Y C, Chuah C H, Julai S and Liou N S 2016 Preparation and characterization of polyvinyl alcohol-chitosan composite films reinforced with cellulose nanofiber *Materials* **9**
- [30] Soltaninejad V and Maleki A 2021 A green, and eco-friendly bionanocomposite film (poly(vinyl alcohol)/TiO₂/chitosan/chlorophyll) by photocatalytic ability, and antibacterial activity under visible-light irradiation *Journal of Photochemistry and Photobiology A: Chemistry* **404** 112906
- [31] Surkatti R, El-Naas M H, van Loosdrecht M C M, Al-Naemi F and Onwusogh U 2019 Improvement of PVA gel properties for cell immobilization *Proceedings of the World Congress on Mechanical, Chemical, and Material Engineering* (Avestia Publishing)
- [32] Dey K K, Kumar P, Yadav R R, Dhar A and Srivastava A K 2014 CuO nanoellipsoids for superior physicochemical response of biodegradable PVA *RSC Advances* **4** 10123–32
- [33] Gupta S, Pramanik A K, Kailath A, Mishra T, Guha A, Nayar S and Sinha A 2009 Composition dependent structural modulations in transparent poly(vinyl alcohol) hydrogels *Colloids and Surfaces B: Biointerfaces* **74** 186–90
- [34] Chavoshizadeh S, Pirsa S and Mohtarami F 2020 Conducting/smart color film based on wheat gluten/chlorophyll/polypyrrole nanocomposite *Food Packaging and Shelf Life* **24**
- [35] Suriyani Che Halin D and Wazira Azhari A 2016 Synthesis of Chlorophyll Thin Film from Noni Leaves via Dip Coating Process *Materials Science Forum* **857** 142-145

Chapter 5

Radiometric analysis of chlorophyll solution and polymer composites

5.1 Introduction

The chlorophylls (a and b) have been extracted from the mango leaves in acetone (80%) for studying the radiation dosimetric properties of the proposed dosimeter. The changes in the absorption spectra with radiation dose have been quantified as a measure of the radiation dose. The chemical dosimetry solution has been found suitable for point dosimetry. The chlorophyll solution has been embedded with PVA to form a 2D composite film. The films are two-dimensional and useful for planar dose verification. Both, the chlorophyll solution, and the polymer composite film have been studied for the effects of therapeutic x-ray radiations from a medical linac. The effects of the range of therapeutic dose, dose rates and energies on these dosimeters have been studied. The detailed results for the chlorophyll solution and the polymer composite film are presented in the following sections.

5.2 Radiation dosimetric properties of chlorophyll solution

5.2.1 Physical properties of the dosimeter

The chlorophyll solution obtained in acetone (80%) contained 86.899 nmol/ml *chl-a* and 30.483 nmol/ml *chl-b*. The effective density of 1 ml of the solution has been found to be 0.941 kg/m³ while the effective density of the chlorophylls has been 1.073 kg/m³. The chemical composition and nature of the chlorophylls are similar to the haemoglobin molecules found in human blood except for the presence of the central Mg²⁺ atom in the former [1]. The density is nearly equivalent to that of water and human soft tissues. It is expected that the dosimeter shall possess radiological properties like the soft tissues in the therapeutic range of x-rays [2,3]. This dosimeter is expected to be suitable for dosimetry of therapeutic x-rays and electron beams.

5.2.2 UV-Vis absorption spectra

The UV-Vis absorbance spectroscopy has been performed to characterize the radiation dosimetric properties of the chlorophyll dosimeter. The absorbance spectra have shown a pattern like that observed in chapter 3. A broad and strong absorbance has been observed in the red region of the spectrum peaked around 664 nm. Other peaks in the blue region around 434 nm and 460 nm have been observed. These peaks are a result of the delocalized π electron cloud of the chlorophyll molecules [4]. The peaks at 664 nm and 434 nm have been attributed to *chl-a* while that at 460 nm have been due to *chl-b* (figure 5.1). The green-yellow region of the spectrum has shown absorbance of less than 10% of the red absorbance maxima. It indicates negligible amount of xanthophylls in the solution [5].

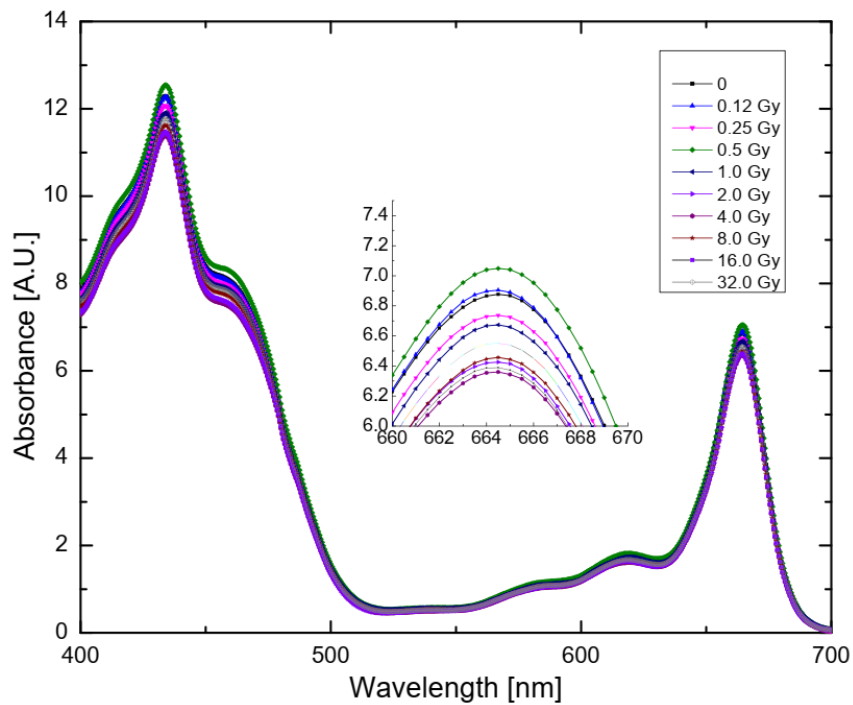


Figure 5.1 The UV-Vis absorption spectra of the chlorophyll dosimeter irradiated to therapeutic range of doses. The dose-response has been observed by A664.

A decrease in the absorbance values at 664 nm and 434 nm have been observed with an increase in radiation dose of 6 MV x-rays. This decrease indicates the degradation of *chl-a* molecules in the solution. This decrease in the absorbance at 664 nm has been further studied to characterize the chlorophyll dosimeter. There has not been any significant change in the absorbance in the green-yellow region of the spectra. The effect of radiation dose has been attributed to the fact that the x-rays are associated with the production of free radicals in the solutions, these free radicals can initiate a polymerization chain reaction most likely at the C=C and C=O bonds. These bonds are in large numbers in the chlorophyll molecules and hence the possible changes due to the absorbed x-rays can be expected at these bonds. Similar observations have been reported by the authors [6] for the chlorophyll solution obtained from spinach in ethanol. However, in contrast to the present study, the dose studied in that research has been in the range of kGy.

5.2.3. Accuracy and Precision

The chlorophyll solution has been found sensitive to the tested therapeutic range of doses and energies. It has shown a response towards the lowest dose of 0.12 Gy of 6 MV x-rays. A decrease in the absorbance at 664 nm (A_{664}) has been observed with increasing radiation dose, at different beam qualities and dose rates. The dosimeter has shown a good response in the therapeutic range of x-rays. The precision of the dosimeter has been tested by irradiation of several samples of the same batch under the same conditions of irradiation setup, temperature, light, and humidity. 2 Gy of radiation dose has been delivered to each sample to estimate the precision of this dosimeter. The samples have been analysed by UV-Vis spectrophotometry to estimate the radiation effects.

The average value of the absorbance at 664 (A_{664}) is 6.391 with a standard deviation of 0.015 (table 5.1). The plot of the distribution of A_{664} values around the average has been presented in figure 5.2. The precision of the dosimeter has been within 0.3 %. This value of precision is good enough to use in the clinical dosimetry of therapeutic x-rays and electron beam radiations.

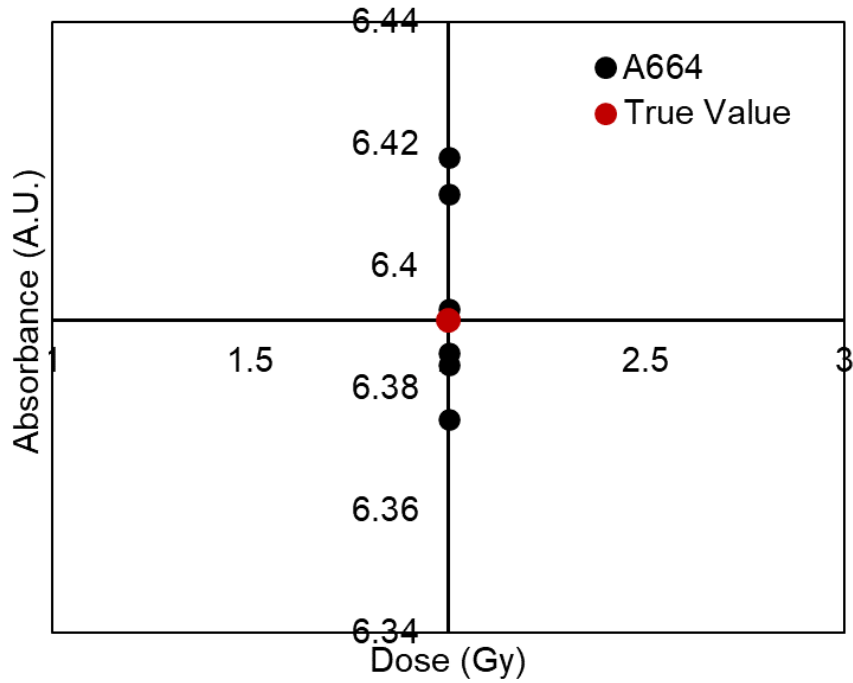


Figure 5.2 The precision of the chlorophyll dosimeter for a dose of 2 Gy of 6 MV x-rays delivered under the same setup conditions.

Table 5.1 The values of A 664 obtained from continuous irradiation of the chlorophyll dosimeter. The precision has been calculated from the standard deviation.

Dose (Gy)	A664	True Value (Avg.)	Standard Deviation	Percentage variation
2	6.393	6.391	0.015	0.002
	6.412			
	6.386			
	6.384			
	6.418			
	6.375			
	6.364			
	6.366			
	6.422			
	6.393			

5.2.4 Dose linearity

The dosimeter has been found sensitive toward small doses of 0.12 Gy of 6 MV x-rays. Figure 5.1 shows a decrease in OD at 664 nm for the tested therapeutic x-ray doses. It is clear from figure 5.3 that the chlorophyll dosimeter once standardised shall be feasible for application in the conventional radiotherapy fractionation of 2 Gy per fraction. The x-ray dose versus absorbance follows a linear response up to 2 Gy. The observations are indicative of the dosimetric potential of this device (figure 5.2). Beyond 2 Gy, saturation in the response of the dosimeter has been observed. Figure 5.3 shows the dose linearity plot for the dose-response up to 2 Gy. The dose-response in the full dose range has been illustrated in figure 5.4. The response saturation has been observed with a small increase in absorbance at higher doses.

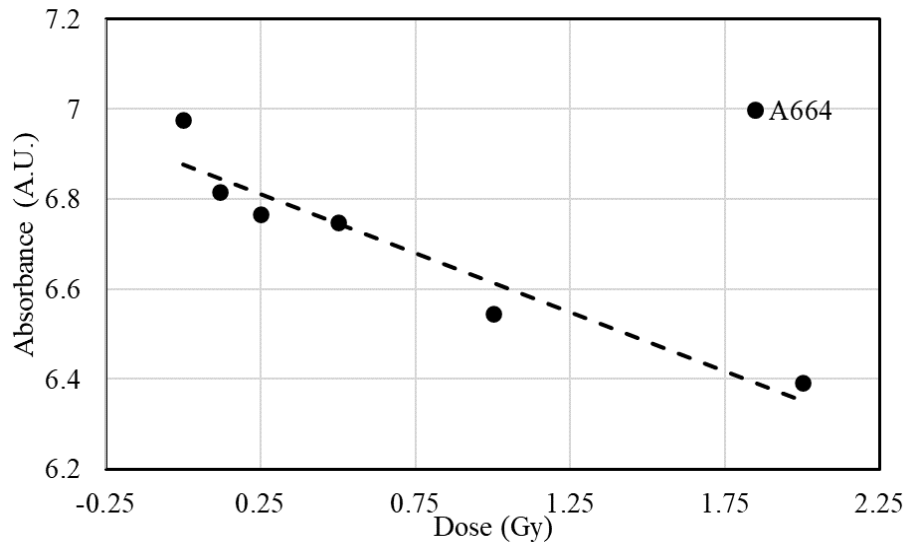


Figure 5.3 The dose linearity region of the chlorophyll dosimeter. The dose, A664 linearity has been observed up to 2 Gy.

A null hypothesis that there is no statistically significant relationship between the absorbed dose and absorbance has been tested and Pearson's Correlation coefficient (R) has been calculated. A correlation coefficient of 0.91 has been obtained for the tested data.

A P-value of 0.003 has been obtained. The results show that there is a statistically significant small negative relationship between the absorbed dose and the absorption values.

5.2.5 Energy Dependence

The dosimetry solution is dependent on the tested range of therapeutic x-rays and electron beam energies. Differences in the OD values at 664 nm have been observed at different beam energies as indicated in figure 5.5. The response has been normalized to 6 MV x-rays. The highest decrease in the OD values has been noted for 15 MV x-ray with a decrease of absorbance by 5.8 % to that of 6 MV x-rays. A minimum change of 1.2 % has been observed for 10 MV x-rays. It has been found that the changes in OD for FFF x-ray beams have been less than that for the flattened counterpart, indicating its higher sensitivity towards the flattened x-ray beams.

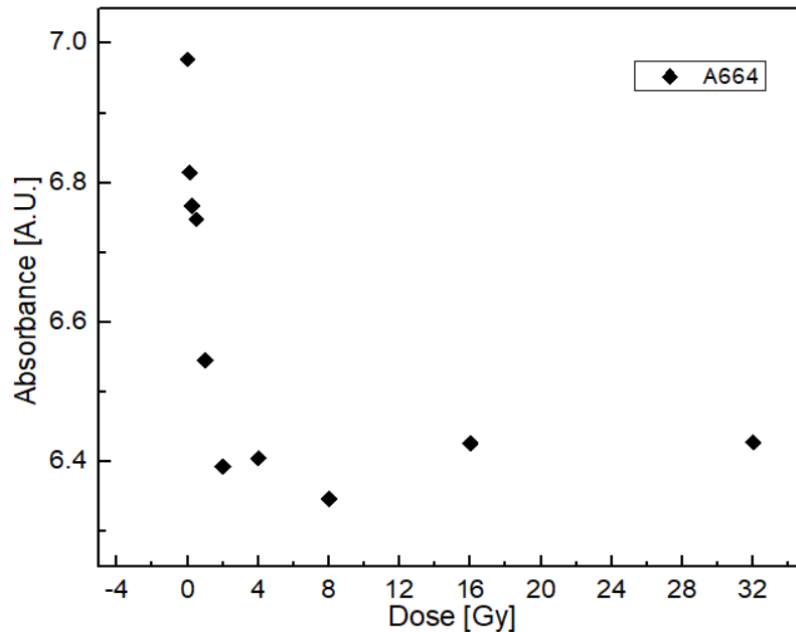
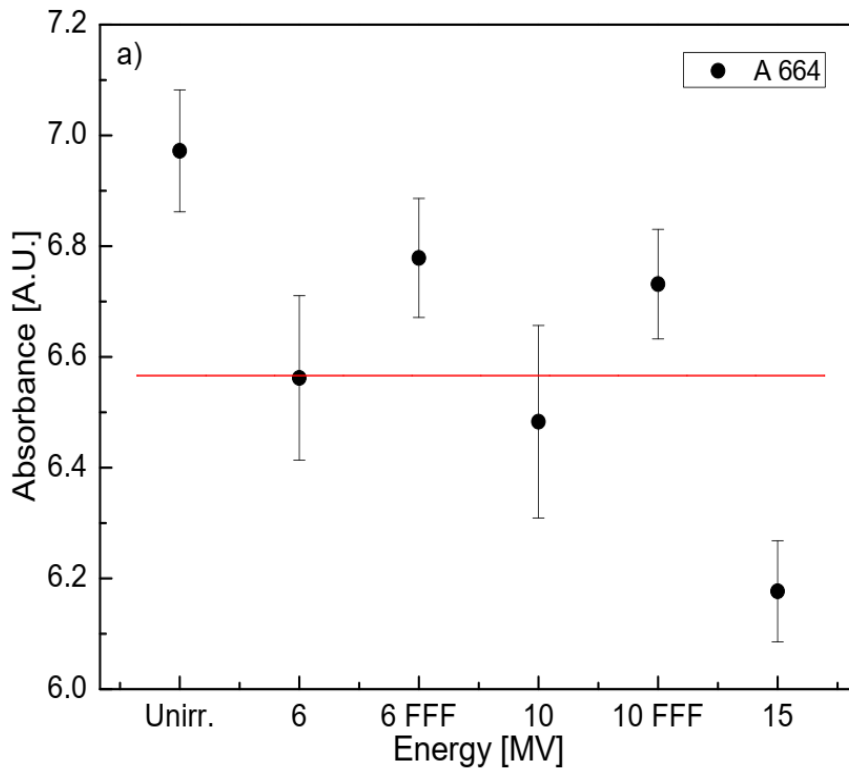


Figure 5.4 The radiation response of the chlorophyll dosimeter in the tested range of therapeutic doses.

The dosimeter has also shown dependence on the electron beam energies. The data indicated in figure 5.5 (b) shows the behaviour of the dosimetry solution in electron beams. The response has been normalized to a 15 MeV electron beam. It has been found that the 8 MeV beam shows minimum variations with the radiation dose as compared to the unirradiated sample. Its response to 4 MeV has varied by 4.7 %. The electron energies shows nearly similar response show nearly close responses and are most closely associated with the response at 4 MeV.



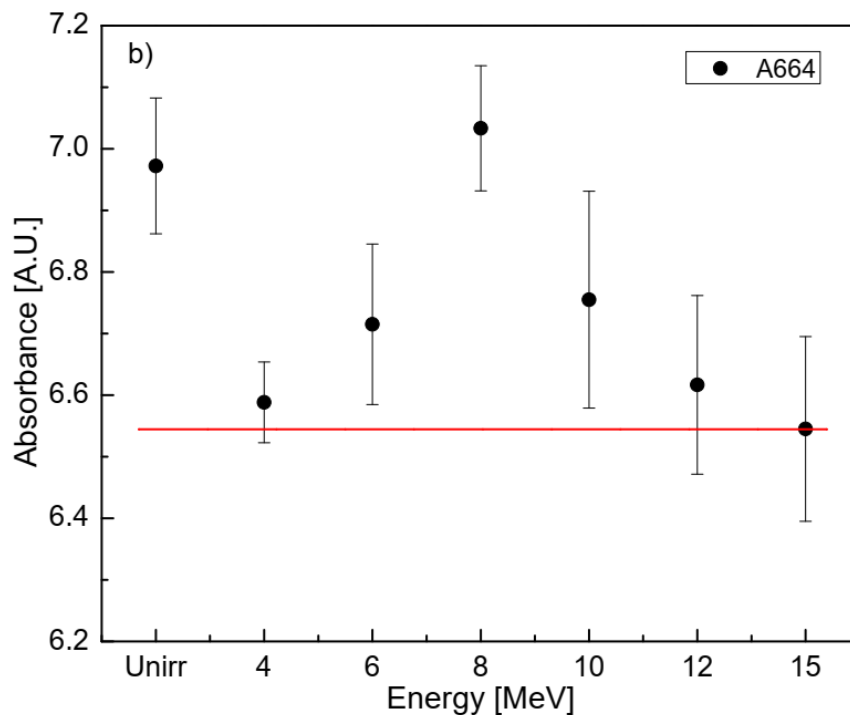


Figure 5.5 The energy dependence of the chlorophyll dosimeter in the therapeutic range of x-rays (a) and electron beams (b).

The dosimeter has shown sensitivity towards all the tested x-rays and electron energies showing its usefulness in the range of therapeutic x-ray energies. This behaviour encourages the investigation of chlorophyll dosimeters at even smaller doses and low-energy photon beams in diagnostic radiology and brachytherapy ranges. The diagnostic radiology and brachytherapy photon beams have been found to have higher linear energy transfer (LET) [7] and hence are expected to produce larger changes in the absorbance at the same doses as tested in the present study.

5.2.6 Dose rate dependence

The chlorophyll dosimeter studied in this work has been tested at different dose rates of 6 MV x-ray beams. Different absorbance values at 664 nm have been observed for the samples irradiated at five different dose rates. The decrease in OD values at 664 nm against the pristine sample has been consistent up to 200 cGy/min, however, very small

changes have been observed afterwards up to 600 cGy/min dose rate. The trend presented in figure 5.6 shows that the dose rate effect is more pronounced at lower dose rates than that at higher dose rates. However, the associated uncertainties as depicted in figure 5.6, indicates that the dosimeter response is independent of dose rates above the therapeutic dose rate of 300 cGy/min.

A decrease of 4.04 % in the absorbance has been observed from pristine samples to the sample irradiated at 100 cGy/min for a dose of 1 Gy. The absorbance value at 100 cGy/min was 6.690, which has been decreased to 6.562 ± 0.142 at the dose rate of 600 cGy/min. This 5.9 % change in absorbance is small but significant and has indicated that the proposed dosimeter can be used to distinguish two different dose rates. The change in absorbance at 400 cGy/min has been less than 1 %, showing that the dosimeter at higher dose rates shows a similar effect at a given dose.

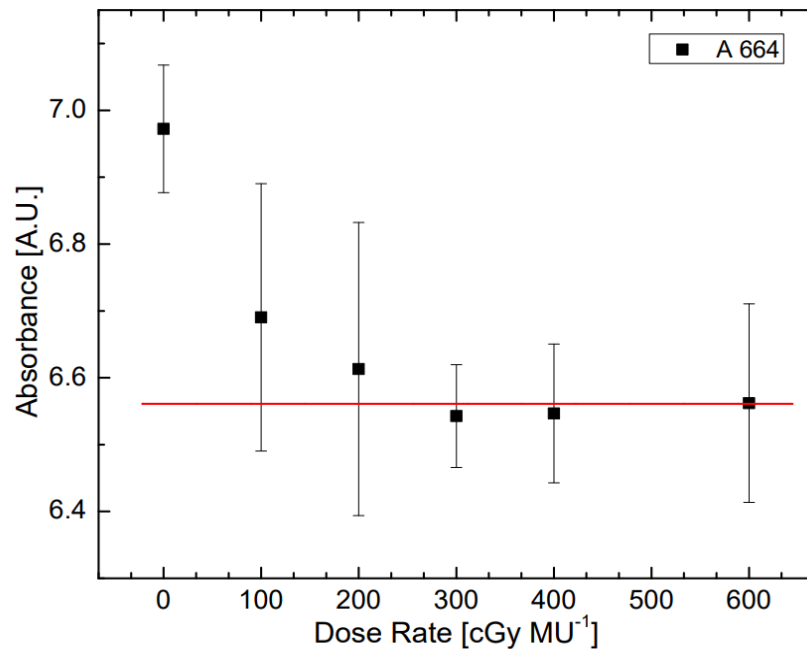


Figure 5.6 Effect of different dose rates utilized to deliver 1 Gy dose of 6 MV x-ray beam to the chlorophyll dosimeter. The figure presents the mean \pm standard deviation (indicated by bars) for all energies compared against 600 cGy/min.

5.2.7 Determination of absorbed dose to water using chlorophyll dosimeter

Following the testing of the dosimeter for radiation dosimetric properties, the chlorophyll dosimeter has been used to measure the radiation dose. In the present study, the dosimeter has shown linear response up to 2 Gy of the therapeutic dose. The statistical analysis of the dosimetric data has been performed. The following relationship between the absorbed dose to chlorophyll (D_{chl}) and the A664 (O.D.) has been obtained.

$$D_{chl} = -3.465 \times O.D. + 23.888 \quad (\text{Gy}) \quad (5.1)$$

The fundamentals of radiation dosimetry rely on the cavity theory and the concept of electronic equilibrium in the cavity. The Bragg Gray cavity theory considers the dosimeter as a small cavity made entirely of the detector material [8]. The presence of the container having electron density different from that of the detector material can perturb the fluence reaching the detector material. This causes a change in the response of the dosimeter with a wall as compared to that without the wall. The effect of the container wall on the x-ray dose in the dosimeter has been discussed by several investigators [9,10].

The correction factors for different wall materials such as PMMA and polyacrylate are in the range between 0.999 – 1.001. These correction factors have been shown to have insignificant effects at higher energies of x-rays due to negligible differences in the energy absorption coefficients [10,11]. In the current study, the sample vials used were those of polypropylene having a density of 0.92 g/cm³. The walls are expected to cause small changes in the dose-response in the dosimeter and these must be corrected by employing Monte Carlo simulations.

Considering the effects of these factors and using the correction factors determined using the MC simulations (Chapter 6), the following equation can be used to calculate the dose from chlorophyll to water

$$D_w = D_{chl} \times P_{wall} \times P_v \times f_{w,chl} \quad (\text{Gy}) \quad (5.2)$$

Where P_{wall} , P_v , and $f_{w,chl}$, are the wall correction factor, volume averaging correction factor and non-water equivalence of the chlorophyll correction factor

respectively. The values of these factors have been determined in chapter 6 and can be utilized for dose calculation.

5.3 Radiation Dosimetric properties of *chl-PVA* composite films

The chlorophyll-PVA composite films have been prepared by the casting method. Those films have been characterized by various characterization techniques. The films have been studied for their radiation dosimetric properties under a range of doses from therapeutic x-rays from a medical linear accelerator. The radiation response on these films has been analyzed by different characterization methods. The proceeding sections give a detailed report of the findings of the radiation dosimetric properties of the composite films.

5.3.1 UV-Vis spectrophotometry

The UV-Vis spectrophotometry of the *chl-PVA* composites has been performed in a range of wavelengths from 250 to 750 nm. The films have been aligned in a standing position with their plane perpendicular to the incident UV-Vis beams. The spectra have been characterized by several peaks in the red, green, yellow, and blue regions of the visible radiations. However, due to the static nature of the red absorbance maxima around 670 nm and its characteristic correspondence to the *chl-a* molecule, the absorbance at this peak (A_{670}) has been related to the radiation absorbed dose. The irradiation of the composite film has been carried out under 6 MV x-rays in a dose range from 0.25 to 32 Gy. The A_{670} has been found to decrease with the absorbed dose. This decrease has been attributed to the decrease in the *chl-a* concentrations in the composites as has been observed for the chlorophyll dosimeter. The absorbance spectra have been presented in figure 5.7 indicating the decrease in the absorbance with increasing dose.

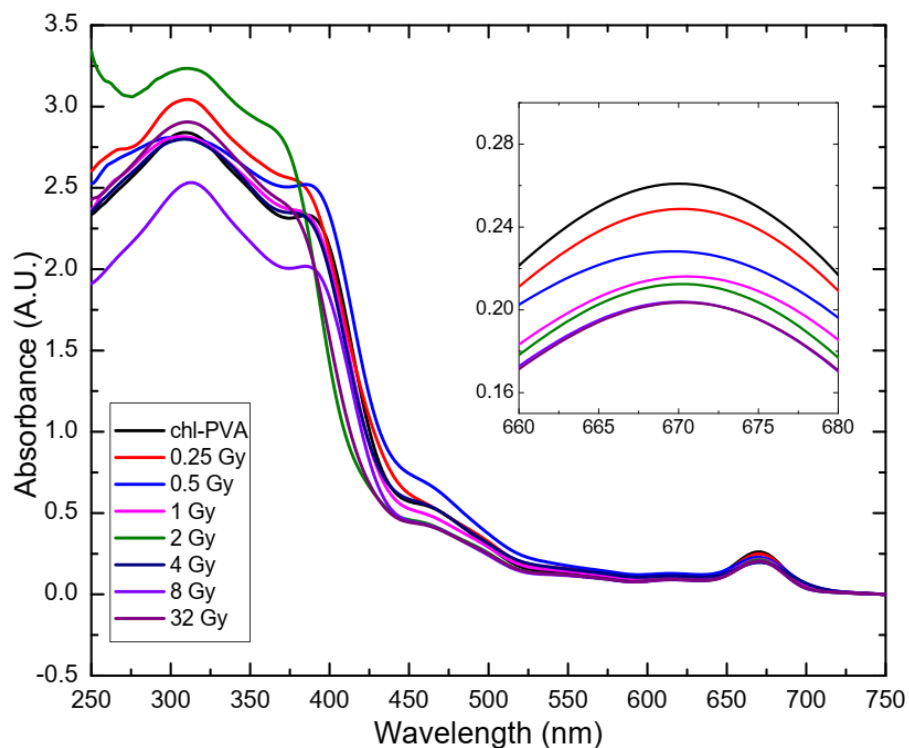


Figure 5.7 The UV-Vis absorption spectra of the composite films show the change in absorbance with radiation dose at around 670 nm.

5.3.2 Flatbed scanning

The films have been scanned on the flatbed scanner and the RGB analysis was done to determine the effect of radiation dose on it. The results of the RGB analysis are presented in table 5.2. There has been a decrease in the grayscale and luminescence values of the films with increasing doses from 0 to 2 Gy. However, saturation in the response has been observed at doses above 2 Gy up to 32 Gy.

Table 5.2 the RGB analysis of the chl-PVA films irradiated up to 32 Gy.

	0 cGy	200 cGy	800 cGy	3200 cGy
RED	216.53	185.06	198.37	198.05
Green	226.49	198.21	212.64	213.19
Blue	129.46	63.56	74.20	71.30
Greyscale	190.83	148.95	161.77	160.84
Luminescence	191.02	160.61	172.98	172.88

The 3D surface analysis of the film has been performed to analyse the distribution and relative intensity mapping of the green colour in the film. The green colour has been found to decrease with increasing radiation dose from 2 Gy to 32 Gy. The mapping is presented in figure 5.8.

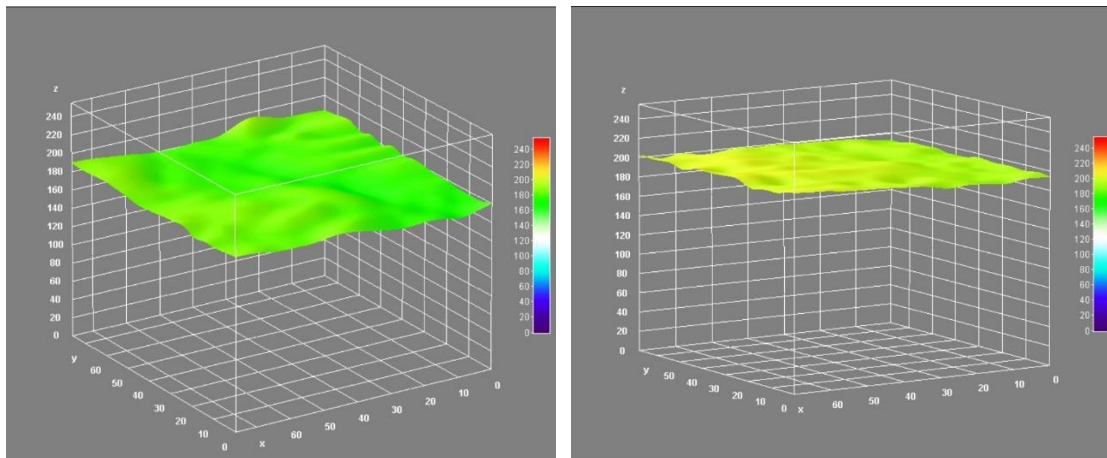


Figure 5.8 The 3D surface analysis of the *chl-PVA* films at 2 Gy and 32 Gy doses shows a decrease in the green colour content in the film.

5.3.3 Dose linearity

The film dosimeter has been tested for dose linearity over the range of doses as mentioned in the preceding section. The dosimeter has shown a similar response as that of the chlorophyll dosimeter. There has been a decrease in A670 up to 4 Gy dose. Beyond that, the saturation in the response has been observed. The linearity in the response has been observed up to 1 Gy dose with a Pearson's correlation coefficient of 0.96, indicating a significant and small negative correlation between the absorbed dose and A670. Up to 2 Gy dose, the correlation coefficient of 0.89 has been obtained indicating a non-significant correlation between the dose and A670.

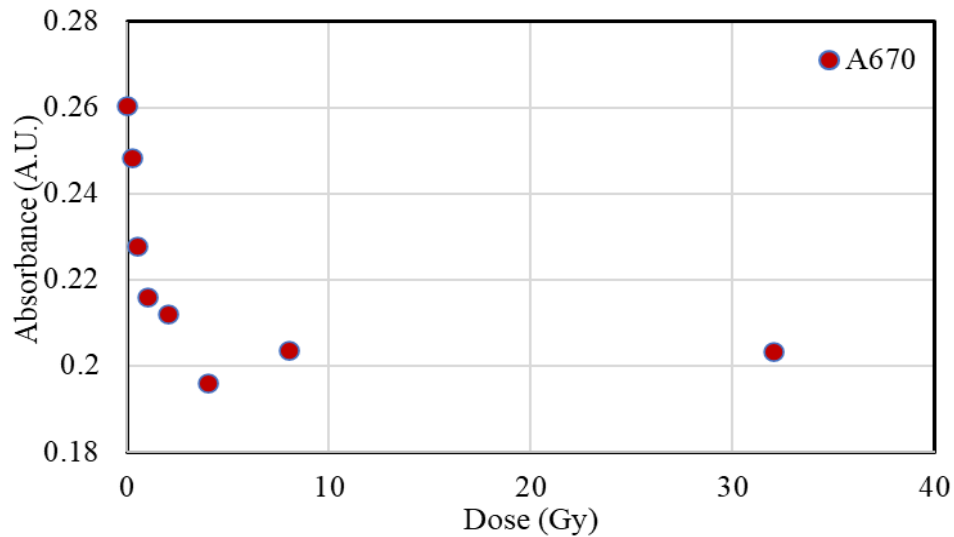


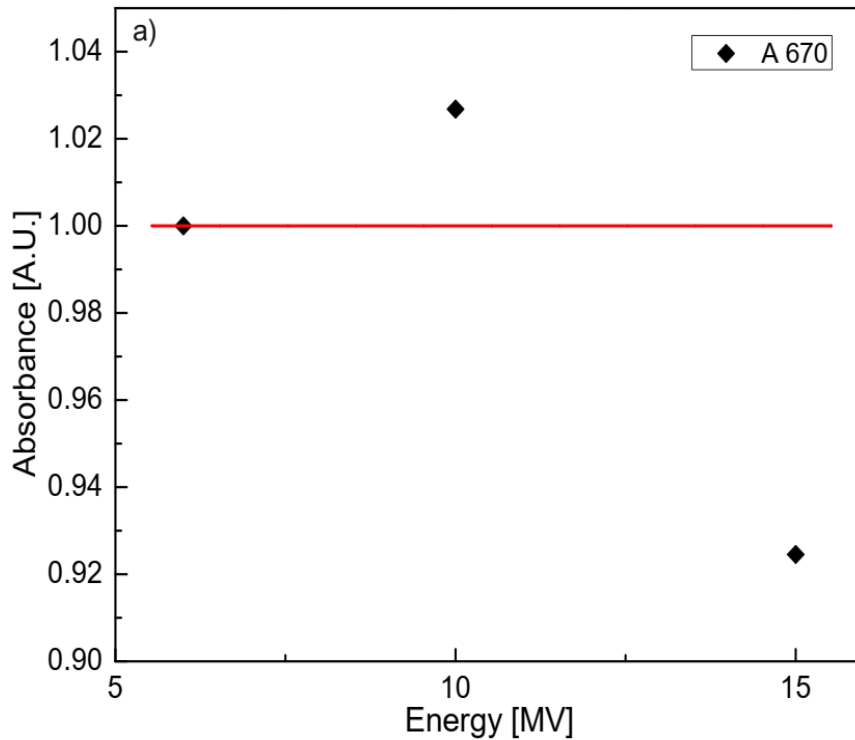
Figure 5.9 The dose-response up to 32 Gy of therapeutic dose shown by the chl-PVA films.

5.3.4 Energy dependence

The *chl-PVA* film dosimeter has been found to be dependent on the radiation beam energies of x-rays and electron beam radiations. The radiation response for x-rays and electron beam radiations has been evaluated by irradiating the dosimeter to 2 Gy dose of 6 MV, 10 MV and 15 MV x-rays and 6 MeV, 10 MeV, and 15 MeV electron beam radiations.

The response of x-rays and electrons has been normalized to 6 MV x-rays and 6 MeV electron beams respectively. The absorbance has shown an increase of response by nearly 3 % for 10 MV x-rays while for 15 MV there has been a decrease in the absorbance by nearly 8 %. A similar trend has been observed for electron beam radiations. These observations are suggestive of the energy dependence of this dosimeter. It further shows that the dosimeter has a better response at higher energy x-rays and electron beam radiations (figure 5.10 a,b)

The energy dependence is more pronounced in the electron beams. The effects may be due to the particle nature of the electron beams and its interaction pattern with the chlorophyll molecules in the film.



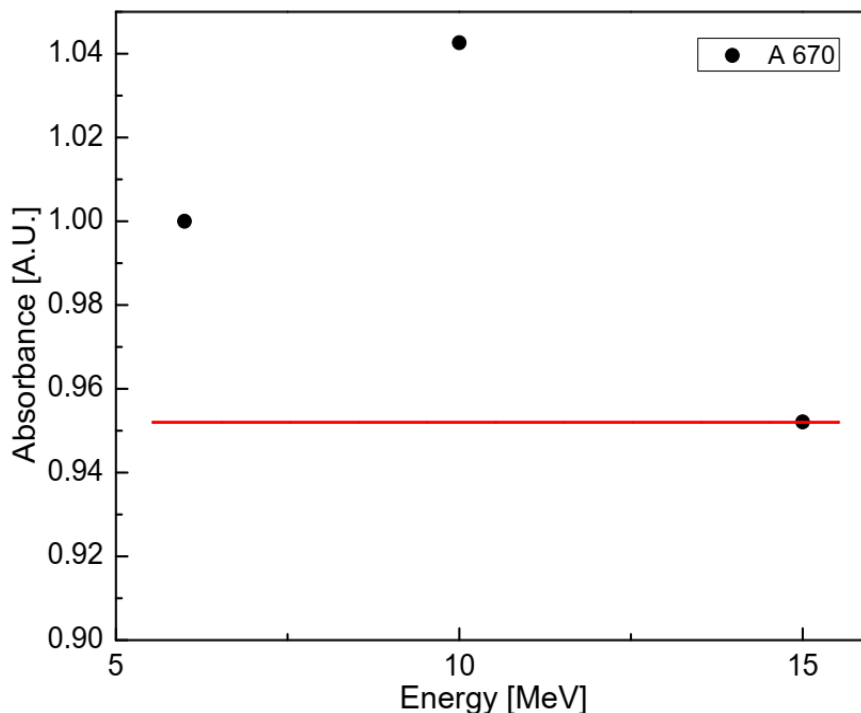


Figure 5.10 The energy dependence of the chl-PVA film dosimeter for x-ray beam energies (a) and electron beam energies (b).

5.4 Characterization of the radiation effects on chlorophyll solution

The *chl-PVA* dosimeter has been characterized for the radiation dosimetry of therapeutic x-rays and electron beam radiations. The dosimetric effect has been attributed mainly to the radiation-induced degradation of the *chl-a* molecules in the solution. The effects have been studied by the UV-Vis absorption spectra and 2D flatbed scanning by RGB analysis. Further, the radiation-induced changes in the dosimetry films have been characterized by other analytical techniques viz. PL spectroscopy, FTIR spectroscopy, X-Ray diffraction, and SEM. A brief description of these techniques has been presented in the proceeding sections.

5.4.1 PL spectroscopy

The PL spectroscopy of the composite films irradiated in the range of dose has been performed and excitation and emission spectra have been acquired. The excitation spectra

have been recorded at 550 nm with excitation wavelengths varying from 200 to 450 nm. The emission spectra have been acquired for an excitation wavelength of 320 nm over a range from 400 to 800 nm. Excitation spectra have shown bands at 235 nm, 266 nm, and 400 nm. The emission spectra have shown peaks around 442 nm, and 688 nm in the blue and red regions of the spectra. The emission intensity at 688 nm has shown a decrease with increasing radiation dose up to 32 Gy. However, no fixed trend has been noted in the excitation spectra (figure 5.11).

The decrease in the peak intensities with increasing radiation dose indicates that there is a radiation-induced decrease in the photogenerated charge carriers' recombination, especially in the energy band gaps corresponding to the $\pi - \pi^*$ transitions. With increasing radiation dose, the number of electron-hole pairs losing the ability to recombine leading to PL quenching also increases.

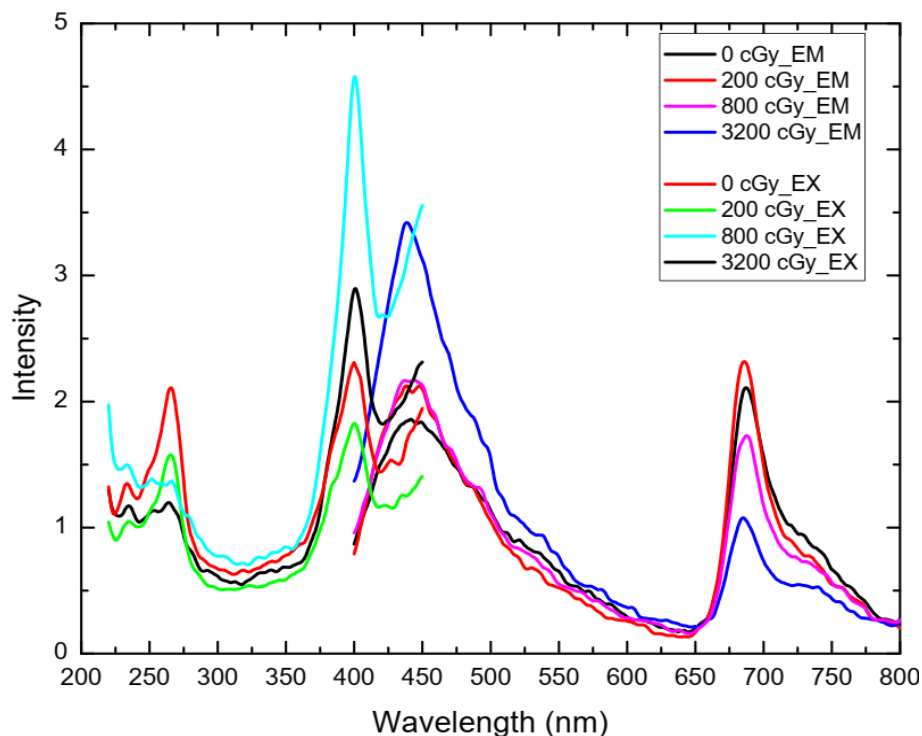


Figure 5.11 The excitation and emission spectra of the *chl-PVA* dosimeter.

5.4.2 FTIR spectroscopy

The FTIR peaks of the *chl-PVA* irradiated to different radiation doses have been analyzed over a range of wavenumbers from 400 cm^{-1} to 4000 cm^{-1} . The peak intensities at different locations are a result of the conjugation of *chl-a* and PVA in the *chl-PVA* composite films. The x-ray dose may cause structural changes in the composition, geometry and polarity of the composite film that may result in changing polarities of different bonds which eventually affects the relative locations and intensities of the FTIR peaks. In the present study, there have been consistent peak locations at different radiation doses, attributed to different groups as explained in chapter 4. However, it has been noted that the peak intensities for the bands corresponding to 32 Gy have shown decreased transmission as compared to 2 Gy.

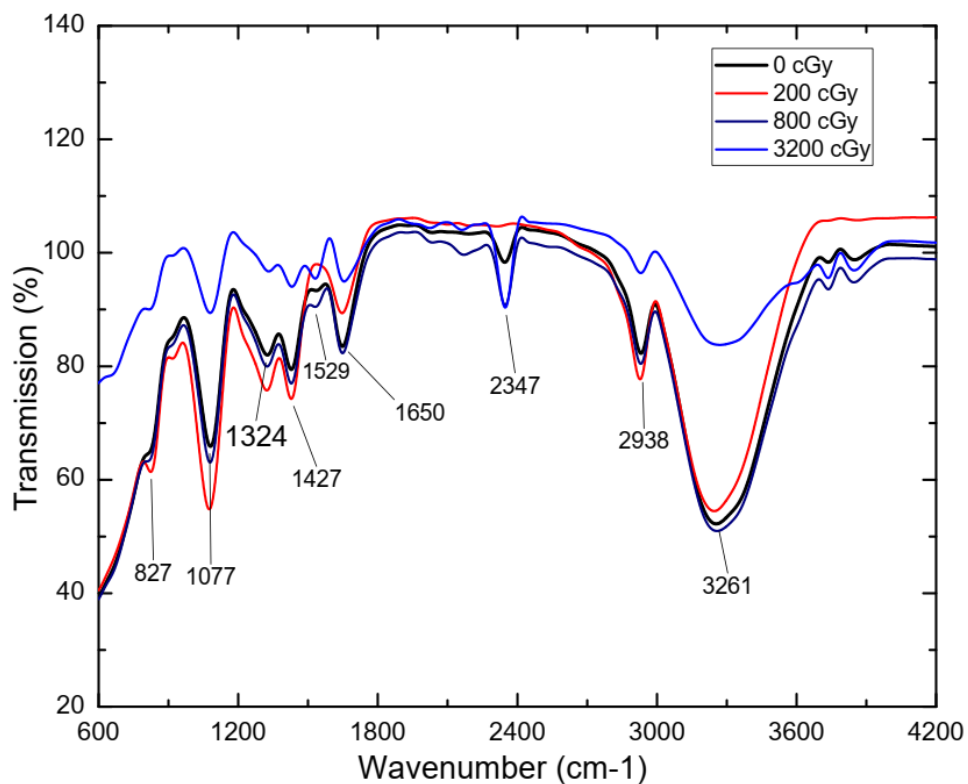


Figure 5.12 The FTIR spectra of *chl-PVA* composite films irradiated to different doses of 6 MV x-rays.

5.4.3 X-Ray Diffraction analysis

The crystallographic analysis of the irradiated *chl*-PVA composite films has been performed. Major peaks around 19.39° , 17.22° , 14.42° , 29.31° , and 40.24° of 2θ have been obtained. There has been a decrease in the peak intensity around all the peaks with increasing radiation dose. These changes are attributed to the change in the chemical state of the molecule that may cause changes in the orientation of the molecules in the composite leading to a change in the peak intensities. From figure 5.13 it can be deduced that the diffraction signal is coming from the (101) plane of PVA. However, due to radiation-induced changes in its orientation, the same plane diffracts the x-rays differently and hence causing the decrease in the intensity. The peaks at the lower 2θ side have indicated that the changes have been induced in the orientations of the planes of chlorophyll molecules also producing small changes in the intensity around these peaks.

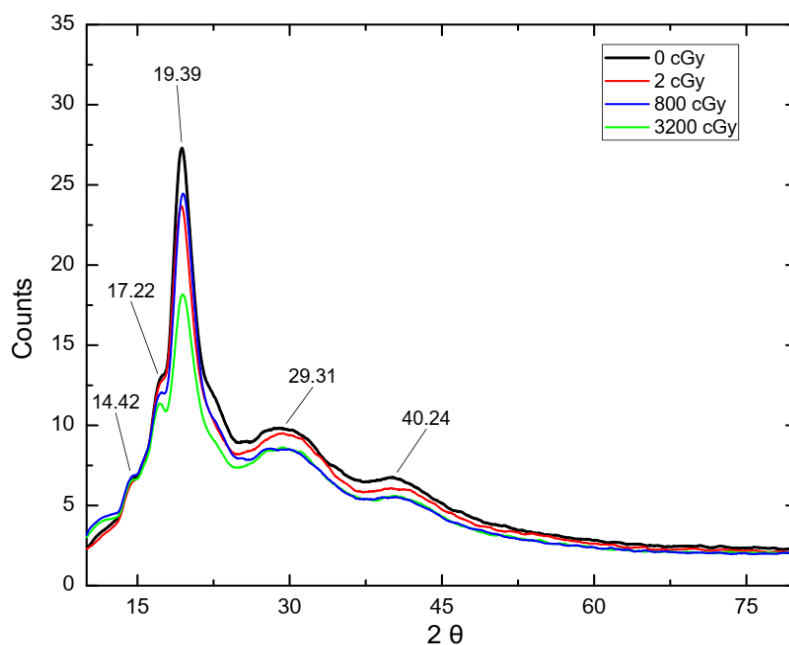
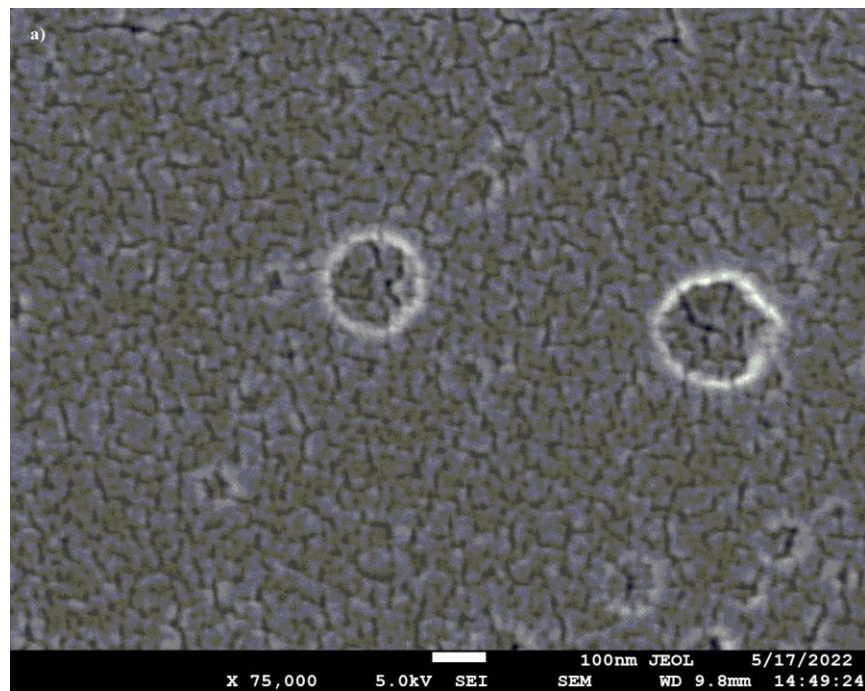


Figure 5.13 The XRD spectra of the *chl*-PVA composite films irradiated to different doses of 6MV x-rays.

5.4.4 SEM analysis

The morphological changes caused by the therapeutic radiations on the *chl-PVA* films have been studied by SEM analysis. The un-irradiated SEM images have shown the distribution of *chl-a* on the PVA matrix. The *chl-a* molecules are randomly distributed on the PVA matrix making it rough and uneven in morphology. The molecules have been found to produce cracks and pores in the PVA matrix. With increasing the radiation dose from 2 Gy to 32 Gy, there has been increasing localized pitting and cracks especially focused on the regions containing the chlorophyll molecules. The radiation-induced pitting effect has been an effect of the localized radiation-induced destruction of the composite film. Figure 5.14 shows the pitting effect of the x-rays on the *chl-PVA* composites.



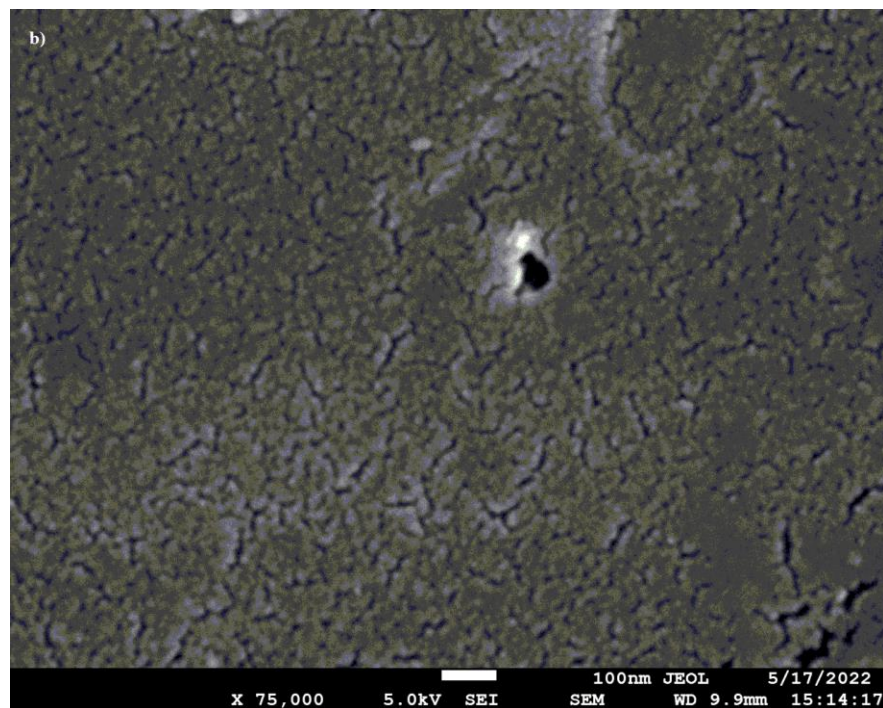


Figure 5.14 The SEM images of the *chl*-PVA composite films irradiated at 2 Gy(a) and 32 Gy (b) dose of 6 MV x-rays. The radiation-induced damage can be visualized in the film irradiated at 32 Gy.

The radiations are associated with the production of free radicals and ion pairs in the matter [12]. Certain materials possess the properties of photoluminescence, emitting light on radiation absorption. The radiation-induced changes in the materials form the basics of the radiation dosimeter [13–15]. If the radiation-induced effects are consistent and can be quantified simply, that material can be used as a radiation dosimeter. However, the applications of the radiation dosimeters vary widely and hence a wide variety of dosimeters are in use [16–18].

The current research has studied a chlorophyll-based solution and film dosimeter. Both the dosimeters have employed *chl-a* as the sensitive material. The dosimeter show response toward the therapeutic x-rays in the therapeutic range of doses [19]. The radiation effects in this dosimeter have been characterized by several different techniques. These techniques are suggestive of a structural and molecular change produced in the solution as

well as in the composite films. Similar observations have been made for the irradiation of organic materials and chlorophyll-doped silica gel films [20,21]. Hasan et al., [22] have reported the effects of gamma rays on *chl-PVA* films in the kGy dose ranges. They observed the decrease in absorption peaks of the composite films and attributed the effects to cleavage of C=C bonds and C–H bonds and polymer chain cessation producing a structural change in the composite film.

Abdelrazak et al., [23] have made similar observations for chl-PMMA composite films at high doses of gamma rays. Researchers have made similar observations for gamma ray irradiated PVA films analyzed by XRD, SEM, absorption spectra, and FTIR [24]. They have observed changes in the major diffraction peaks of PVA with increasing dose. The surface of the PVA matrix is rougher with increasing radiation doses. Also, the disappearance and shifting of the IR peaks have been reported.

5.5 Convenience of use and cost effectiveness

The proposed chlorophyll dosimeter and the *chl-PVA* films have shown good response in the therapeutic x-rays and electron beam radiations. The dosimeter has been prepared from organic materials. The chlorophylls have been extracted from the plant leaves (Mango) commonly available in the region using common lab solvents (acetone (80%)). The process of preparation of the chlorophyll dosimeter and the composite films is simple and can be carried out simply with common lab instruments. Further, the dosimeter has been found affected by the storage and irradiation temperature and light. Since most radiotherapy centres have a dedicated air conditioning system and a temperature in the range from 18°C – 20 °C is maintained, hence the irradiation and analysis temperature can be kept constant. The storage of the dosimeter has been recommended at a temperature of 5°C in darkness which can be achieved in a refrigerator used for drug storage in hospitals. In this way, the dosimeter can be managed in the radiotherapy department with all the previously available resources.

Further, the dosimeter is made up of biodegradable materials and hence pose no threat of environmental pollution. Further, the chlorophylls are present in all the plant

species and the solvents required for its extraction are very common lab reagents, available locally at low costs. In this way the dosimeter is expected to be non-expensive and cost-effective for the users. This is expected to not to pose any additional cost to the patient's treatment also.

5.6 Conclusion

The chlorophyll dosimeter proposed in the present study has been tested under the x-rays and electron beam radiations from a medical linac. The chlorophyll dosimeter has been characterized by UV-Vis spectrophotometry. The dosimeter has shown a response toward the low therapeutic doses of x-rays in the range of 0.12 Gy. There has been a decrease in A664 with increasing radiation dose. It has exhibited linearity in response up to 2 Gy dose with an R-value of 0.91. Beyond 2 Gy, the dosimeter has shown saturation in its response. The dosimeter has shown a precision of 0.3% which is acceptable for dosimetry of therapeutic x-rays. The dosimeter has shown dependence on the radiation beam energies of x-rays and electron beam radiations with the highest change in A664 for 15 MV x-rays. The observation has indicated that this dosimeter can be used to distinguish the radiation beams' qualities. Similarly, the dosimeter has shown dose rate dependence at low dose rates up to 2 Gy/min. At higher dose rates, this effect has been insignificant.

For the *chl-PVA* composite films, the A670 has been found to decrease with increasing radiation dose. The RGB analysis of the flatbed scanned images of the *chl-PVA* films has shown a decrease in luminescence and greyscale values at 2 Gy dose, however, the values have not changed significantly at 8 Gy and 32 Gy. The film dosimeter has shown linearity up to 1 Gy dose with an R-value of 0.96, while the linearity decreased for dose range up to 2 Gy with the R-value of 0.89. The A670 has possessed a significant negative correlation with the absorbed dose. The dosimeter has shown energy dependence for electron and x-ray beam radiations. The response of the composite films has been assessed by characterized by PL, FTIR, XRD and SEM. The PL emission spectra have shown a change in the concentration of photoelectrons with increasing radiation dose. The spectra indicate changes in the physical properties of the films with increasing doses. The IR

spectra have also shown a decrease in transmission intensity at 32 Gy due to possible radiation-induced changes leading to changes in dipole moment and geometry of the composite structure.

The XRD spectra have also indicated the radiation-induced change in the composite films leading to change in the orientations of the composite molecules and hence a decrease in the intensity of the diffraction peaks. The peak intensities around XRD have been found to decrease with increasing doses. The SEM images have also confirmed the radiation-induced structural changes with localized cracks and pitting observed with increasing radiation dose. The highest level of pitting effect has been observed at 32 Gy dose.

The results of the present study have shown that the proposed chlorophyll solution and composite films possess the properties and feasibility of a radiation dosimeter. Considering its convenience and cost-effectiveness, the proposed dosimeters can be utilized for relative dosimetry in radiotherapy.

Bibliography

- [1] Yuniarti E, Hasanah L, Advinda L and Indika P M 2019 Effect of wheat grass juice (*triticum aestivum* l.) against the erythrocytes and hemoglobin in male mice (*mus musculus* l.) anemia induced by sodium nitrite *Journal of Physics: Conference Series* **1317** 012069
- [2] IAEA 2000 *Absorbed Dose Determination in External Beam Radiotherapy An International Code of Practice for Dosimetry Based on Standards of Absorbed Dose to Water*
- [3] IAEA 2017 *Dosimetry of Small Static Fields Used in External Beam Radiotherapy An International Code of Practice for Reference And Relative Dose Determination* (Vienna)

- [4] Nayak P K, Mohan C C and Radhakrishnan K 2018 Effect of microwave pretreatment on the color degradation kinetics in mustard greens (*Brassica juncea*) *Chemical Engineering Communications* **205** 1261–73
- [5] Lefebvre T, Destandau E and Lesellier E 2020 Evaluation of the extraction and stability of chlorophyll-rich extracts by supercritical fluid chromatography *Analytical and Bioanalytical Chemistry* **412** 7263–73
- [6] Ramírez-Niño J, Mendoza D and Castaño V M 1999 Design and fabrication of an optical dosimeter for UV and gamma irradiation *Radiation Measurements* **30** 181–7
- [7] International Commission on Radiological Protection 2007 The 2007 Recommendations of the International Commission on Radiological Protection. ICRP publication 103 *Ann ICRP* **37** 1–332
- [8] Attix F H 2007 Cavity Theory *Introduction to Radiological Physics and Radiation Dosimetry* (Weinheim, Germany: Wiley-VCH Verlag GmbH) pp 231–63
- [9] el Gamal I, Cojocaru C, Mainegra-Hing E and McEwen M 2015 The Fricke dosimeter as an absorbed dose to water primary standard for Ir-192 brachytherapy *Physics in Medicine and Biology* **60** 4481–95
- [10] Chang M M and Nahum A E 1993 Dose conversion and wall correction factors for Fricke dosimetry in high-energy photon beams: Analytical model and Monte Carlo calculations *Physics in Medicine and Biology* **38** 93–114
- [11] Mazurier J, Gouriou J, Chauvenet B and Barthe J 2001 Calculation of perturbation correction factors for some reference dosimeters in high-energy photon beams with the Monte Carlo code PENELOPE *Physics in Medicine and Biology* **46** 1707–17
- [12] Seco J, Clasié B and Partridge M 2014 Review on the characteristics of radiation detectors for dosimetry and imaging *Physics in Medicine and Biology* **59** R303–47
- [13] Kelsey C A 1986 Fundamentals of Radiation Dosimetry *Radiology* **159** 422–422

- [14] Knoll G F 2010 *Radiation detection and measurement* (John Wiley)
- [15] Andreo P, Burns D T, Nahum A E, Seuntjens J and Attix F H 2016 *Fundamentals of Ionizing Radiation Dosimetry (Introduction to Radiological Physics and Radiation Dosimetry, 2nd ed.)* vol 1, ed P Andreo, D T Burns, A E Nahum, J Seuntjens and F H Attix (Wiley-VCH)
- [16] Shani Gad 1991 *Radiation dosimetry: instrumentation and methods* (CRC Press)
- [17] Chu R D H, McLaughlin W L, Miller A and Sharpe P H G 2008 Dosimetry Systems for Use in Radiation Processing *Journal of the ICRU* vol 8 (SAGE Publications) pp 1–2
- [18] Das, I.J., Downes, M.B., Kassaei A et al. Choice of Radiation Detector in Dosimetry of Stereotactic Radiosurgery-Radiotherapy *Journal of Radiosurgery* (2000) 3: 177.
- [19] Chand B, Priyamvda, Kumar M, Prasher S and Kumar M 2021 Feasibility study of a chlorophyll dosimeter for high energy x-ray beam used in radiotherapy *Journal of Radioanalytical and Nuclear Chemistry*
- [20] Egerton R F, Li P and Malac M 2004 Radiation damage in the TEM and SEM *Micron* **35** 399–409
- [21] Ramírez-Niño, José & PEREZ-ABAD, C & Rodriguez, Joaquin & GARCIA, J & CASTANO, M & Castaño V 1997 Optical properties of chlorophyll-doped silica gels *Journal of Materials Science: Materials in Electronics* **8**
- [22] Hassan G M, Sokker H H, Lotfy S and City N 2011 Studying the dosimetric properties of γ -rays irradiated chlorophyll polyvinyl alcohol *Isotope and Radiation Research*
- [23] Abdelrazek E M, el Damrawi G, Elashmawi I S and El-Shahawy A 2010 The influence of γ -irradiation on some physical properties of chlorophyll/PMMA films *Applied Surface Science* **256** 2711–8

- [24] Ahmed Jassim T and Abdulmunem Saeed A 2020 Effect of Gamma Irradiation on the Physical Properties of PVA Polymer *IOP Conf. Series: Materials Science and Engineering* **928** 072137

Chapter 6

Monte Carlo simulation of chlorophyll dosimeter

6.1 Introduction

The chlorophyll dosimeter has been investigated for its dosimetric properties under radiotherapy beams from a medical linear accelerator. The dosimeter has shown a response towards the therapeutic x-ray and electron beam radiations from the linac. In the present study, the chlorophyll solution has been contained in polypropylene vials of 1 ml volume. The vials have a polypropylene wall thickness of 0.5 mm. The chlorophyll solution on the other hand has an electron density different from that of water. Hence, it is mandatory that the correction factors for these quantities be determined to obtain the absorbed dose to water accurately.

The determination of the effect of the walls of the containing vessel i.e., polypropylene, the effect of the finite volume of the dosimeter and the non-water equivalence of the dosimetry material by measurement methods require a lot of setup modifications and tedious calculations. This process is prone to errors and may result in inaccurate values of desired quantities. On the other hand, the Monte Carlo (MC) techniques are one of the most accurate and commonly utilized methods for the determination of the effect of different parameters affecting radiation dosimetry [1]. The present study has utilized the MC technique for the determination of the correction factors for the chlorophyll dosimeter developed in this study.

6.2 MC Simulation of the linac

Elekta VersaHD (Elekta Medical Systems, UK) has been simulated using its geometric and dosimetric parameters for a 6 MV x-ray beam. The initial beam parameters have been obtained from the published literature and the open-access user manuals of the linac [2–7]. The components of the linac viz. the target, primary collimator, flattening filter (FF), monitoring ion chambers, multileaf collimators (MLCs), jaws and the mylar sheet

have been simulated using best possible geometrical and physical data at a fixed distance from the source. The target has been made up of tungsten (W) and Rhodium (Rh) 9:1, the primary collimator, jaws, and MLCs have been made up of tungsten alloy while the flattening filter has been made up of steel placed on an Aluminium plate. The transmission type monitoring ion chambers have been made up of air and copper wires.

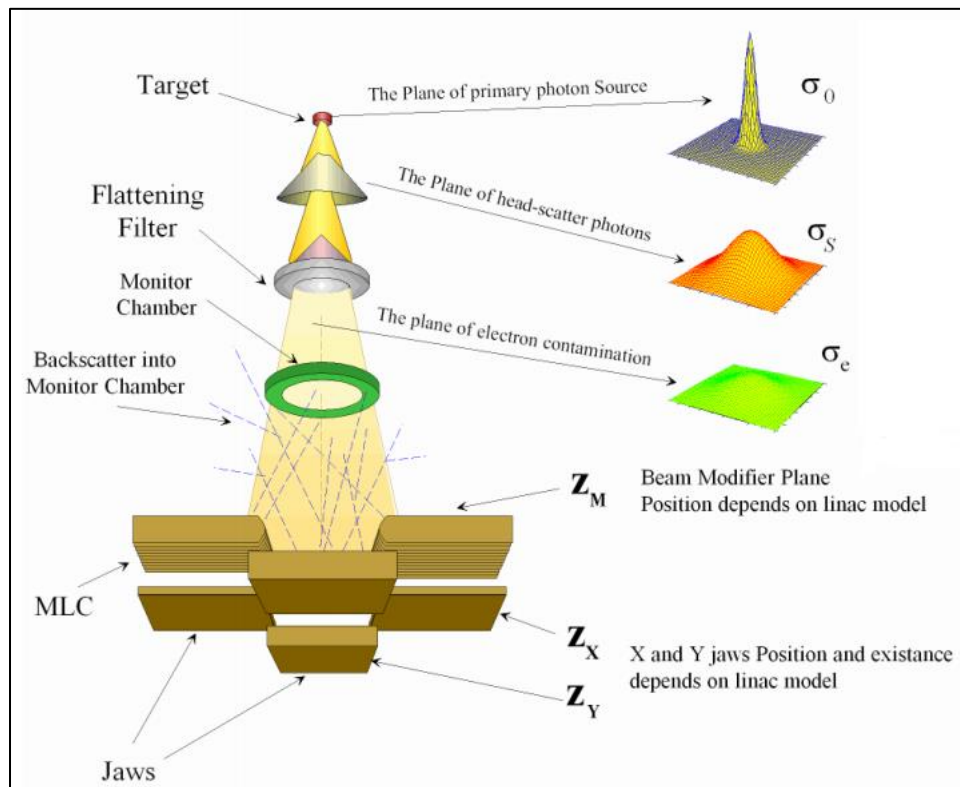


Figure 6.1 The relative locations of the components in Agility treatment head installed in Elekta VersaHD linac [Source: Monaco TPS reference manual [6].

The EGSnrc (National Research Centre, Canada) MC simulation toolkit has been used for the simulation of the linac and estimation of the radiation dose. The toolkit consists of different user codes and applications for simulation of a variety of x-ray, gamma-ray and electron sources, generators, phantoms, detectors, dosimeter cavities etc. The linac components have been simulated in BEAMnrc user code; an MC simulation toolkit

specifically programmed for geometrical and physical simulation of various electron and photon sources and generators. The BEAMnrc toolkit can give the radiation dose directly or a phase space file can be scored at the desired location. A 3D vocalised phantom for estimation of radiation dose has been simulated in the DOSXYZnrc user code.

The exact radiological properties of the materials can be simulated in EGSnrc toolkit by applying appropriate density correction data. This data has been presented in the form of a density correction file called pegs4 data file. The pegs4 data file for all the materials has been created using the stopping power and density effect values over different energy ranges using the NIST algorithm [<https://physics.nist.gov/PhysRefData/Star/Text/ESTAR.html>; May 2020]. The materials have been simulated in the EGS application using the AE and AP value respectively, 0.7 MeV and 0.01 MeV and material specific ICRU density corrections have been applied. Other MC simulation parameters for MC simulations have been set at default values of the toolkit.

Initially, 3×10^8 electron histories have been used to obtain the phase space data. The variance reduction techniques have been applied to enhance the accuracy of simulation and reduce simulation time. The directional bremsstrahlung splitting has been used with a splitting field radius of 8 cm and splitting number 40. The global electron cut off (ESAVE) has been turned on and its values set at 2 MeV.

The simulations have been performed in a phased manner. In the first phase, the patient independent part of the linac has been simulated. An initial phase space data has been scored at a plane just above the MLCs at 30.9 cm. This phase space has been used as a source in the second phase for the patient dependent part of the linac head. In this second phase the MLCs, jaws, Mylar sheet and intervening air has been simulated. The benchmarking process of the linac has been established at 100 cm source to surface distance (SSD) for a 10×10 cm². The beam profiles, output factors and percentage depth dose (PDD) profiles have been calculated at 90 cm source to axis distance (SAD) at 1.5, 10 and 20 cm depth for square fields of side length 5, 10, 20 and 30 cm.

The MC calculated data has been validated for its accuracy and consistency against the measured data. The depth dose profiles, and beam profiles have been analysed by two-dimensional (2D) gamma analysis criteria by comparing the 2D dose planes [7]. The gamma criteria of 3 % local dose difference (DD) and 3 mm distance to agreement (DTA) have been set as an acceptance criterion in this study and a relaxation of 5% DD has been used for comparative analysis of the data. The accuracy of the MC model has also been evaluated by a dose error estimator (ϵ) quantity also [8,10]. The accuracy of MLC modelling has also been validated. The beam output factors have also been analysed to further validate the model.

$$\epsilon = \frac{1}{N} \sum_i \frac{D_{cal_i} - D_{meas_i}}{D_{meas_i}} \quad (6.1)$$

Where, N is the total number of points observed, D_{cal_i} , and D_{meas_i} , are the dose obtained at i^{th} point by the MC calculated and measured dose profile, respectively. The beam quality parameter $TPR_{20,10}$ has been determined using an empirical formula based [10].

$$TPR_{20,10} = 1.2661 (D_{20/10}) - 0.0595 \quad (6.2) \text{ [9 ; pg.no. 68]}$$

$D_{20/10}$ is the PDD ratio at 20 cm and 10 cm depth respectively.

The 6 MV x-ray beam of the Agility collimator system installed on VersaHD linac has been modelled. The independent validation of the linac parameters has been done by comparing the modelled depth dose data and radiation beam profiles against the experimentally measured data. The MLCs leakage and leaf end model has been validated from the penumbra profiles. The beam output factors have also been validated for a set of field sizes to check the exact matching of the modelled collimator opening to that of the experimental values. Gamma analysis of the dose has been performed to check the local dose difference (DD) and distance to agreement (DTA) within the tolerance values of 3 % DD / 3 mm DTA. All the points in the SAD and SSD setups have been found to follow the

gamma criteria. An overall error (ϵ) of less than 1% has been obtained for the beam profiles and depth dose profiles. The depth dose at 10 cm depth, the beam quality index and the depth of maximum dose are within acceptable tolerances as given in table 6.1.

Table 6.1 The value of estimated errors (ϵ) and gamma index (3%/3mm) for PDD, inline and crossline profiles at 100 cm SSD and 10×10 cm² field size.

	estimated errors (ϵ)	gamma (3% / 3mm)
PDD	0.0066	1.00
Inline	0.0344	1.00
Crossline	0.0601	1.00

6.2.1 Radiation beam profiles

The PDD and off-axis beam profiles have been tested by local dose difference between the MC calculated and measured dose. Figures 6.2 and 6.3 show these results. An extensive set of beam profiles and depth doses have been tested for a range of square field sizes of the side length ranging from 5 cm to 30 cm in the SAD setup. These depth dose and beam profiles are presented in Figures 6.2(b) and 6.4 respectively.

Table 6.2 Comparison of the parameters describing radiation beam quality of a 6 MV photon beam for 10×10 cm² field size.

	Measured PDD (%)	MC Calculated PDD (%)	Error (%)
D₁₀	67.7	68.1	0.59
D₂₀	39.6	40.0	1.01
TPR_{20,10}	68.2	68.4	0.293
d_{max} (cm)	1.5	1.5	0

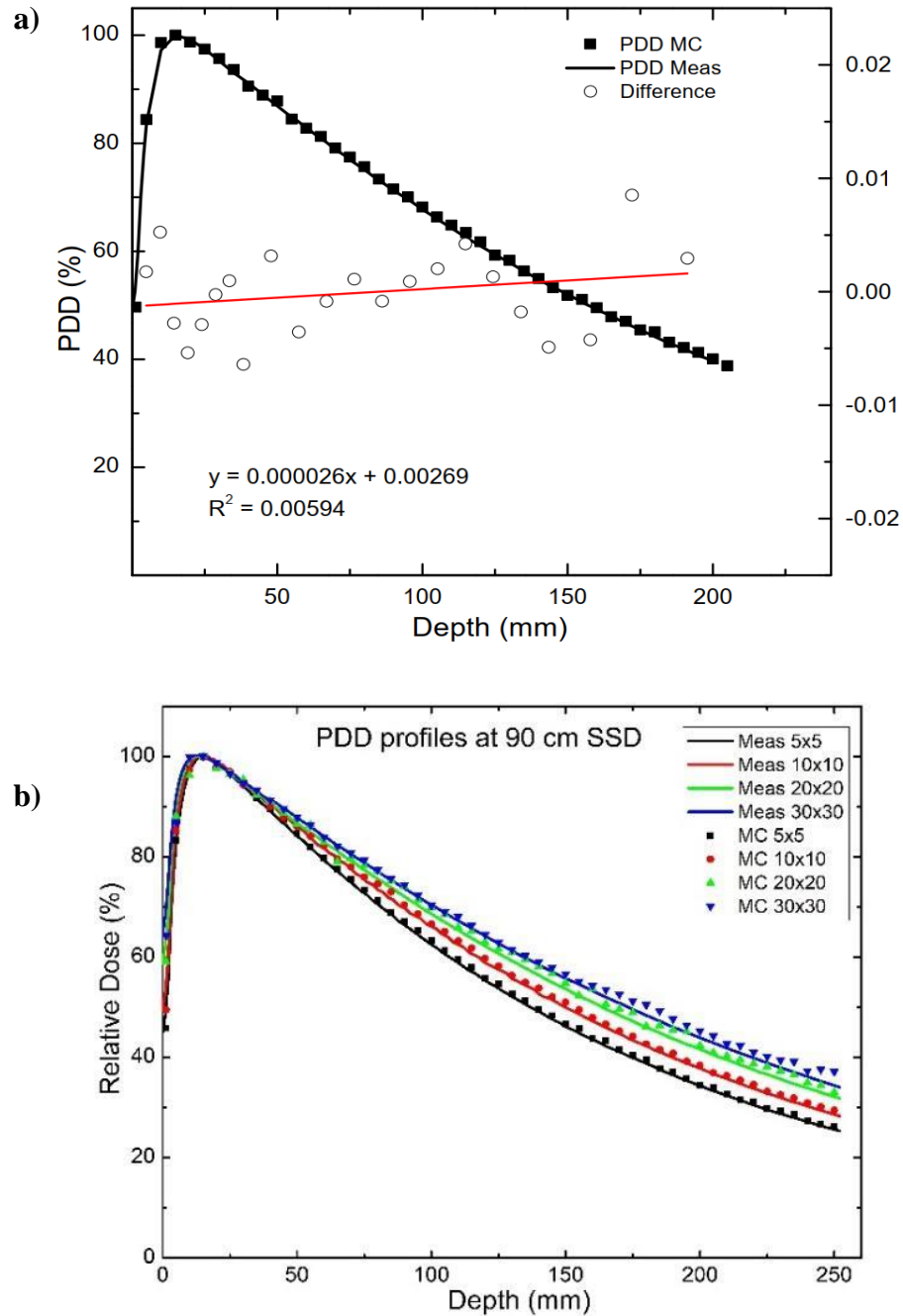


Figure 6.2 The comparative analysis of MC calculated and measured PDD profiles in SSD setup shows the dose difference at respective depths (a) and SAD setup for a range of field sizes (b).

The inline and crossline beam profiles and depth dose profiles have been tested for point dose differences and point to point gamma analysis. The profiles at small field sizes ($<10 \times 10 \text{ cm}^2$) have been found to pass the gamma criteria at lower tolerance values of 2%/2mm. The profiles for larger field size ($>10 \times 10 \text{ cm}^2$) have been found to follow the gamma criteria of 3%/3mm for all the field sizes up to $20 \times 20 \text{ cm}^2$, above that the points for $30 \times 30 \text{ cm}^2$ at the highest depth of 20 cm have been found to follow the gamma criteria at extended DD range of 5%.

The 2D gamma has also been tested for these profiles at different depths and set of tested field sizes. These profiles have been found to pass the gamma criteria of 3%/3mm for most of the field sizes except the largest field of $30 \times 30 \text{ cm}^2$ for which the extended criteria of 5%/5mm has been used (Figure .

Least square linear regression has been analysed for the dose difference as a function of depth for the PDD curve (Fig 6.2 a). In an ideal energy match with zero dose difference, the slope of the line is zero. An R^2 value of 0.006 has been obtained for the dose difference fitting line. The d_{max} has been 1.5 cm for both the measured and MC calculated PDD profiles (table 6.2). A maximum discrepancy of 1.01 % has been found for the PDD at 20 cm depth. Once the accurate model of the linac has been achieved and validated, this model has been used to calculate the correction factors for the dosimeter under study. The chlorophyll solution of standard concentration in the vessel contained in a water phantom has been simulated.

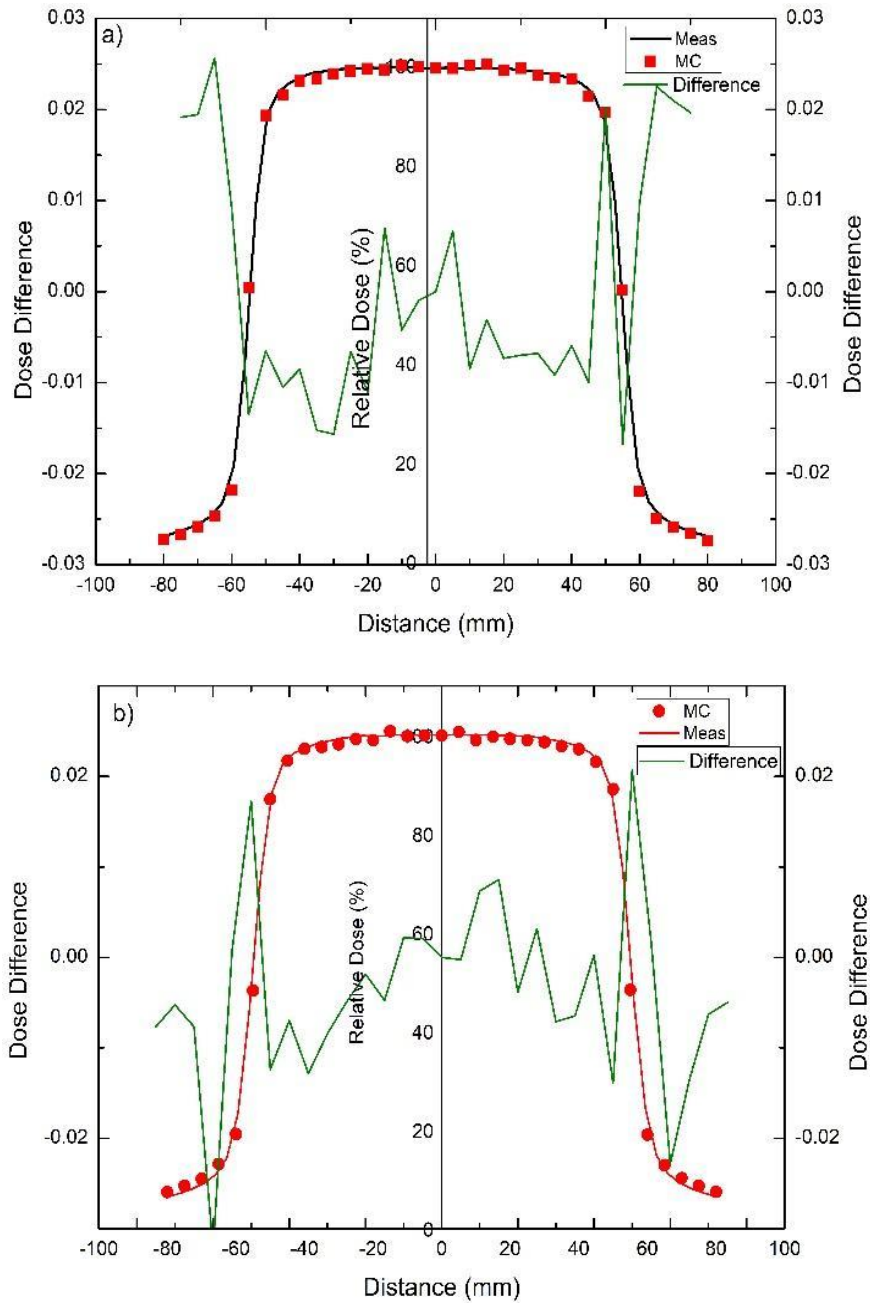


Figure 6.3 Dose difference in measured and calculated off-axis beam profiles in crossline (a) and inline (b) directions.

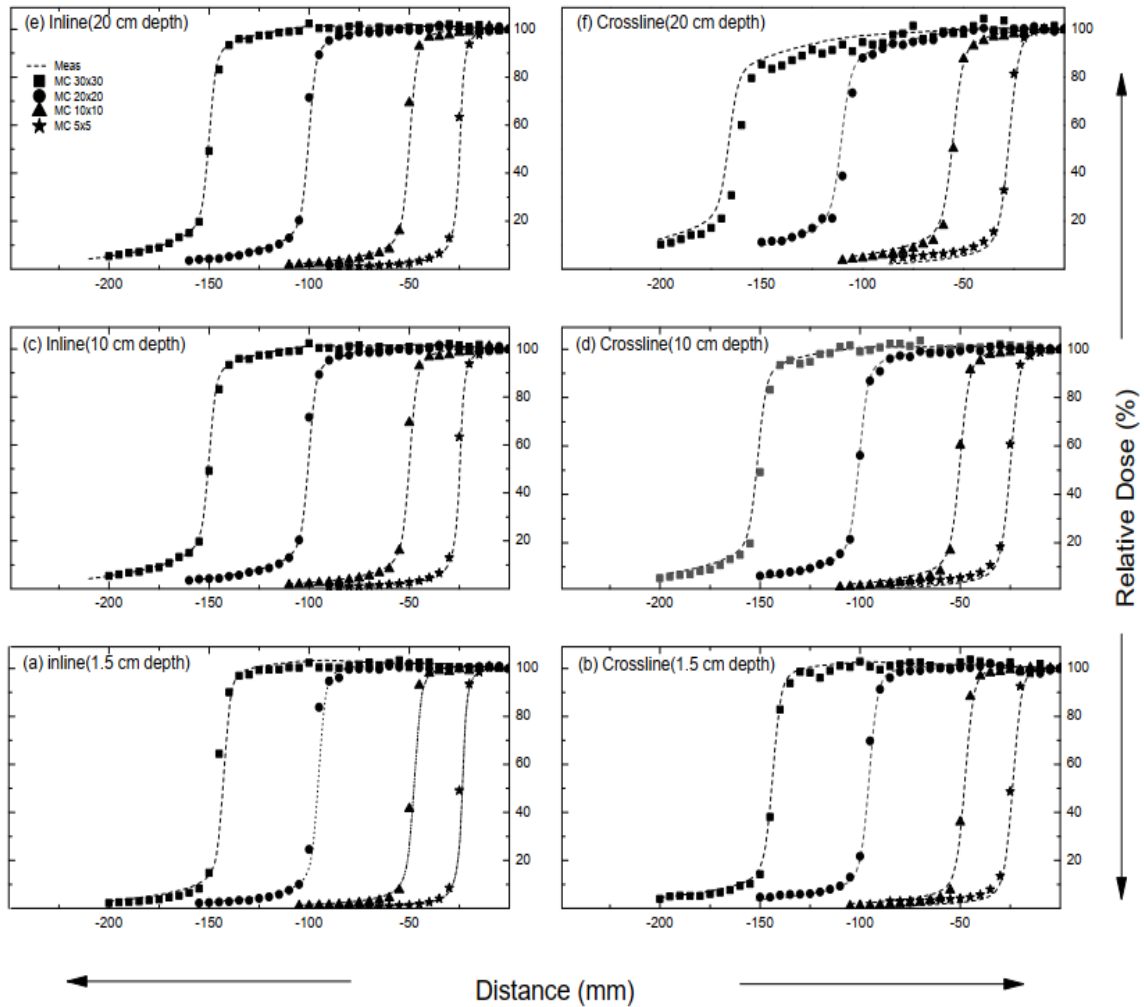


Figure 6.4 The inline and cross-line beam profiles for a range of square field sizes of sides of length ranging from 5 cm to 30 cm.

6.2.2. MLC modelling

The MC calculated beam profiles and PDD profiles at SSD and SAD setup are in good agreement with the measured profiles. The matching of the MC calculated results against the measurements has demonstrated the accuracy of the MC model. The leaf bank rotation (LBROT) value of 9.4 m radians, isocentre interleaf gap of 0.1 cm, step width of 0.04 cm, and radius of the leaf ends of 17 cm have been found to match the calculated

profiles most closely with measured profiles. These results have further been validated by match in the penumbra profile of the MLC field (figure 6.5). Similar results have been obtained for the jaws as indicated in the inline profiles calculated for SSD and SAD setup.

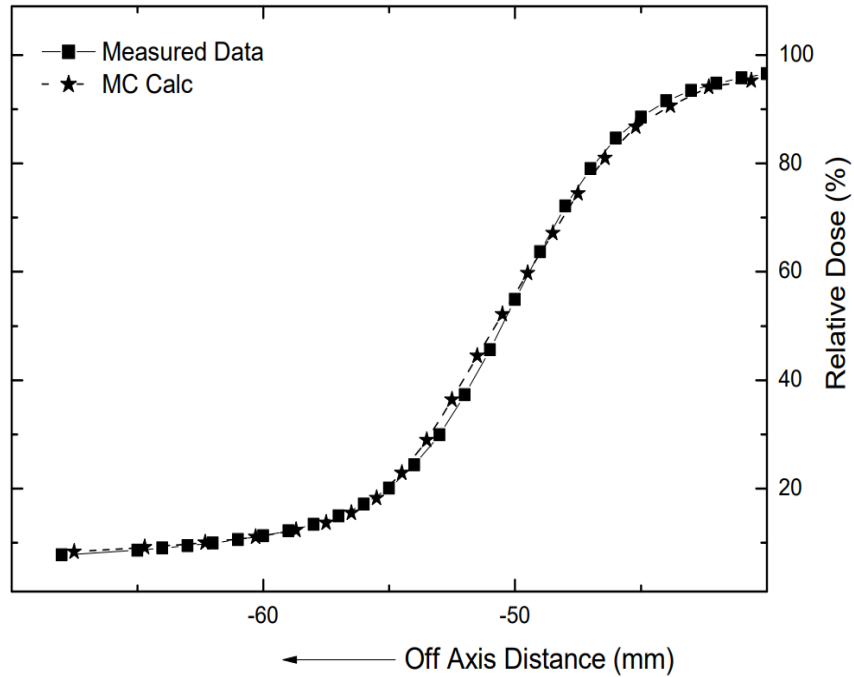


Figure 6.5 The radiation beam penumbra for Agility 160 leaves MLCs for a $10 \times 10 \text{ cm}^2$ field size. The congruence of measured and MC simulated parameters show the accuracy of the model parameters used to define the MLCs.

6.2.3 Output factors

The field output factors for the MC model have been obtained for the square fields of the length of the side ranging from 5 cm to 30 cm. These calculated factors have been compared against the measurements. These factors for different field sizes have been normalized at $10 \times 10 \text{ cm}^2$ field size for calculated and measured data respectively (figure 6.6). A maximum variation of 0.7% has been observed in the beam output factors for the $20 \times 20 \text{ cm}^2$ field.

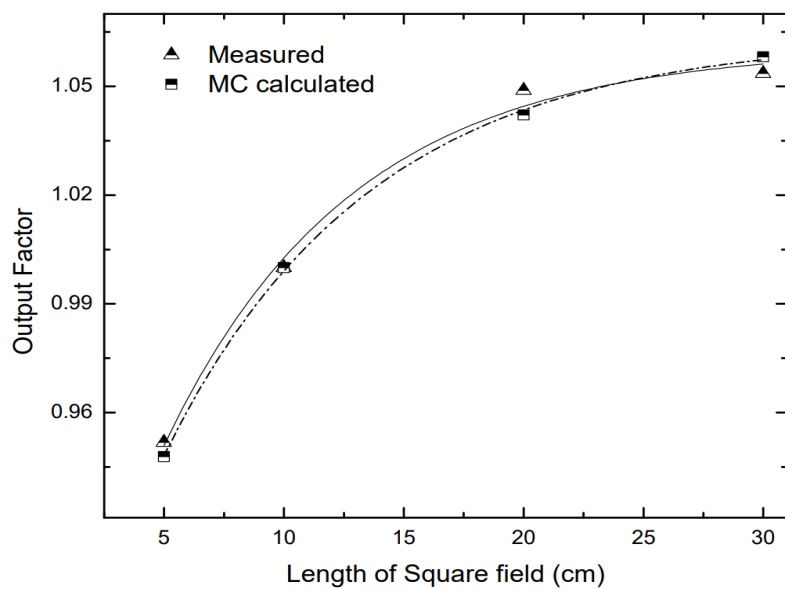


Figure 6.6 Calculated and measured beam output factors as a function of field sizes.

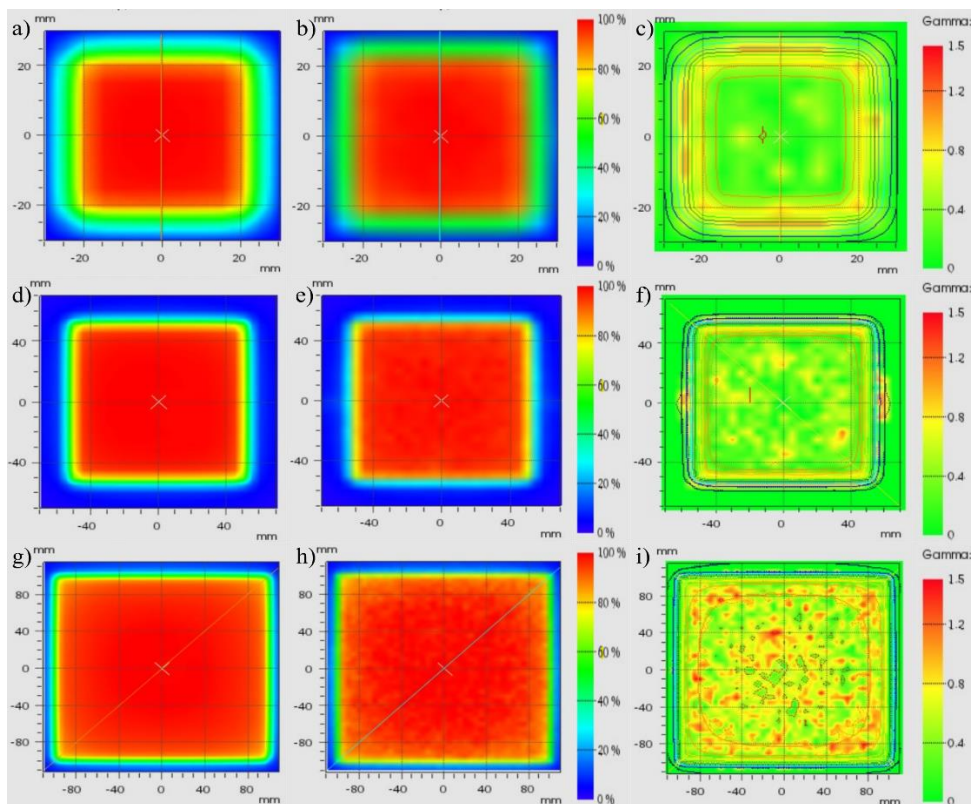


Figure 6.7 2D gamma analysis of the measured (a, d, and g) and MC calculated (b, e and, h) dose distributions at 90 cm SSD, 10 cm depth for $5 \times 5 \text{ cm}^2$ (a-c), $10 \times 10 \text{ cm}^2$ (d-f), and $20 \times 20 \text{ cm}^2$ (g-i).

6.3 MC Simulation of the chlorophyll dosimeter

The MC simulation of the chlorophyll dosimeter has been performed to determine the correction factors. The 6MV x-ray beam of the linac simulated in the previous section has been used as a radiation source. The density correction file for *chl-a* concentration 1 nmol /ml of acetone (80%) has been generated in the EGS software from the radiological density correction data obtained from the NIST database. The chlorophyll solution has been modelled inside a cylindrical vessel made up of polypropylene plastic. The vessel has been supplied by the Thermo Scientific company. It is 0.7 cm in diameter, and 1 cm in height with a wall thickness of 0.05 cm. The vessel has been modelled inside a uniform phantom at 10 cm depth and 100 cm SSD from the radiation source. The following set of simulations has been performed to determine the correction factors:

1. Full beam simulation on the water phantom to determine the dose to water at the point of placement of the dosimeter.
2. Full beam simulation with modelling of the chlorophyll solution inside the polypropylene vessel placed in a water phantom.

These correction factors for the chlorophyll dosimeter have been determined using the following formulae:

1. **Volume averaging correction factor (P_{vol}):** The volume of the dosimetry vessel has been simulated keeping water as medium and the following equation as per the IAEA TRS 480 [11] has been used:

$$P_{vol} = \frac{D_{w,v}}{D_w} \quad (6.3)$$

Where, $D_{w,v}$ = Average dose to water over the volume of the dosimeter in water in the absence of dosimetry material.

D_w = Actual dose to water at the point of measurement in water.

2. **Non-water equivalence of the dosimeter ($f_{w,chl}$):** The factor accounts for the difference in radiation absorption characteristics of chlorophyll dosimeter from that of water. The factor is calculated by the following equation:

$$f_{w,chl} = \frac{D_w}{D_{chl}} \quad (6.4)$$

Where, $\underline{D_w}$ is the average dose to water and D_{chl} is the average dose to the chlorophyll dosimeter.

3. **Wall correction factor for non-water equivalence of the dosimeter wall (P_{wall}):** the factor accounts for the perturbation caused by the wall of the dosimetry vessel. This factor is calculated by using the following equation:

$$P_{wall} = \frac{[D_{chl}]_{ww}}{[D_{chl}]_w} \quad (6.5)$$

Where, $[D_{chl}]_{ww}$ is the average dose to chlorophyll dosimeter without the polypropylene vessel and $[D_{chl}]_w$ is the average dose to the chlorophyll dosimeter with polypropylene vessel.

The correction factors for the chlorophyll dosimeter have been determined in DOSXYZnrc user code. The correction factors are given in table 6.3.

Table 6.3 The MC calculated values of the correction factors for the chlorophyll dosimeter.

Correction factor	Calculated values
P_{wall}	0.995 ± 0.011
$f_{w,chl}$	0.969 ± 0.009
P_{vol}	0.999 ± 0.007

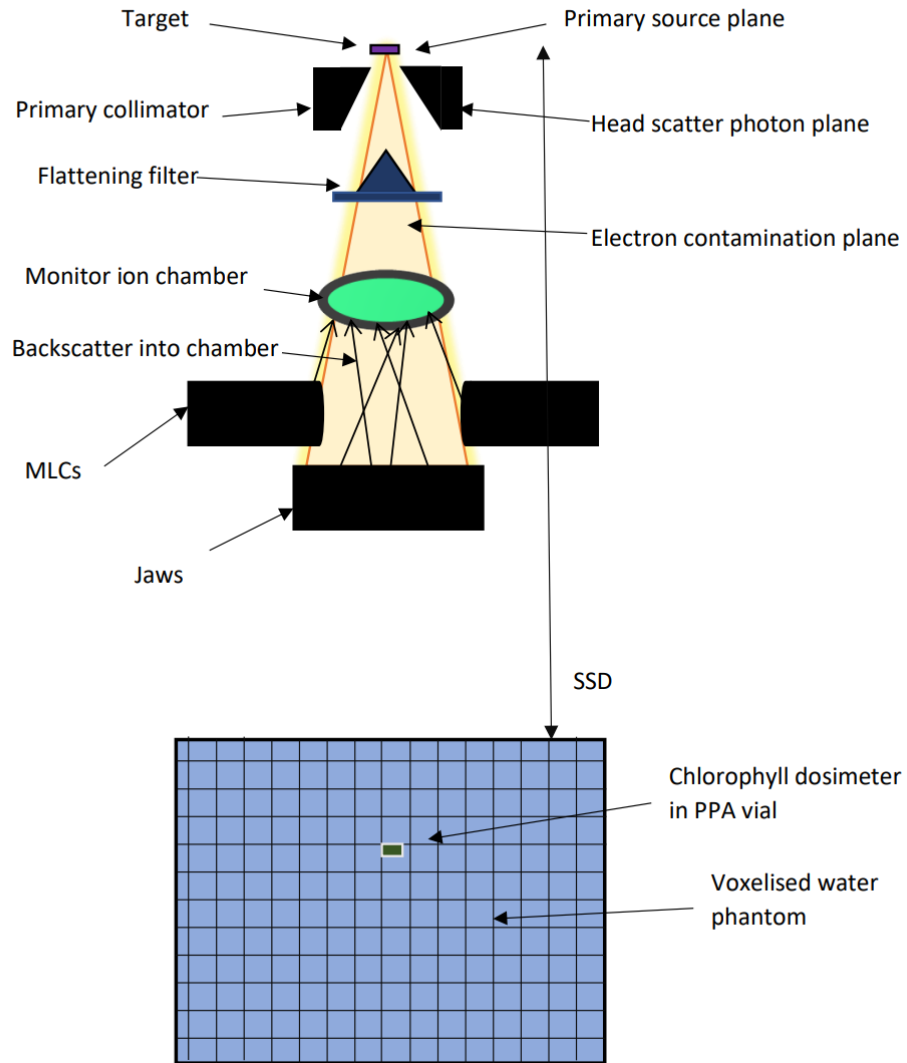


Figure 6.8 Illustration of the irradiation setup for a chlorophyll dosimeter and Agility head simulated in EGSnrc MC simulation toolkit for determination of the correction factors.

The MC simulations have been used by numerous researchers to calculate the beam-related parameters, model the physical properties of the detectors, and determine different types of calibration and correction factors. The application of MC simulations for chemical dosimeters has been focused mainly on Fricke dosimeters. Researchers [12] have

determined the correction factors for applications of Fricke dosimeter in HDR brachytherapy. They obtained the factors with minimal uncertainty. Similarly, ElGamal et al., and David Mariano et al have utilized the MC methods to determine the correction factors for a Fricke dosimeter in HDR brachytherapy. For Fricke, the values of $f_{w,F}$ have been 1.003 [13] for 6 MV x-ray while for Ir¹⁹² brachytherapy 1.004 [10] and 1.0004 [14] have been observed. The P_{wall} values of 0.994 for glass wall, and 0.999 [10–12] for PMMA walls have been observed.

The correction factors are dependent on the dosimeter composition, the volume of the dosimeter and irradiation conditions. The P_{wall} values obtained in the present study are closely associated with those obtained by Moussous et al., for 6 MV x-ray beams. The $f_{w,chl}$ values have differences owing to the difference in the composition and electron density values of Fricke and chlorophyll dosimeters. Similarly, P_{vol} is dependent on the dosimetry vessel's volume and may vary greatly for different vessel designs. The correction factors in the present study have been obtained for a standard chlorophyll dosimeter and can be used to correct the dose obtained in a chlorophyll dosimeter to accurately determine the dose to water.

6.4 Conclusion

The MC simulation methods have been used to determine the correction factors for the chlorophyll-based chemical dosimeter. For this purpose, the MC model of the radiation source i.e., the medical linac collimator head has been produced. The independent model of the collimator head has been validated against the experimentally measured beam data to ascertain the accuracy of the MC model. The beam profiles and depth dose profiles have been validated by testing the gamma criteria. An error estimator quantity has also been determined. The beam profiles and depth dose profiles for most field sizes have been found to follow the gamma criteria of 3%/3mm. The error estimator for the inline and crossline profiles at 10 cm depth has been 0.034 and 0.060 respectively and for the PDD profile 0.0066. On validation of the MC model, the chlorophyll dosimeter has been simulated with a standard concentration of 1 nmol/ml of *chl-a* in acetone (80%) and maintaining the *chl-*

a/b of 3:1. The correction factors have been determined and found to be; $P_{wall} = 0.995 \pm 0.011$, $f_{w,chl} = 0.969 \pm 0.009$, $P_{vol} = 0.999 \pm 0.007$. The factors can be used to determine the absorbed dose to water from the absorbed dose to chlorophyll.

Bibliography

- [1] Andreo, P. (2018). Monte Carlo simulations in radiotherapy dosimetry. *Radiation Oncology* 1–15. <https://doi.org/10.1186/S13014-018-1065-3/FIGURES/8>
- [2] Gholampourkashi S, Cygler J E, Belec J, Vujicic M and Heath E 2019 Monte Carlo and analytic modeling of an Elekta Infinity linac with Agility MLC: Investigating the significance of accurate model parameters for small radiation fields *Journal of Applied Clinical Medical Physics* **20** 55–67
- [3] Tayalati Y, Didi S, Zerfaoui M and Moussaa A 2013 Monte Carlo Simulation of 6MV Elekta Synergy Platform Linac photon beam using Gate/Geant4
- [4] Onizuka R, Araki F and Ohno T 2018 Monte Carlo dose verification of VMAT treatment plans using Elekta Agility 160-leaf MLC *Physica Medica* **51** 22–31
- [5] Vujicic M, Belec J, Heath E, Gholampourkashi S and Cygler J 2015 SU-E-T-627: Precision Modelling of the Leaf-Bank Rotation in Elekta's Agility MLC: Is It Necessary? *Medical Physics* **42** 3480–3480
- [6] Elekta. (2016). *Monaco Dose Calculation Technical Reference*.
- [7] Low D A, Harms W B, Mutic S and Purdy J A 1998 A technique for the quantitative evaluation of dose distributions *Medical Physics* **25** 656–61
- [8] Sarin B, Bindhu B, Saju B and Nair R 2020 Validation of PRIMO monte carlo model of clinac®IX 6mv photon beam *Journal of Medical Physics* **45** 24–35
- [9] Grevillot L, Frisson T, Maneval D, Zahra N, Badel J N and Sarrut D 2011 Simulation of a 6 MV Elekta Precise Linac photon beam using GATE/GEANT4 *Physics in Medicine and Biology* **56** 903–18

- [10] INTERNATIONAL ATOMIC ENERGY AGENCY 2000, *Absorbed Dose Determination in External Beam Radiotherapy*, Technical Reports Series No. 398, IAEA, Vienna
- [11] INTERNATIONAL ATOMIC ENERGY AGENCY 2017, *Dosimetry of Small Static Fields Used in External Beam Radiotherapy*, Technical Reports Series No. 483, IAEA, Vienna
- [12] deAlmeida C E, Ochoa R, Lima M C de, David M G, Pires E J, Peixoto J G, Salata C and Bernal M A 2014 A Feasibility Study of Fricke Dosimetry as an Absorbed Dose to Water Standard for ^{192}Ir HDR Sources *PLoS ONE* **9** e115155
- [13] Moussous O, Khoudri S and Benguerba M 2011 Characterization of a Fricke dosimeter at high energy photon and electron beams used in radiotherapy *Australasian Physical and Engineering Sciences in Medicine* **34** 523–8
- [14] David M G, Salata C and de Almeida C E 2021 Determination of the correction factors used in Fricke dosimetry for HDR ^{192}Ir sources employing the Monte Carlo method *Physica Medica* **84** 50–5

Chapter 7

Summary and conclusion

This thesis has proposed a novel dosimeter for application in the radiation dosimetry of therapeutic x-rays and electron beam radiations.

The research has been started with the identification of an optimal pair of plant leaf and solvent yielding the highest chlorophyll content. Chemical factors like solvent toxicity and the seasonal availability of the leaves have also been considered. The presence of chlorophylls in the solution has been identified by IR analysis. Following the selection of the optimal pair, the solution has been tested for radiation response under the therapeutic x-rays and electron beam radiations from a linac. The dosimetric properties have been tested for energy dependence and dose rate dependence at different x-ray and electron beam energies and dose rates available in the linac.

A 2D film dosimeter has been synthesized by incorporating the chlorophylls in the PVA matrix. The film dosimeter has been characterized for its preparation by several techniques. The 2D film has been tested for its dosimetric properties under similar conditions of irradiation. The dose response and energy dependence has been tested under therapeutic x-rays and electron beam radiations. Further, owing to the temperature and light induced effects in the chlorophylls, the storage conditions for the chlorophyll dosimeter has been tested at four different conditions of temperatures and light. After, studying the dosimetric properties of chlorophylls, the correction factors for this dosimeter have been determined using the MC simulations to determine D_w from D_{chl} .

The dosimeter in its present form has strong feasibility for application in therapeutic x-rays and electron beams. It can be a potential candidate in the radiation dosimetry of therapeutic and industrial radiation if successfully standardised and made available. Above all the dosimeter has the advantage of cost effectiveness and biodegradability. This dosimeter shall be helpful in reducing the cost burden and enhancing cancer care.

The thesis has been aimed at completion of certain specific objectives mainly concentrated on study of the feasibility of chlorophyll molecule as a radiation dosimeter. In future the authors aim to extensively study the chlorophyll dosimeter at different concentrations for best response in the therapeutic radiations. The energy and dose rate dependence will also be investigated with more detailed manner.

Appendix - 1

List of Patents and Publications

Patent

1. Chand B. and Kumar M., **Chlorophyll based radiation dosimeter for radiotherapy**; Submitted to Indian patent office.

Publications

1. Chand B, Singh R and Kumar M 2022 Determination and validation of the initial beam parameters of Elekta Agility collimator head by Monte Carlo simulations. *Physical and Engineering Sciences in Medicine*; 45(3):889-899. <https://doi.org/10.1007/s13246-022-01159-7/>
2. Chand B, Priyamvda, Kumar M. Prasher S and Kumar M 2022 Feasibility study of a chlorophyll dosimeter for high energy x-ray beam used in radiotherapy. *Journal of Radioanalytical and Nuclear Chemistry* **331(4)** 1881-1887. <https://doi.org/10.1007/s10967-021-08106-y>
3. Chand B, Kumar M, Prasher S, Sharma A and Kumar M 2022 Aprotic and protic solvent based extraction of chlorophyll from various plants: Chemical characteristic and analysis *Journal of Physics: Conference Series* **2267(1)** 012143. <https://doi.org/10.1088/1742-6596/2267/1/012143>
4. Chand B., Priyamvda, Kumar M. Prasher S and Kumar M Effect of CT number to relative electron density curves acquired at different tube voltage and current on radiotherapy dose calculation. *Journal of Physics: Conference Series* **2267(1)** 012140. <https://doi.org/10.1088/1742-6596/2267/1/012140>
5. Bhagat Chand B, Trivedi G, Prasher S and Kumar M 2020 Commissioning of Clinac IX Trilogy Linear Accelerator for Stereotactic Radiosurgery *Journal of Physics: Conference Series* **1531(1)** 012032. <https://doi.org/10.1088/1742-6596/1531/1/012032>.

6. Chand B, Kumar M, Kumar M and Priyamvda 2020 Comprehensive Review of Small Field Dosimetry *European Journal of Molecular & Clinical Medicine* **7(7)** 3595-3607.
7. Chand B and Kumar M Estimation of Correction Factors for Chlorophyll Based Chemical Dosimeter. *AIP Conference Proceedings*; Accepted.
8. Chand B., Priyamvda, Kumar M. Prasher S and Kumar M Analysis of thermal and photodegradation kinetics of mangifera indica leaf extracts for determination of optimum storage conditions. *Journal of the Indian Chemical Society*; Under review.

List of Conference Presentations

1. **Poster Presentation** 2nd International Conference on Recent Advances in Fundamental and Applied Sciences, 2019, LPU Phagwara.
2. **Oral Presentation** 3rd International Conference on Recent Advances in Fundamental and Applied Sciences, 2021, LPU Phagwara.; **Best paper award.**
3. **Oral Presentation** 3rd National Conference on Radiation Awareness and Detection in Natural Environment, 2021, Hemvati Nandan Bahuguna Gharwal University, Tehri.
4. **Oral Presentation** 21st National Conference on Solid-state Nuclear Track Detector and their application, 2021, Ramjas College; Delhi University.
5. CME on Recent Updates in Medical Physics Practices, 2021, AIIMS Bhopal.
6. **Oral Presentation** International Conference on Materials for Emerging Technologies, 2021, LPU Phagwara.